

POLITECNICO DI TORINO

Master of Science in Civil Engineering



**Half-joint assessment of concrete bridges:
strut and tie model development and
FEM validation**

Master Thesis

Relatori

Politecnico di Torino

Prof. Maurizio Taliano

TU Delft

Dr. Yuguang Yang

Candidato

Rebecca Asso

Accademic year 2019/2020

Abstract

Monitoring and assessment of structures is one of the most interesting and urgent topics that occupies a central role in research. Bridges are no exception: due to their location and structure they are often subjected to critical environmental conditions and load cases. A widely exploited structural scheme is the dapped-end beam, obtained by using a particular joint (half-joint) which geometry does not allow direct inspections in its critical zones. The aim of the thesis is to provide a useful generic tool: a safe, fast, reliable indication of the strength of the element, a model that can be of a vast application, with different reinforcement layouts, different geometries. A lower bound of strength based on the strut and tie method is identified in order to have an indication of the ultimate resistance of the joint. Existing strut and tie models are studied and implemented, until a new model is defined and applied to several existing half-joints in order to test its adaptability. The analytical model is then validated by means of the finite element program ATENA 2D, with non-linear analysis of selected cases among the analytical model applications. The numerical analysis confirms all results coming from the analytical model application, also providing an excellent agreement with a laboratory test output. This thesis result can be of spread use and basis for further interesting research topics, since it can represent the first step towards a new strategy for half-joint monitoring.

Ringraziamenti

Siamo arrivati alla fine di questo percorso. E dico “siamo” non per esaltarmi ma perché ho avuto la fortuna di condividere questi sei anni con tante persone che mi hanno supportato e sopportato, e quindi tutto questo giro di giostra se lo sono dovuto sorbire in tanti. Quello che sono oggi, o perlomeno il lato buono, è frutto soprattutto al meraviglioso esempio e insegnamento di persone che ho avuto la grandissima fortuna di conoscere e apprezzare.

Voglio prima di tutto ringraziare i miei genitori, due persone intelligenti e capaci, che hanno sempre avuto una grande fiducia negli insegnamenti diretti e indiretti, guidandoci con l'esempio, la gentilezza, il dialogo, l'apertura e il coraggio. E la tecnica del ricatto, che devo dire porta sempre i suoi risultati. Pietro, Anna e Marta vi ringrazio perché sopportare una sorella maggiore come me non deve essere facile, sono un po' ingombrante (cit.). Da parte mia devo dire che arricchite tutti i giorni che passiamo insieme, siete brillanti e tenaci, non vorrei staccarmi mai.

Ci sono stati dei Maestri nella mia vita precedente, quella che non era fatta solo di Università. Vorrei ringraziare Jojo e Luciano, e vorrei ringraziare l'insieme di coincidenze che mi hanno permesso di conoscervi e apprezzarvi. Grazie.

E adesso due colonne portanti, due colonnane importantissime. Tere e Ly, mi meraviglio continuamente del nostro rapporto e della naturalezza che ci lega. Ci vorrebbero giornate da 50 ore per fare tutte le cose che vorremmo. Un'altra parte della mia struttura portante è Ila, che fa vedere il mondo a colori.

Dal punto di vista “tecnico”, grazie a Massimo e Nicolò che avete avuto sempre una pazienza da certosini, sopportando le mie domande e dubbi esistenziali.

Questi ultimi anni sono stati ricchissimi, pieni di persone belle, divertenti e intelligenti. Sicuramente tutto questo percorso non sarebbe stato possibile se non ci foste stati. Grazie Boba, Matte, Mara, Leo, Ale, Fede, Sandro, Nicco e tutti quelli che non ho modo di scrivere qui, senno' viene lunga da morire. Lo sapete che vi penso e che se ci penso troppo mi commuovo.

Che anni belli che sono passati.

TABLE OF CONTENTS

1. INTRODUCTION	1
1.1. Background.....	1
1.2. Scope of the research	1
1.3. Thesis overview	2
1.4. Overview of the 20th century infrastructures	3
1.4.1. Italian and Dutch roads network	3
1.4.2. Concrete: use and codes	6
2. BRIDGES WITH GERBER BEAMS.....	8
2.1. Use, advantages and experience.....	9
2.2. Collapses of bridges with half-joints	11
2.2.1. Polcevera Viaduct (2018).....	12
2.2.2. Concorde Overpass (2006)	13
2.2.3. Annone Overpass (2016)	15
2.3. Theories, Codes, Publications	17
2.3.1. Modelling and testing of half joint in literature	19
2.3.2. Monitoring and strengthening	22
2.4. Conclusions.....	24
3. STRUT AND TIE: A LOWER BOUND.....	26
3.1. Definition of the <i>Disturbed and Bernoulli</i> zones.....	26

3.2. Truss identification	28
3.3. Elements dimensioning	29
3.3.1. Struts.....	29
3.3.2. Ties.....	32
3.3.3. Nodes.....	32
3.4. Model development	35
3.4.1. Literature references to the superposition of the two models	38
3.4.2. Trusses superposition assessment	39
3.4.3. Stirrups concurring to a single tie	40
3.4.4. Prestressing aspect	41
4. KINEMATIC METHOD: AN UPPER BOUND	43
4.1. Upper bound model limits.....	44
5. ANALYTICAL MODEL APPLICATION	47
5.1. Dutch bridge practice: analysis of selected existing joints	48
5.1.1. Beam 3	49
5.1.2. Beam 5	51
5.1.3. Beam 14.....	53
5.1.4. Beam 27.....	55
5.1.5. Beam 30.....	57
5.2. Laboratory test carried out by Desnerck et al	59
5.3. Conclusions	62
6. NUMERICAL ANALYSIS.....	64
6.1. Introduction to ATENA 2D	64
6.2. Desnerck et al. laboratory test: validation of the FEM model	68
6.2.1. Inputs.....	68
6.2.2. Outputs.....	72
6.3. Selected database joint: validation of the analytical models	80

6.3.1. Inputs.....	80
6.3.2. Outputs.....	87
6.4. Discussion of obtained results	101
6.5. Conclusions.....	105
7. GENERAL GUIDELINE.....	107
8. FURTHER RESEARCH	111
9. CONCLUSIONS	114
10. REFERENCES	116
APPENDIX	126
A. ANALYTICAL MODELS: LOWER AND UPPER BOUNDS	126
A.1 Beam 3	126
A.2 Beam 5	131
A.3 Beam 14	136
A.4 Beam 27	142
A.5 Beam 30	146
A.6 Laboratory test.....	152

1 . INTRODUCTION

1.1. BACKGROUND

Most of the infrastructural networks existing nowadays have been designed and built in the 1950s and 1960s, according to different regulations, under the action of lower loads and with a more limited knowledge about the behaviour of structures. Half-joints were widely used, because of their easy application and prefabrication, and we are now inheriting structures that are getting to the end of their service time, subjected to years of environmental attacks, maybe with small damages and repairing, maybe strengthened or apparently in a perfect shape of their materials and functionality. Moreover, in recent years traffic loads increased and codes changed, with more precise specifications and limits: the non-conformity of existing structures to actual codes' requirements and the limit load can be identified and structures can be verified to actual circumstances.

It appears that a precise and accurate plan of assessment must be identified, based on theoretical knowledge and supported by numerical and laboratory validations, in order to provide a general and applicable model that can guide the assessment of the existing half-joints. The topic may appear limited, since it is focussed on a specific type of bridges' joint. Nevertheless, it can provide an important basis for a further research on this type of structures or similar.

Many authors and researchers dealt with half-joints, particularly in the design phase^{1,2}, studying reinforcement optimization, some focussed on service loads and cracks development^{3,4}, a few on strengthening techniques^{5,6} or deteriorate elements⁷.

1.2. SCOPE OF THE RESEARCH

The aim of the thesis is not to develop a new theory, but to provide a useful universal tool: a safe, fast, reliable indication of the strength of the element, a model that can be of a vast

application, with different reinforcement layouts, different geometries. The output of this thesis can be of useful in order to define or recalculate the strength of half-joints, to be compared to the increasing loads acting on such structural elements.

The proposed model will be validated with a non-linear finite element program, ATENA. Since one the principal purposes is its applicability to a large number of structures, this aspect will be considered with the analysis of some examples of existing structures derived from the Dutch practice and the nonlinear FEM approach will also be validated by the laboratory tests carried out by Desnerck, Lees and Morley⁷⁻¹⁰.

The model should be applicable and adaptable to different half-joints geometries and reinforcement layout and type, different standards and it must provide a lower bound of strength. The optimum value of a lower bound is the one that is closer to the real resistance of the element, however in this case it is more useful to have a conservative output. Degradation processes cannot be considered because the most damageable parts are not accessible for inspections and qualitative indications provided by field surveys are not possible to be included in the model: a lower indication of the ultimate resistance of the element can be on the safe side also when dealing with deteriorated elements.

The thesis produces a good compromise: a conservative result achieved in a not-demanding approach, that could have a good use in a wide application to define the strength of half-joints.

1.3. THESIS OVERVIEW

The first two chapters of this thesis are devoted to a general overview of the current structures, materials, half-joints' applications, advantages and disadvantages. Moreover, in the second chapter of the thesis two collapses caused by failure of half-joints are reported. In the third chapter there will be a first insight in strut and tie practices, providing a lower bound of strength computation. As a counterpart, in the fourth chapter an alternative method will be introduced and analysed: it consists in the hypothesis of an equilibrated mechanism in the beam, thus bringing about an upper bound of strength, whose results are higher or equal to the real failure load of the structure. This method has been widely used in determining the strength of existing half-joints and some aspects showing its non-reliability will be discussed. Nevertheless, it is a valid complementary method to the lower bound of strength, and for this purpose it will be used in

the following chapters. Regarding the application of the models, an analytical study is provided in chapter five, and a numerical validation will be provided in chapter six. A general guideline for an easy application of the model will be introduced in chapter seven.

The author is aware that the thesis can only give a rather limited contribution, a rough result in a wide and complex field. More studies will be necessary and in chapter 8 further research topics will be discussed.

1.4. OVERVIEW OF THE 20TH CENTURY INFRASTRUCTURES

During the 1950's and 1960's of the 20th century, most Western European countries enjoyed a strong economic development and change. In fact, after wartime reconstruction was completed, beginning with the early 1950s, a "Golden Age" of fast growth involved many European countries, that lasted until the late 60s when a progressive and inevitable slowdown spread across countries¹¹. In a continent devastated by a World War, many factors contributed to this era of great social conquests and tumultuous economic change. One of them regarded a vast program of public works affecting mainly a very articulated network of new road and rail infrastructures. Thanks to public provisions to infrastructures, the construction and rebuild of European roads and railways network could be possible¹².

1.4.1. Italian and Dutch roads network

Nowadays, the Netherlands has one of the densest public road networks of 139 000 *km*, denser than the German's and French's, and with 5 350 *km* of motorways it also has the densest motorway networks in the world (Benelux countries are in the first three positions). About 5200 *km* of national roads are managed by the central government agency Rijkswaterstaat, while other 7200 *km* of provincial roads are controlled by the twelve provinces¹³. The first motorway was built in 1936, and the construction accelerated in the 1960s and 1970s, slowed down in the 80s. Dutch flat landscape allows a good optimization in the production of roads' elements, rendering possible an ideal "standardization" of structures like bridges or viaducts. Construction time, costs and safety standards are the three main factors that influence the use of precast elements to build bridges, and in the growth years there was an intensive use of industrial production, also because of the introduction of prestressing: nowadays 90% or more of Dutch

bridges are built with precast elements. Bridge beams can be of various shapes, mainly inverted T or box beams. Gerber beams could optimize the total height of the structure, so the material used, construction time and cost; moreover, they are usually precast and prestressed, and these characteristics caused a widespread use of such elements.

In Italy the National Autonomous Agency for roads (ANAS) is the main player in road infrastructures, but it only controls 12% of the total road network, with more than 14600 bridges¹⁴. Italian morphology necessitates a very high number of bridges and viaducts (around 60000 bridges are present, even though an accurate estimate does not exist). Moreover, compared to the Netherlands, infrastructures are characterised by a high variety in construction materials, methodology, age of structures and environmental conditions. This is partly due to the fact that the use of new techniques such as reinforced and prestressed concrete was widely exploited and implemented at an early stage too.

One interesting case was the construction of a 1176 m long bridge on the Po river in North Italy in 1958: the designer Silvano Zorzi decided to build a multi-span bridge with precast prestressed concrete beams, so the newly born prestressing technique was used for the first time making it urgent to be regulated (first large-scale application was on the Rio Paz between El Salvador and Guatemala, 1949¹⁵). In fact, an Italian code on prestressed structures was missing, since it had never been necessary. To test the finished bridge an extraordinary variable load was used: a line of ten tanks and several trucks full of gravel passed on the bridge in both directions to validate its bearing capacity¹⁶ (Figure 1.1).



*Figure 1.1: Load test on the Po Bridge (Italy)*¹⁷

Starting from the 1950s, Italian transport culture radically changed moving from train- to a car-based, due to incentives and the greater efficiency provided by the general political strategies on public works that clearly supported the enlargement and the improvement of the road networks, aiming to a more modern, more connected and faster country.

In fact, from 1926 to 1950 more than 13000 km of roads have been built, and in 1964 the national Italian highway *Autostrada del Sole*^{16,18} was constructed: a masterpiece of infrastructure that connects Milan, Bologna, Florence, Rome and Naples in 755 km (Figure 1.2). Italian variegated morphology tested designers' and constructors' audacity and fantasy: moving from the flat lands of the north, the central mountain chain had to be crossed, the *Appennino*, going towards the completely different landscape of Tuscany, with its soft, green hills.



Figure 1.2: Italian *Autostrada del Sole*

That part of highway connecting Bologna to Florence, was 90 km long with 67 bridges and viaducts, together with 24 galleries. In order to speed up the construction, in the *Appennino* section every firm or company could work on one lottery only: 27 different designers worked on that part, and this led to a great variety of bridges and viaducts, in steel, reinforced concrete, prestressed concrete or composite¹⁸.



Figure 1.3: *Aglio viaduct*

Aglio viaduct in Figure 1.3 is one of the bridges connecting Bologna to Florence and it is a magnificent reinforced concrete arch bridge, built between 1957 and 1959, spanning 164 m and 440 m long. This is only one example of the many bridges and viaducts that were built with the arch shape in a relatively short time-span.

As it is possible to notice from these few lines, construction was surprisingly fast in those years. New infrastructures were designed, and many new techniques were exploited. Our inheritance is therefore various, built in a moment of lower knowledge and with limited tools that caused

the use of simplifications. The use of “good practices” and “rule of thumbs” was common procedure at that time and it deeply affected design choices. Nowadays we have finer research and technological tools to better support design and maintenance of new and existing structures.

1.4.2. Concrete: use and codes

During the 1950s and 1960s knowledge on concrete was limited, because of lack of experience and computational issues, that could not support the power and level of complexity of the research. This mainly affected the prediction of prestressing loss, the calculation of complex static schemes, the exact knowledge of factors that affect reinforced concrete durability, strength and resistance to the environment^{19–22}. As a direct consequence, building codes were dealing with critical aspects giving qualitative indications, biased by oversimplifications and assumptions. In recent years many topics were analysed: correlation between aggregate size, water/cement ratio, concrete porosity and reinforcement corrosion²³ so that plasticizers and fluidifying solutions were introduced, minimum concrete cover in correlation to the environment aggressiveness²⁴, minimum shear reinforcement even though it appears not to be required are just some of the aspects that are implemented nowadays.

Regulations of the building industry in the 1950s and 1960s were mainly pertained to a National scale, and this led to a non-uniformity in construction techniques, experiences, culture and tolerances. Since 1975, the Infrastructure Commission of the European Community started to work on a project of harmonization of technical specifications: today, National Building Codes of European countries are all referred to a wider and common standard, the Eurocode. This modern code is based on a probabilistic approach on safety, serviceability, strength, resistance to fire, durability and risk class.

It is very common that structures built in the Golden Age are not fulfilling the actual code requirements, and it is obvious that it is not possible to rebuild all structures or infrastructures that do not overcome such limitations of modern codes. To have a correct and feasible monitoring and repairing plan it is necessary to proceed with a multi-level approach, with risk classes and different levels of danger depending on the type of detail considered²⁵.

The International Federation for Structural Concrete (*fib*) is working on the elaboration of codes that aim to merge international rules on concrete, ISO codes and Eurocodes, producing Model Codes and setting goals for the incoming research topics that varied during years: in the last

Model Code (MC2020) monitoring of structures occupies a central role. In fact, MC2020 aims to be a *model code that gives particular attention to the issues specific for existing structures, such as the effect of material degradation and/or insufficient or deficient detailing on the provided material and member behaviour models, the need for model improvement and the treatment of uncertainties in models and model parameters for existing structures and (phased) interventions*²⁶.

Now that the background of the research has been presented, it will be easier to introduce the main character of the thesis: the Gerber beam. This structural element has been of wide application in the discussed period, and the next chapter will all be devoted to its discussion: advantages and disadvantages, a few cases of failed bridges with Gerber joints and a quick scan on past and present studies will be provided.

2. BRIDGES WITH GERBER BEAMS

A half-joint, Gerber joint or dapped-end, referred as nib, consists in a Gerber deck, suspended span or reduced end beam, supported on nibs of abutments or adjacent beams, as shown in Figure 2.1). It takes the name of its inventor, Heinrich Gottfried Gerber²⁷, a German engineer who lived in the XIX century.

Only for the *Autostrada del Sole* (Figure 1.2), around 400 bridges were built, many of them following the standard scheme of multi-span simply supported beam with Gerber scheme^{18,28,29}. In fact, starting from the 1950s the use of prestressed reinforced concrete gained popularity and when applied to Gerber beams it could allow the production of long beams, of comparable dimension to steel beams³⁰.

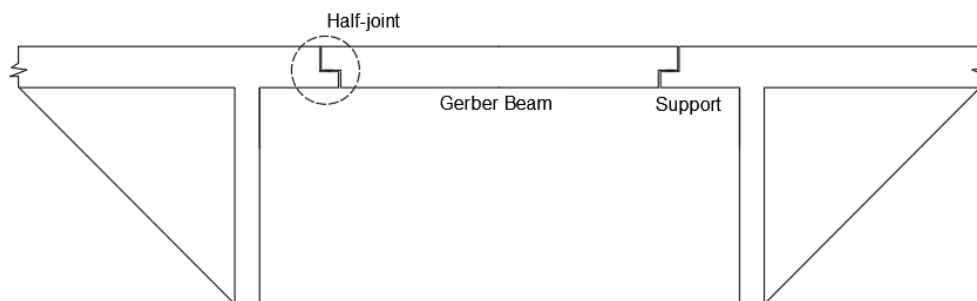


Figure 2.1: Suspended beam

As reported from Desnerck et al.¹⁰ geometries of half-joints can be various, with a height reduction often higher than 50% and a ratio length over height of the nib that can be equal or higher than 1. Geometry of the half-joint is shown in Figure 2.2.

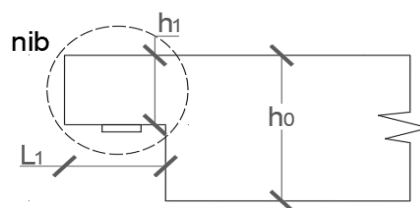


Figure 2.2: geometry of the half-joint

2.1. USE, ADVANTAGES AND EXPERIENCE

The choice of static scheme directly affects the magnitude of stresses and the sensitivity to actions such as differential settlements or thermal variations. The simply supported scheme allows simpler force calculation of each element and does not develop internal actions due to settlements and thermal variations³¹. However, mid-span moments are higher compare to that of the continuous supported beam which redistributes the moment on the supports: their final distribution, depending on the number of spans, tends towards the diagram of a beam clamped on both extremes (see Figure 2.3).

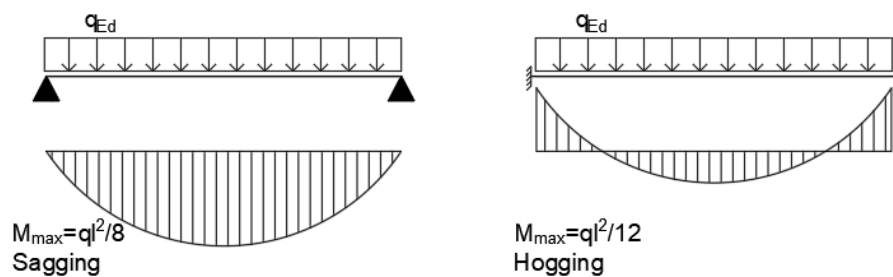


Figure 2.3: static schemes comparison

So, the continuous beam has a better moment distribution, but it is not forgiving differential settlements or thermal variations: the beam inflects, and additional internal stresses are developed. The comparison is shown in Figure 2.4.

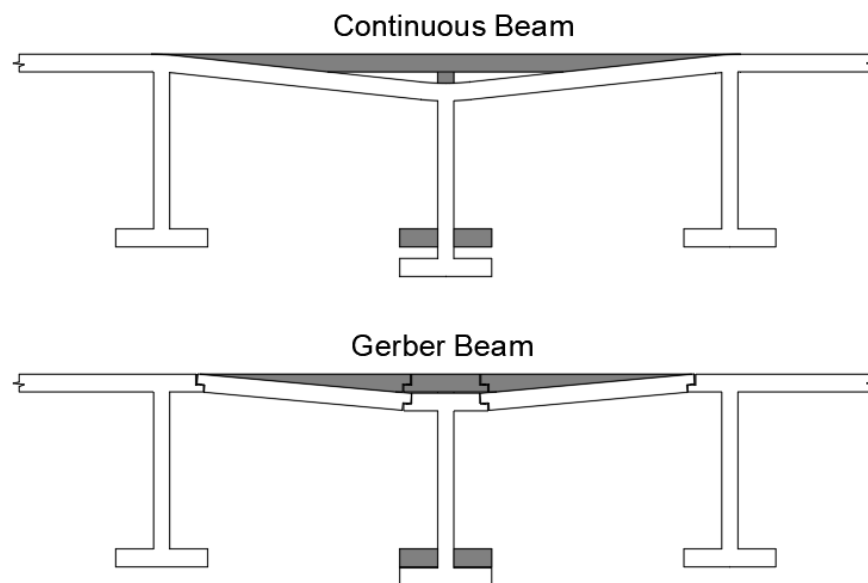


Figure 2.4: behaviour of continuous or simply supported beam

The use of a Gerber beam exploits the positive aspects of the two systems: the joints allow rotations, so can be schematized as hinges, and they are placed in strategic points where the bending moment is zero (see Figure 2.6). This leads to a simply supported static scheme with the moment distribution of a continuous beam. Forces transmitted from the joint are horizontal and vertical reactions, bending moments are very limited. Moreover, the use of half-joints can easily take advantage of precast production of beams, of common use nowadays.

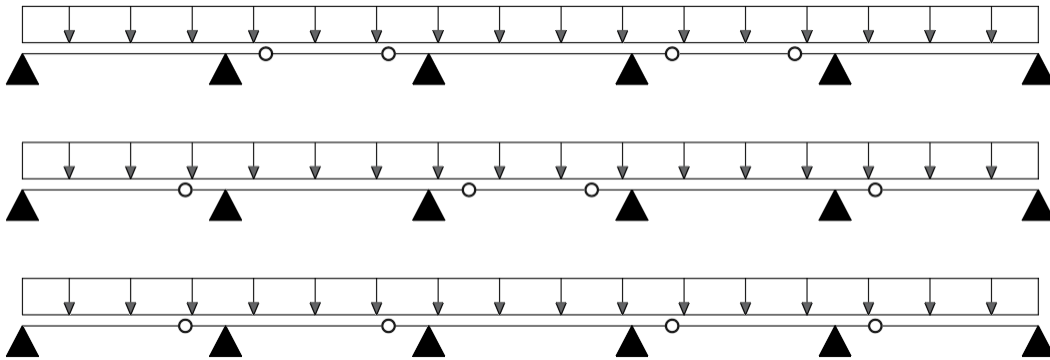


Figure 2.5: possible positions of hinges in continuous beams

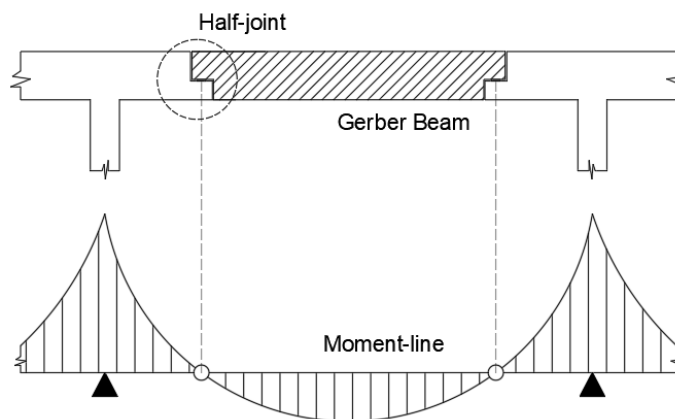


Figure 2.6: strategic position of the half-joint

However, the geometry of the joint itself is the cause of some disadvantages that must be considered and that are crucial to be solved:

- Inspections are not possible in the most problematic regions of the joint where water can easily infiltrate and accumulate, enhancing its vulnerability to chloride corrosion due to seepage of sealant coming from the road surface²⁴;
- Reinforcement layout of existing joints is not designed referring to a unique standard configuration, but it is possible to find many different geometries, as shown in Figure

2.7. This last aspect creates problems when trying to have a unique law of assessment or localize the most critical regions of the joints.

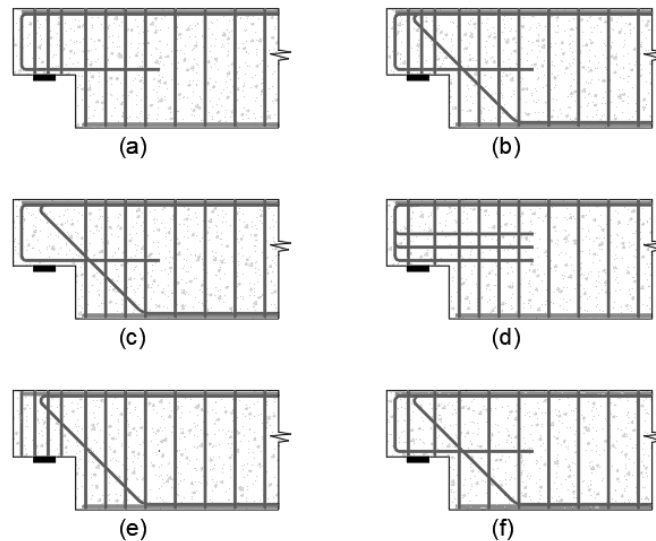


Figure 2.7: possible configuration of reinforced concrete half-joints⁹.

On one side there is a non-conformity to nowadays standards and a questionable design and construction, (e.g. absence of shear reinforcement in The Concorde viaduct), on the other side there are problems that affect all structures, also the ones with non-arguable design aspects: traffic load has increased from the reference loads of the 1960s, many existing structures are about to reach their end-of-life and environmental effects cause inevitable degradation on materials. Hence, a plan of control and maintenance of an incredibly high number of elements is becoming more and more urgent.

Technologies, theories and strategies must be updated and functional to face and solve actual problems of existing structures, in order to have adequate monitoring and repairing plans and avoid catastrophic episodes.

2.2. COLLAPSES OF BRIDGES WITH HALF-JOINTS

Several cases of disastrous failure have unfortunately been observed. Sad examples^{14,28,32,33} are the collapses of the Concorde in 2006, Petrulla viaduct in 2014, Annone viaduct in 2016, Ancona overpass and Fossano viaduct in 2017, Bologna and Polcevera bridges in 2018. Among the

reported cases, three of them were including a Gerber scheme and two collapses can be directly addressed to the half-joint.

2.2.1. Polcevera Viaduct (2018)

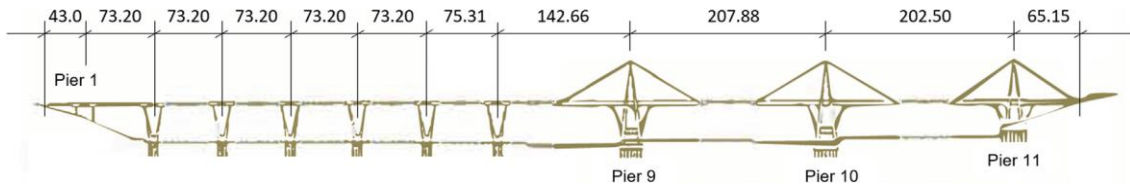


Figure 2.8: Polcevera viaduct [m]²⁹

Polcevera viaduct, known as Morandi bridge, was finished in 1967 and for that time it represented one of the most pioneering structures ever built (Figure 2.8). The causes of collapse on August 14, 2018 are many, the aggressive environment^{19–21} (the viaduct was 1 km distant from the sea), the absence of structural redundancy³⁴ and the negligence in construction and initial maintenance (“most of the ducts did not have grouts, that supposed to have been injected in during the construction, and strands showed extensive corrosion and some cables had loose strands³⁵”) are, among others, the most crucial factors in this catastrophe³⁶. Several assessments had been carried out throughout the years, some of them guided by the designer Riccardo Morandi himself^{19,29}, showing the necessity of continuous repairing actions, external prestressing cables substitution, rust removal, protective layers application. When Tower 9 collapsed, a replacement intervention of its strands was planned for the following two months, and ongoing maintenance was present on the deck.



Figure 2.9: Polcevera viaduct before failure, highlight on Gerber beams and collapsed tower²⁸

Gerber beams were used to connect adjacent piers and were exploited in their best functionality since they managed to increase the length of the bridge without introducing bending moments. The collapse cause is not attributed to a half-joint failure, in fact the two Gerber decks that were

supported by the Tower 9 (Figure 2.9) fell as a consequence of the support failure. The collapse caused 43 casualties.

2.2.2. Concorde Overpass (2006)

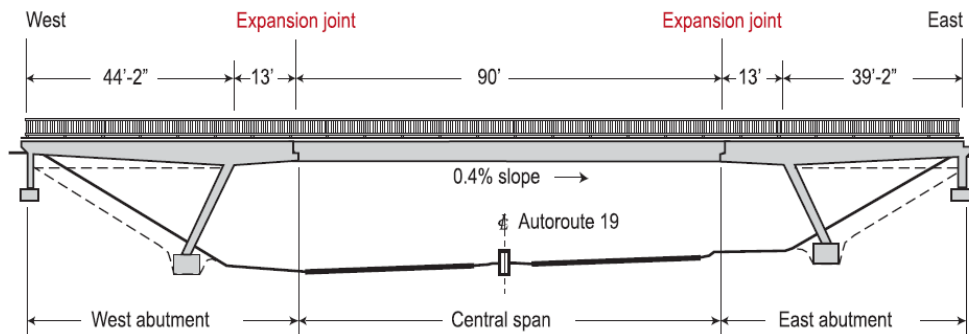


Figure 2.10: The Concorde overpass static scheme [1 ft=0.3048 m]³³

This overpass was a skew-bridge situated close to Montreal, Canada, built in 1968 and collapsed in 2006. It was built with precast box beams with dapped ends.

The failure of this bridge can be directly assigned to the inadequate design of the Gerber joint. The collapse happened in a brittle shear mode, under the action of the self-weight and almost no live load. This experience showed how dramatically the building codes of its construction time were inadequate:

- The load analysis only assumed a uniformly distributed load on the whole span with no consideration, among the others, of the concentrated moment and shear coming from the skew supports³³.
- Anchorage of diagonal bars was not properly designed.
- Shear reinforcement was absent, but according to the regulations in the design phase it was not required³⁷.

Moreover, reinforcement layout of the joint as built did not reflect the design indication, producing a further decrease in the bars' anchorage. This topic has been investigated by Desnerck et al.⁸, whose studies on reinforced concrete half-joints show how a reduced anchorage can cause a loss of 10% of the strength of the joint. Moreover, this malfunction is often in combination with other inevitable weakening actions, such as concrete spalling and reinforcement corrosion: in these cases the resistance reduction is more severe and due to the difficulties in

reaching the inner nib for inspections, it is often challenging to have an accurate indication of the residual strength of the joint.

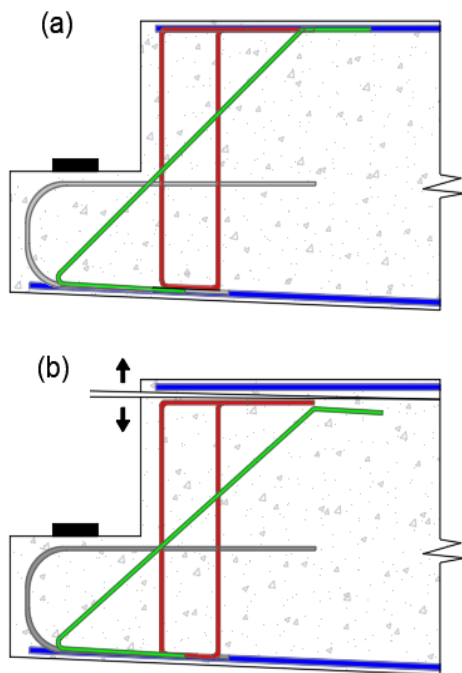


Figure 2.11: reinforcement layout as-designed (a) and as-built (b). Highlight on crack initiation (b)

The critical crack that led to the failure of the bridge initiated at the half-joint, in the gap generated by the reinforcement misalignment, between the longitudinal upper reinforcement and the anchorage of the hangers (red stirrups in Figure 2.11). The weak concrete area supported the formation and development of the crack, which simplified water and de-icing salts access, resulting in an accelerated process of reinforcement corrosion and resistance reduction.

Degradation of the concrete above the reinforcement hooks plays a crucial role in reducing the half-joint strength, causing the premature failure under dead loads and very limited live loads (595 kN is the acting load on the bridge).

Investigations carried out by Mitchell et al.³³ on full scale laboratory tests and numerical simulations, surprisingly show that the as-built reinforcement layout could bear a higher load (1075 kN) when compared to the ultimate load of the as-designed (810 kN) joint. The collapse mode was a brittle shear failure in both cases.

One more aspect of importance in this collapse case is the so-called *size effect in shear*: in absence of vertical reinforcement, shear resistance decreases with the increase of reinforcement depth. In 1968 it was not known yet, and no shear reinforced slab would have resulted in an unsafe design choice. From this dramatic experience it is possible to see how the combined action of insufficient misplaced reinforcement and lack of anchorage can have severe consequences.

It must be again highlighted that this design would not be fulfilling modern codes, minimum shear reinforcement is always required, precise indication about anchorage design are provided and skewed bridges undergo more limitations, regarding load distribution calculation and detailing. Nevertheless 5 people have died and 6 were injured³⁸(see Figure 2.12).



Figure 2.12: The Concorde after collapse

2.2.3. Annone Overpass (2016)

The bridge has been built between 1960 and 1962 and collapsed in October 2016 causing the death of one person and injuring of 5 others. It consisted in precast prestressed beams, and the suspended dapped-end beam was 18.7 m long.

During its lifetime it went through many repairing works, mainly because of its reduced clearance (less than 5 meters), that caused impacts of high trucks against the lower side of the edge beam. CFRP strips had been applied in the half-joints in order to strengthen and renovate the bridge after the umpteenth impact in 2006, as it is possible to notice in Figure 2.13. At least four impacts have been registered: 1988, 1990, 2006 and 2009³².



Figure 2.13: Annone overpass before collapse

The very same day of the failure, a 25 mm settlement of the joint had been measured by specialists who went to check the bridge after some material fell on the road. It probably was the outcome of a progressive decline of the health of the bridge, consequent to extensive reinforcement corrosion that caused the formation of a major crack in the edge beam. However, this settlement could redistribute the loads on the structure and reduce the loads acting on the joint. The collapse of the overpass was not due to an impact, but it was caused by the passage of a 107.6 t heavy truck, travelling at 6.6 km/h²⁸, shown in Figure 2.14.

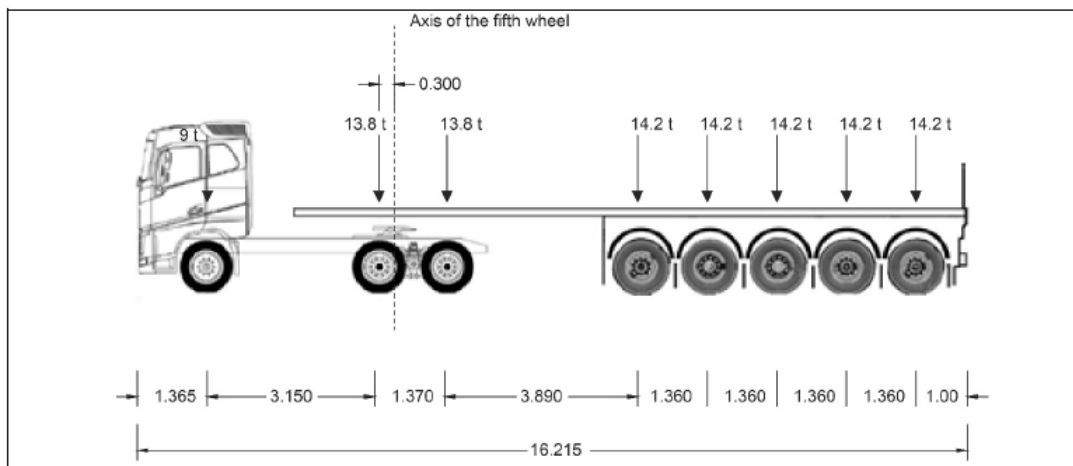


Figure 2.14: truck that caused the bridge collapse³²

After a load analysis, an investigation on the load acting on the bridge during the day of the collapse, a test carried out on the non-destroyed half-joint and a strut-and-tie model, M. di Prisco et al.³² concluded in a technical report on the failure of the bridge with the following:

- The dead load calculated was lower than the real dead load of the bridge (155 tons against 172.3 tons).
- The design live load of a category II bridge of that type was, according to the code in 1962 *Circolare 14 febbraio 1962 n.384*, **55 tons** on one lane. According to the code in force at the collapse time, *NTC 2008*, the same category of bridges could withstand **92 t** in one lane, 150 t on both lanes.
- In the day of the collapse four trucks weighting more than 70 t passed on the bridge, and the critical load was **107.6 t**, double of the original design value.
- The resistance of the Gerber beam was estimated 24.7 t with a strut and tie model by Di Prisco et al.³², and resulted equal to the acting load of 22.8 t in a direct laboratory test

carried on the available bridge beam. With no settlement of the joint, so no redistribution of loads, the acting load would have been 46.7 t.

- The failure of the horizontal reinforcement in the nib caused the joint collapse.

The bridge fell as a consequence of degradation of the material that decreased the strength of the joint, but a lack of attention in controlling the bridge bearing capacity played a major role.



Figure 2.15: Annone overpass collapsed

2.3. THEORIES, CODES, PUBLICATIONS

From the late 1960s research started to move its interest towards half-joints, first focussing on design strategies, then in direction of other important aspects such as crack monitoring, specific geometries assessment, and strengthening techniques.

Strut and tie model is an important method to design and assess regions where the Euler-Bernoulli hypothesis in Timoshenko³⁹ beam theory is not fulfilled, so the *plain sections do not remain plain*. Hence, two regions are defined: the D-region where the discontinuity causes stress variations not complying to Euler-Bernoulli hypothesis and the B-regions where Bernoulli principle is respected, see Figure 2.16.

The next chapter will describe the available strut and tie models for half-joint in detail. Here some half-joints' studies in the past years are reported.

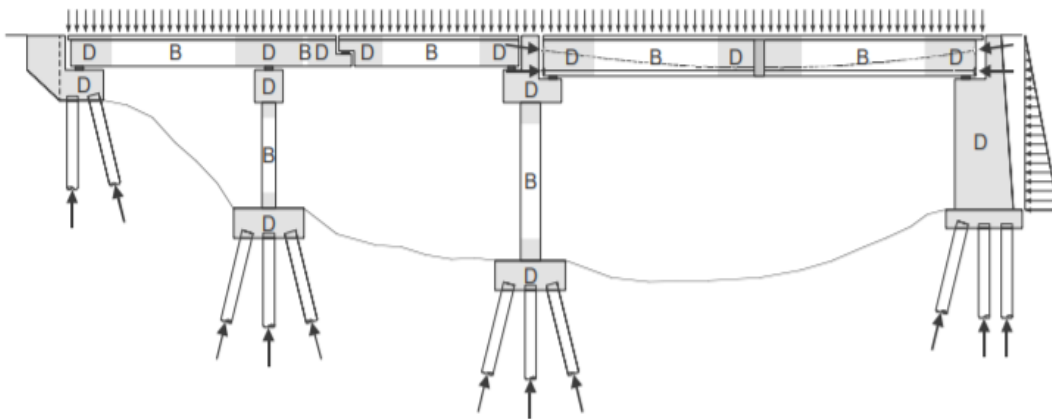


Figure 2.16: typical example of D- and B- regions of a structure

The strut and tie model is based on the truss analogy introduced by Ritter⁴⁰ and Morsch⁴¹ (see Figure 2.17), which states that cracked reinforced concrete acts like a truss, where steel reinforcement is loaded in tension and concrete is loaded in compression. The truss is composed by a lower chord and vertical elements in steel while upper chord and 45° diagonals are concrete struts. In the model, the tension resistance of concrete is neglected.

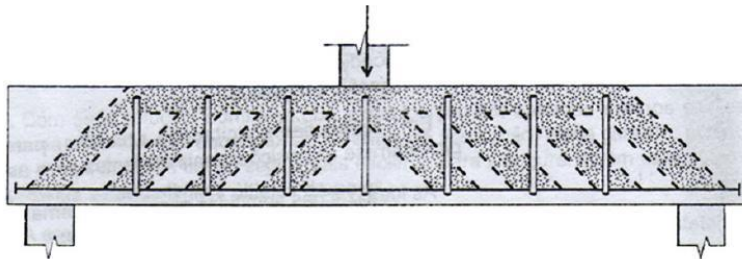


Figure 2.17: Ritter and Morsch truss

The traditional truss model used in shear design of reinforced concrete beams has been generalized to allow the analysis of discontinuities which could be caused by the geometry (holes, cross section variations) or by loads applications (anchorage zones, support areas or concentrated loads). The strut and tie model is widely used in the design phase of reinforced concrete elements such as half-joints, and the generalization that brought this method from dealing with the B-regions of shear reinforced concrete beams to a wider application form was achieved in several passages, which will be briefly introduced in the following few lines.

Strut and tie model for shear resistance of beams with vertical reinforcement has been the object of many studies and has drawn the attention of many researchers, including Kupfer⁴², Leonhardt⁴³, Collins and Mitchell⁴⁴, Marti⁴⁵. In 1971 Lampert and Thürlimann⁴⁶ first generalized the angle θ of concrete struts, studying the behaviour of reinforced beams in torsion: this has been

then included in the CEB-FIB code of 1978 that allowed values for tangent of θ between $3/5$ and $5/3$. The assumption of 45° diagonal struts was done observing the initial crack slope, also according to Mohr circle of pure shear stresses.

Based on the tension-field theory developed by Wagner⁴⁷ on the observation of the development of diagonal tension ties in post-buckling of thin web metallic of steel beams, Collins and Mitchell^{39,44} identified and validated a specular theory: the compression-field theory. According to Wagner the diagonal tension field has the same direction of the principal tensile strain, and the same approach shifted to concrete defines the inclination of the diagonal compressed elements in the beam.

The compression-field theory and strut-and-tie model have many common points, in fact according to Schlaich⁴⁸, a strut-and-tie is a schematization of the stress field in elastic (uncracked) phase. In 1996, Muttoni et al.⁴⁹ produced an extensive work on the application of the compression field (see the truss in Figure 2.18) and in 2007, Muttoni and Ruiz⁵⁰ investigated the development of truss models based on the stress fields, with a Finite Element Programme.

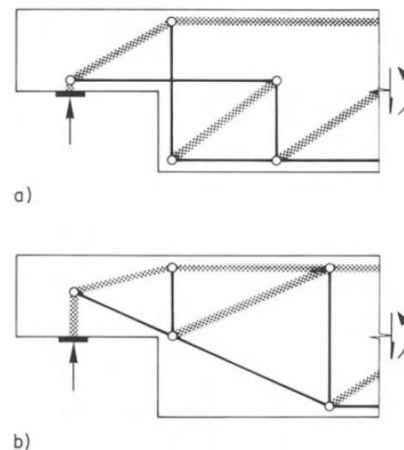


Figure 2.18: Truss based on the stress-field, Muttoni et al.¹

2.3.1. Modelling and testing of half joint in literature

Many authors faced the difficult task of defining design strategies that could maximise reinforcement, usually by means of strut and tie schematizations and laboratory tests. In 1969 Reynolds⁵¹ first carried on important extensive studies about half-joints, resulting in a reinforcement layout proposition and a procedure for quantifying each bar contribution to the strength of the joint.

Ten years later Mattock and Chan¹ studied dapped-end beams (Figure 2.19), comparing internal force flows to corbels on a column, based on the studies by Mattock in 1976⁵². Important results have been achieved: following the stress flow, possible crack locations are identified, and based on bending equilibrium in the crack cross section, steel amount is identified and set in strategical points, as shown in Figure 2.20.

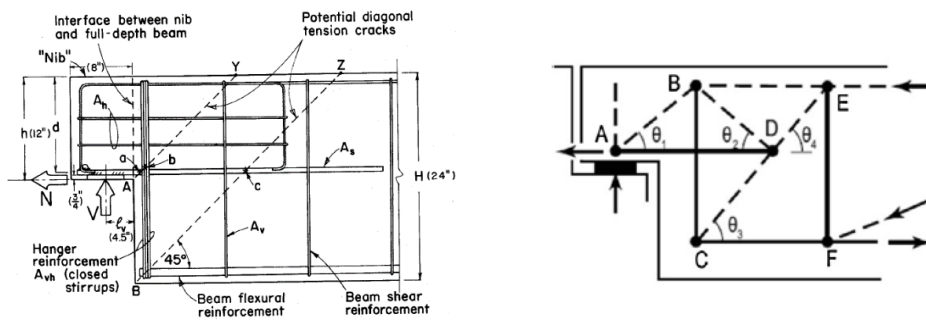


Figure 2.19: typical reinforcement layout suggested by Mattock and Chan¹

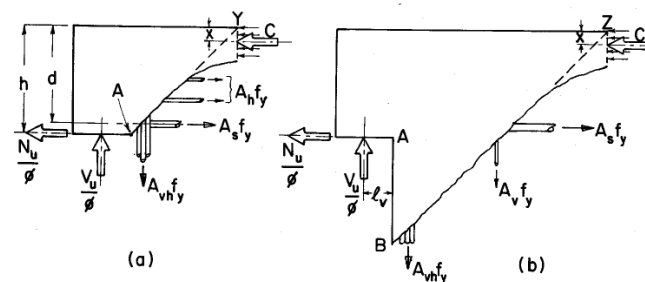


Figure 2.20: possible cracks cross sections and acting forces¹

Note that the model behind the reinforcement layout in Figure 2.19 is not compatible to the failure mode in Figure 2.20: the diagonal crack AY is not represented with diagonal compressed strut in the same direction, nor a diagonal stretched steel element in the opposite direction.

To overcome this non-conformity, Liem in 1983⁵³ introduced the diagonal reinforcement to avoid big cracks at the inner part of the corner, Figure 2.21. This reinforcement layout was validated and considered to be important to enhance the ultimate strength of the joint^{10,54}. Nowadays most of existing half-joints are obtained with this reinforcement layout, very often in combination with the orthogonal one.

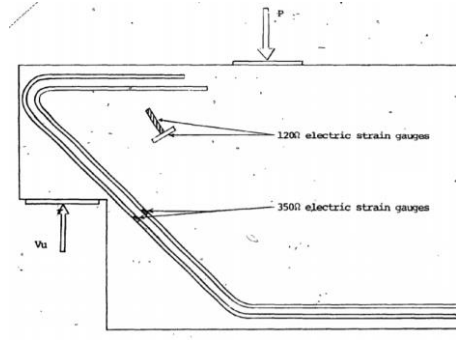


Figure 2.21: Liem reinforcement layout tested in 1983

In 1984 Canadian codes introduced a strut and tie method in half-joint's design, following Collins and Mitchell⁵⁵ research; in 1987 Schlaich⁴⁸ et al analysed Gerber joints' disturbed regions and proposed strut and tie schematization according to the compression field theory⁵⁵, in 1988 Cook and Mitchell⁵⁶ validated those models with the help of non-linear Finite Element Analysis FIELDS with the purpose of providing some indications in design with strut and tie models. It is evident how strut and tie models were often exploited, usually trying to consider all possible rebars present in the joint. However, the more complex is the truss, the higher its variability is, hence for the proposed thesis' model another approach is followed, based on Clark and Thorogood research carried out in 1988⁵⁷, who proposed two ways to predict the ultimate strength of the dapped end: as lower bound the S&T model (or sum of the two S&T of Figure 2.22 in case reinforcement is present in the three directions) and as upper bound the study of the mechanism due to a generally inclined crack at the inner nib (similar to model *a*, Figure 2.20).

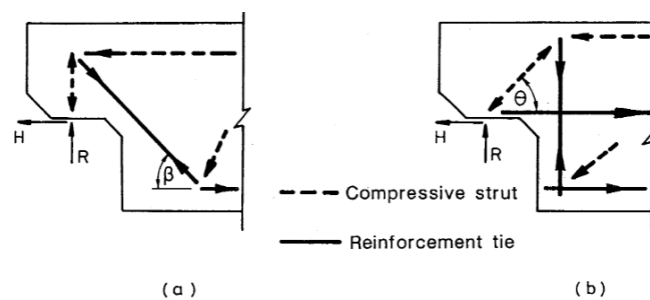


Figure 2.22: two strut and tie models by Clark and Thorogood

The two strut and tie models, when taken individually, are not considering all the possible reinforcement in the nib, but the sum of the two trusses has all rebars that can be present.

To summarize, horizontal rebar in the nib and vertical stirrups in the deep beam are necessary to bear shear coming from the nib reaction applied, and the diagonal reinforcement is essential to reduce the crack width.

Literature on reinforcement layouts and different S&T models is very extensive^{2,58-60}, focussing also on the influence of the contemporary action of horizontal and vertical actions^{61,62}, ribs with length to depth ratio larger than one^{63,64} or design with modified concrete⁶⁵⁻⁶⁷. Indeed, the goal of the present research is the definition of a good assessment method, that must consider design phase of half-joints in order to produce a valid model that can be adjusted on various types of layouts and geometries. Recent research is no longer focussed on design optimization, but mainly on strengthening solutions and crack monitoring.

2.3.2. Monitoring and strengthening

Crack width control has a fundamental role in the service life of the structure: as concrete cracks, oxygen and moisture can easily seep through it reaching rebars and starting one of the most dangerous processes for the durability of the structure: the corrosion of steel reinforcement. It causes structural degradation in two mechanisms, mainly: reduces steel's strength^{63,64} and ductility⁶⁸ and increases steel volume⁶⁹, causing concrete spalling and further increase of crack width. Many authors studied the correlation between the speed of corrosion and crack width^{3,70}, and many researchers tested half-joints^{1,10,57,71} cracking and behaviour under service loads.

In 1973, Werner and Dilger⁴ conducted an interesting test campaign on five prestressed concrete beams, highlighting the influence of shear reinforcement and bearing conditions on the load causing the first crack. They also investigated concrete influence on the total ultimate strength of the beam, concluding the analysis with precise indication on the shear reinforcement position, concrete cover to avoid spalling and bars anchorage loss. In fact, an indirect way to control crack formation and propagation are a proper concrete cover, in dimension and quality, and a limited bars diameter and spacing.

Codes gave empirical formulas or simplified methods to control crack propagation. The American Concrete Institute⁷² provides empirical relations derived from laboratory tests⁷³ and that is then linked to the environment aggressiveness, while the Eurocode 2⁷⁴ and Model Code 1990⁷⁵ use semi-empirical relations to correlate the concrete, steel strain and diameter to the crack width, also influenced in long term by creep.

In 2014 Moreno-Martinez and Meli⁵⁴ tested four specimens with different reinforcement layouts, showing the important role of the diagonal rebar in crack control at the re-entrant corner, followed by Desnerck et al.¹⁰ in 2016 who observed the influence of horizontal reinforcement in the nib, which is highly affecting the crack pattern, so the number of vertical stirrups exploited.

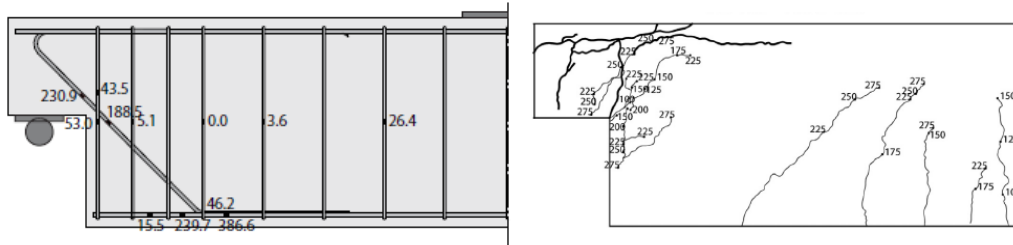


Figure 2.23: reinforcement layout and crack pattern of an half-joint with no horizontal bar, studied by Desnerck et al.⁶

As it is possible to notice from the Figure 2.23 the crack pattern in case of no horizontal rebar in the nib is almost vertical, with little-to-no intersection with the stirrups in the deep cross section: this reduces the load carried by the stirrups and consequently the failure load of the joint.

As the problem of degradation of the material is becoming more and more urgent, many authors tested and analysed strengthening solutions.

In 2004 Taher⁵ studied various solutions and approaches in strengthening half-joints, with bolts, steel plates, fibre reinforced polymers strips, carbon fibre wraps or a combination of different techniques. He obtained good results in terms of ductility and strength enhancement with FRP strengthening after concrete cracked. When only diagonal CFRP strips were applied, a 22% increase of strength was measured, but when the strips were in combination with horizontal carbon fibre wrappings as in Figure 2.24, the measured increase was of 42%.



Figure 2.24: Taher reinforced half-joint, with CFRP strips and carbon fibre wrapping

Other analyses on FRP have been carried by Sas et al.⁶, meanwhile Herzinger and Elbadry⁷⁶ tested the influence of different studs' configurations.

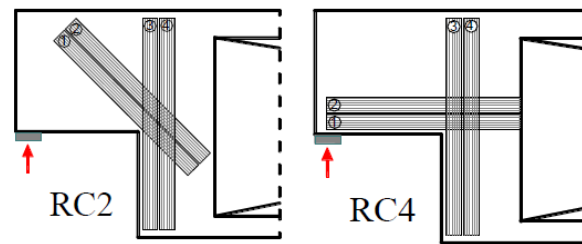


Figure 2.25: Strengthening systems studied by Sas et al.

The two cases studied by Sas et al. reported in Figure 2.25 with FRP produce a strength increase of 20.7% in RC2 and 16.1% in RC4, congruently to Taher et al. results.

Regarding deterioration processes, important tests have been carried by Desnerck et al.⁷ who tested half-joints subjected to rebars corrosion, lack of anchorage and concrete spalling in different reinforcement configuration and concrete class. The deteriorating process that most affects the resistance of the joint is reinforcement corrosion of the rebars in the nib, that can cause an effective area reduction from 30% to 50%⁷⁷, decreasing the strength of the 35%. It is unfortunately the most spread deterioration mechanism, almost impossible to observe and monitor because of the hidden location of the most damaged rebars.

Strengthening solutions are available, deterioration processes are known: the tool missing is missing is a smart model that can help in defining which cases necessitate urgent repairing, and which ones are safe.

2.4. CONCLUSIONS

In this chapter an overview on the thesis' topic has been provided: pros and cons coming from the use of half-joints, three cases of failures of bridges with a Gerber scheme, a review on the ongoing and past researches. Gerber beams provide a good structural compromise in order to have the moment distribution of a multiple-supported beam, and the good attitudes of simply supported beams, with no stress development in case of thermal variation and differential settlements. However, the joint is highly prone to chloride corrosion and fast deterioration that are the main causes of half-joints collapses registered in the recent years. Despite the environmental factors which has an important role in half-joints degradation, loads have increased and codes are changed from the years when the large percentage of structures was built: structures must be checked to be functional and their load bearing capacity sufficient to fulfil the nowadays

requisites. In the next chapter the strut and tie model will be developed and assessed in its theoretical parts. It will be a chapter organized in two parts: the first one presents the method, and the second one defines the model.

3. STRUT AND TIE: A LOWER BOUND

The strut and tie method is a tool which has first been applied to shear resistance of reinforced concrete beams with shear reinforcement^{40,41}, then generalized to deal with stress discontinuities^{48,49}. It provides conservative results, but it allows a safe and precise stress pattern identification and it has been widely used and tested in years of experience. In fact, this method represents an application of the lower bound theorem of plastic analysis which affirms that every schematization of stresses in equilibrium with the external loads that does not exceed in any member the plastic stress is lower or equal to the real structure collapse load. Half-joints are a classic example of geometrical discontinuities, therefore they are commonly treated with strut and tie schematizations.

The first step to design a half-joint is the identification of the part of the beam affected by the discontinuity and the one in which the stresses are following the traditional beam theory. The first region that needs to be mentioned is commonly called the *D-region* since it is the disturbed part, while the undisturbed one that is located at a certain distance from the element that causes disturbance is called the *B-region* because there the Bernoulli hypothesis of conservation of plane sections is valid.

3.1. DEFINITION OF THE *DISTURBED* AND *BERNOULLI* ZONES

The two regions are identified in function of the beam depth following St-Venant's principle⁷⁸, and for half-joints it is usually considered a D-region as deep through the beam as the height of the full cross section beyond the nib (see Figure 3.1).

B-regions are analysed through traditional section properties and forces applied, whereas D-regions are schematized with the Strut and Tie method.

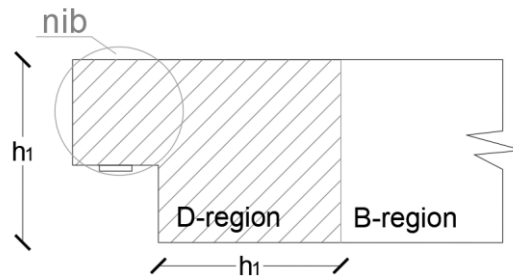


Figure 3.1 schematization of the B- and D-regions

The design of B-regions is congruent to standard beam design and it is of non-negligible importance because in case of complex structures it provides the forces applied at the interface with D-regions. However, in the case of half-joint analysis, the procedure is simplified because the force applied to the D-region is the vertical reaction acting on the nib.

As mentioned before S&T is a lower bound of plasticity, thus the truss requirements are:

- a) Equilibrium with external loads;
- b) Internal stresses in members must not exceed design resistance, assuming materials plasticization.

According to these two conditions, every truss in equilibrium, whose members are in plastic phase and with enough ductility to redistribute internal stresses from elastic to plastic phase represents a lower bound of strength of the structure. In fact, D-regions are the most challenging part in design and assessment because these few conditions allow multiple solutions of possible and correct truss schematization.

For many years, at least until Schlaich work was published in 1987⁴⁸, D-regions were treated with rules of thumb and common practices. Since then, also with further publications in 1990⁷⁹ and 1991⁸⁰, Schlaich and his colleagues radically changed the approach to disturbed regions problems, introducing a precise principle connected to the real behaviour of the cracked beam, in order to schematize a rational, systematic approach.

3.2. TRUSS IDENTIFICATION

The possibility of more than one solution is not a favourable condition, more than ever in the assessment phase: the existing dapped-end beams are in various configurations, with a few common general aspects that can help to discretize different design choices.

How is it possible that more solutions can be achieved, with the same geometry and same load cases? When looking at the stress trajectories in the beam, B-regions are characterized by smooth lines, while D-regions have more abrupt changes in direction, with higher stresses peaks as shown in Figure 3.2. A strut and tie model is a simple schematization, where stress lines are segments in tension or compression, and nodes are changes in direction: more than one schematization is possible. The model identified by the stress path of the elastic theory is obviously neglecting some capacities in plastic field, but this allows a good reliability in Service and Ultimate loads.

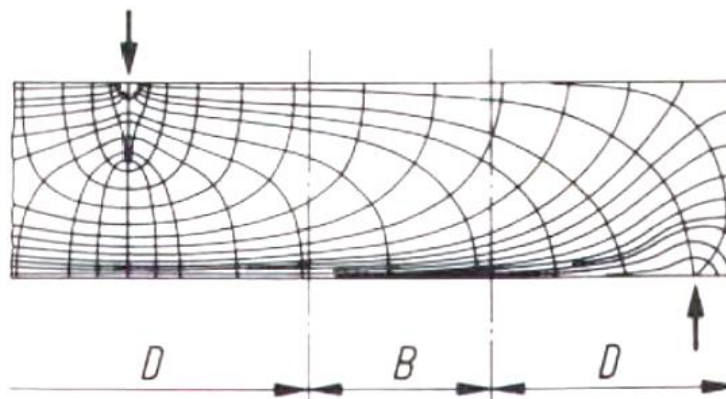


Figure 3.2: stress lines in B- and D-regions, by Schlaich et al.⁴⁸

In the assessment phase, a possible way to define half-joints is by the reinforcement configuration: for example the presence of diagonal and/or horizontal bars that can witness a design pattern, but this choice is done in retrospect, only by observing the position of the bars with no official information about the design scheme used.

The same reinforcement configuration can be addressed to more truss schemes, so involving different forces distribution and overall strength. Possible trusses are reported in Figure 3.3.

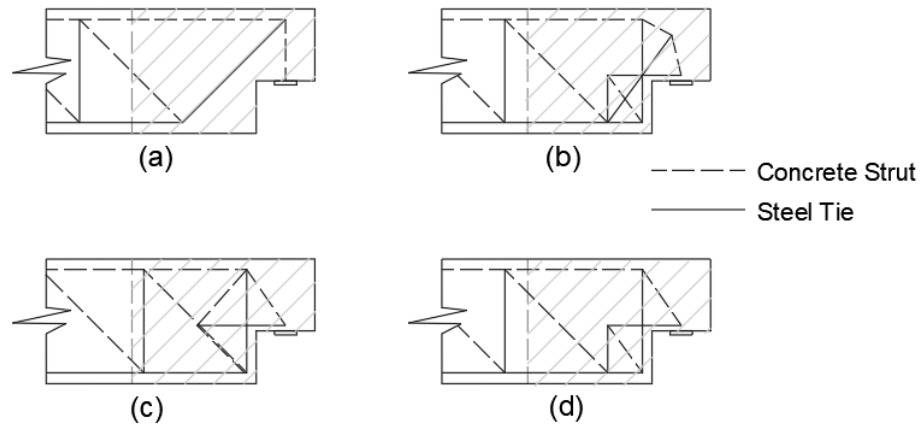


Figure 3.3 possible trusses in the D-region⁹

The identification of the truss defines the forces distribution in the region and the maximum load that can be carried. Every component has a major role: the overall resistance is directly affected by the geometry of the truss (angles and lengths) and the elements' resistance.

3.3. ELEMENTS DIMENSIONING

There are mainly four types of elements that need to be dimensioned: C_c , concrete struts; T_c , concrete ties; T_s , steel ties and nodes. Usually concrete resistance in tension is neglected, so only concrete struts, steel ties and nodes are considered.

3.3.1. Struts

Struts are concrete elements in pure compression and this idealization of concrete as a linear, straight one-dimension element is far away from reality: the real cross-sectional area of concrete causes a spread of stresses in transversal direction that interferes with the other elements, and the simplification of a stress field as a straight line is a gross idealization. Struts can also be considered as bottle-shaped elements, according to some regulations (ACI 318⁷²), as shown in Figure 3.4.

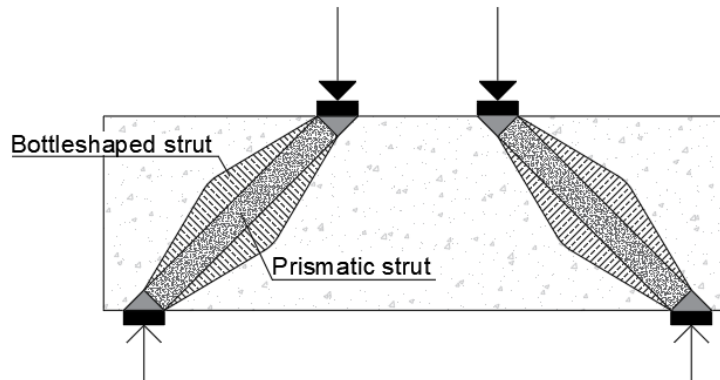


Figure 3.4: Struts schematization

Concrete resistance is affected by the stress applied in transversal direction, and the low tensile strength reduces the compression resistance when tension is applied in transverse direction. In Figure 3.5 this condition is schematized.

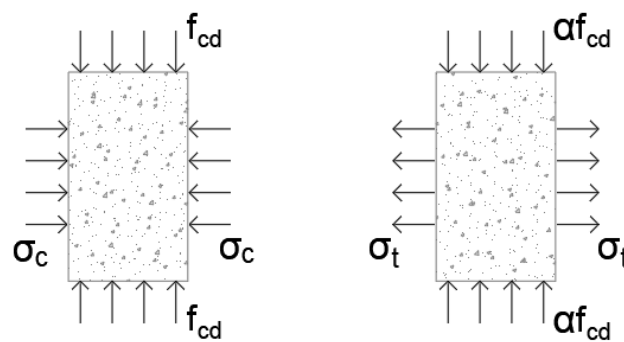


Figure 3.5: cylinder concrete subjected to tension or compression in transverse direction

Codes and authors^{48,72,74,81} give different indications about the reduction factor that applies to the compression strength in the most severe condition, that is also the most likely to have.

Eurocode 2⁷⁴ defines the design compressive strength, referring to the following formulas:

Transverse tension	$\sigma_{Rd} = 0.6 \cdot v' \cdot f_{cd}$ $v' = 1 - f_{ck}/250$	(3. 1)
--------------------	---	--------

Transverse compression	$\sigma_{Rd} = f_{cd}$	(3. 2)
------------------------	------------------------	--------

According to Schlaich et al.⁴⁸:

Undisturbed and uniaxial state of compressive stress $\sigma_{Rd} = f_{cd}$ (3. 3)

Cracking parallel to the strut $\sigma_{Rd} = 0.8 \cdot f_{cd}$ (3. 4)

Skew cracks or skew reinforcement $\sigma_{Rd} = 0.6 \cdot f_{cd}$ (3. 5)

Skew crack of extraordinary crack width $\sigma_{Rd} = 0.4 \cdot f_{cd}$ (3. 6)

Where $f_{cd} = \frac{0.85}{1.5} \cdot f_{ck}$ is the design compressive strength of concrete.

According to ACI 318⁷²:

Struts with uniform compression area along the length $\sigma_{Rd} = 0.85 \cdot f'_c$ (3. 7)

Bottle-shaped struts, with lateral expansion at middle-length $\sigma_{Rd} = 0.64 \cdot f'_c$ (3. 8)

Struts in tension members $\sigma_{Rd} = 0.34 \cdot f'_c$ (3. 9)

According to the Model Code 2010⁸¹, the strut resistance is reduced in function of the concrete compressive characteristic strength:

$$\sigma_{Rd} = k_c \cdot f_{ck} / \gamma_c \quad (3. 10)$$

Transverse compression regions $k_c = 0.75 \left(\frac{30}{f_{ck}} \right)^{1/3} < 0.8$ (3. 11)

Transverse tension regions $k_c = 0.55 \left(\frac{30}{f_{ck}} \right)^{1/3} < 0.55$ (3. 12)

The geometry of the strut changes in function of the truss configuration.

In this thesis the code adopted is the Eurocode 2, because of the application area is in Europe, but other standards can be used.

3.3.2. Ties

Ties can be reinforcing or prestressing steel. Even though steel members are naturally linear elements, the number of rebars that are part of one single tie can vary.

$$F_{tie,Rd} = f_{yd} \cdot A_{tie,r} + \alpha \cdot f_{pd} \cdot A_{tie,p}$$

where:

- f_{yd} is the yielding strength of the reinforcement,
- f_{pd} is the design strength in the prestressing steel,
- $A_{tie,r}$ is the area of reinforcing steel concurring to that tie,
- $A_{tie,p}$ is the area of prestressing steel,
- α is a coefficient that considers the partial exploitation of prestressing steel (the prestressing load is considered to be an external load, only the remaining part of the prestressing capacity can contribute to the tie resistance⁴⁸).

Model Code 2010 considers the influence of post-tensioned steel in the overall strength of the tie as:

$$F_t = A_s \cdot f_{yd} + A_p (f_{pd} - \sigma_{p0})$$

Where σ_{p0} is the initial prestressing force applied to the strands.

3.3.3. Nodes

While struts and ties are linear elements, nodes are bilinear elements, and can be generally made with different combination of elements: compression or tension concrete elements connected to tension ties, in a variable number (see Figure 3.6).

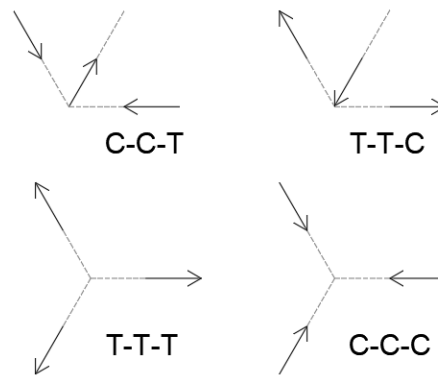


Figure 3.6: Different nodal configuration

In half-joints, the most likely configuration to find is C-C-T or C-T-T nodes (Figure 3.7), and more than three elements are usually joined.

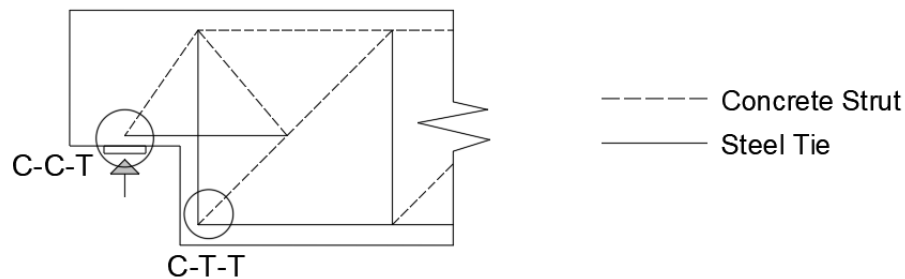


Figure 3.7: two nodal configurations

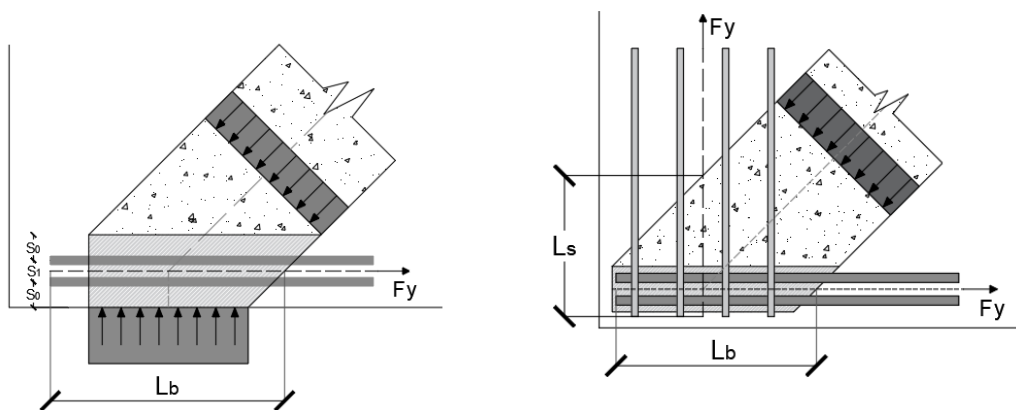


Figure 3.9: Typical C-C-T node

Figure 3.8: Typical C-T-T node

Codes agree in defining the reinforcement anchorage length L_b from the intersection between the resultant of tensile forces and the concrete strut (see Figure 3.9 and Figure 3.8).

Alike strut elements, nodes are the results of a huge simplification: in the model they are identified as the intersection between three linear elements, whereas they are curved three-

dimensions elements. In cases of wide elements composing the node, stresses can be distributed in a larger area (smeared), while in cases of concentrated stress fields nodes are concentrated (singular).

Two aspects of great importance are directly affected by nodes' geometry:

- a) The number of stirrups composing one steel tie,
- b) The anchorage of steel elements.

Moreover, compression resistance of nodes must be assessed, and equilibrium satisfied. Codes give different indications concerning the limit values for nodes' compression strength.

According to the Eurocode 2⁷⁴:

$$\begin{aligned} \sigma_{Rd} &= 0.85 \cdot v \cdot f_{cd} \\ \text{C-C-T node} \quad v &= 1 - f_{ck}/250 \end{aligned} \quad (3.13)$$

$$\begin{aligned} \sigma_{Rd} &= 0.75 \cdot v' \cdot f_{cd} \\ \text{C-T-T} \quad v' &= 1 - f_{ck}/250 \end{aligned} \quad (3.14)$$

According to Schlaich et al.⁴⁸:

$$\text{C-C-T node} \quad \sigma_{Rd} = 0.62 \cdot f_{ck} \quad (3.15)$$

According to ACI 318⁷²:

$$\text{C-C-T} \quad \sigma_{Rd} = 0.68 \cdot f'_c \quad (3.16)$$

$$\text{C-T-T} \quad \sigma_{Rd} = 0.51 \cdot f'_c \quad (3.17)$$

According to the Model Code 2010⁸¹:

$$\sigma_{Rd} = k_c \cdot f_{ck}/\gamma_c \quad (3.18)$$

Compression and tension node with
bars anchorage $k_c = 0.75 \left(\frac{30}{f_{ck}} \right)^{1/3} < 1.0$ (3. 19)

C-C-C nodes exhibit a higher strength, also according to the concrete behaviour described in Figure 3.5, therefore the analysis is on the safe side in case prestressing stresses are neglected.

Barton² tested nine C-T-T and ten C-T-T nodes, to verify the reliability of strut and tie models in simplifying the real geometry of nodes. Comparing test results to recommended values by Schlaich⁴⁸, Ramirez⁸² and Mitchell and Collins⁴⁴, he noticed a conservative trend in analytical estimation of the compression strength of the strut. However, several variables deeply affect the node resistance, and in the assessment phase of deteriorated elements.

In this thesis the node strength is calculated according to the Eurocode 2 indications.

3.4. MODEL DEVELOPMENT

This thesis aims at defining an appropriate model to assess existing joints. For this purpose, two half-joints schematizations have been considered, according to the Hoepli⁸³ guide. The choice was mainly guided by the possibility to consider all rebars configurations and a lower variability regarding the geometry of the trusses.

Both two trusses schematize the half-joint, each one providing a resisting mechanism. The overall resisting force will be equal to the sum of the two models resistance, and this choice will be validated in chapter 3.4.2: please note that all rebars nearby the nib belong to one model or to the other, and all the stress paths are not repeated more than once. This is the background that allows to split one single element in two models assuming each one independent from the other; nevertheless in the design procedure showed in the Hoepli manual the resistance of the joint is considered as the mean value of the two contributions, and in my opinion this strategy is under-estimating the total strength, also considering that ULS are investigated and that rebars are in plastic phase, the consideration of a mean value is not representative of the total resistance of the element.

The use of two trusses allows a good representation of most cases, since all the possible elements are considered: horizontal bars in the nib, diagonals and stirrups. On the other hand, prestressing strands that are often used in Gerber beams must be carefully treated, and in chapter 3.4.4 this aspect will be discussed and verified.

Vertical reinforcement in the nib is necessary for its shear resistance, but it has no influence in introducing shear stress from the reduced cross section to the remaining part of the beam; hence, the overall resistance is generally not affected by the presence of these type of rebars.

Now that all the elements composing the Gerber beam have been introduced, the two models are presented in their main characteristics.

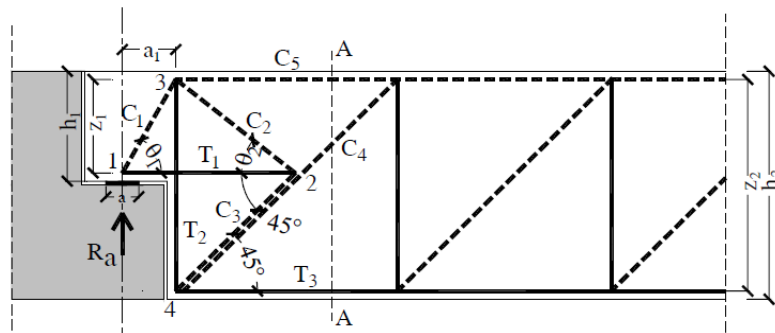


Figure 3.10: strut and tie model "a"

In model *a*, the horizontal bars in the nib and the first stirrups are considered and exploited, as shown in the truss of Figure 3.10. Node 4 geometry at failure of the truss defines the number of stirrups that can be considered in steel tie T_2 , and this will be part of discussion of chapter 3.4.3. In the following table the forces in the truss are reported as function of the force applied and geometry.

C_1	$R_a/\sin\theta_1$
C_2	$R_a/[\tan\theta_1 \cdot (\sin\theta_2 + \cos\theta_2)]$
C_3	$\sqrt{2} R_a/[\tan \theta_1 \cdot (1 + \cotan\theta_2)]$
C_4	$\sqrt{2} R_a$
T_1	$R_a/\tan\theta_1$
T_2	$R_a + R_a/[\tan\theta_1 \cdot (1 + \cotan\theta_2)]$

Table 3.1: stresses in the truss elements in function of the applied force R_a

While it is generally agreed that the inclination of the strut C_1 is function of the geometry of the beam (the tie T_2 is in the centroid of the steel rebars considered and the support coordinates are known), struts C_2 and C_4 can have different slopes depending on the model chosen. In this thesis it has been defined a 45° strut in the deep cross section and depending on it the angle of strut C_2 is found. In other strut and tie applications for half-joints⁹, the strut C_2 has the same slope of strut C_1 , and in function of it, the inclination of strut C_4 is defined.

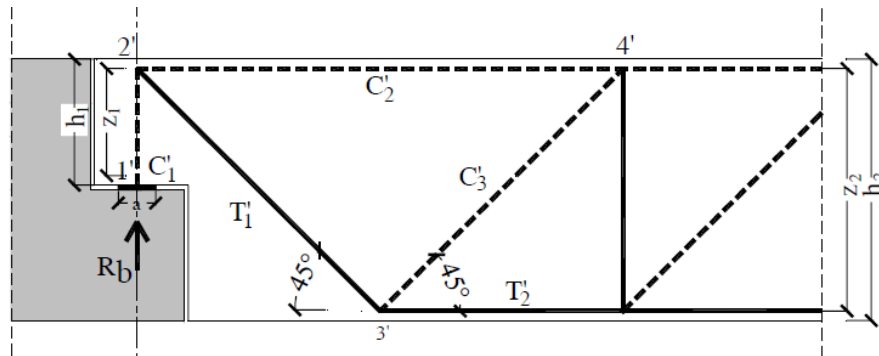


Figure 3.11: strut and tie model "b"

In model *b*, diagonal and longitudinal bars are considered and exploited. To better generalize reinforcement layout, the inclination of the diagonal rebar with the horizontal is of an angle θ , and not 45 degrees as shown in Figure 3.11.

C_1	R_b
C_2	$R_b/\tan\theta$
T_1	$R_b/\sin\theta$
T_2	$R_b/\tan\theta$

Table 3.2: stresses in the truss elements in function of the applied force R_b

This model has lower variability than the previous one, the only consideration is regarding the strut C_1 that has been assumed to have cross section equal to the bearing geometry.

The two models will be of interest in the D-region of the half-joint, in the incipient B-region the main assessment is regarding shear failure.

In each model the procedure is the following:

1. *Identify* the weakest steel element that first yields and its resistance R_i ;

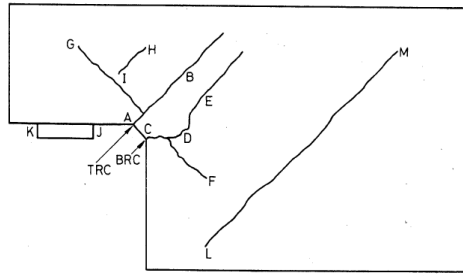


Figure 3.13: Clark and Thorogood upper bound

Desnerck, Lees and Morley tested reinforcement layout influence on half-joints ultimate resistance. They show by direct tests on three-directions reinforced half-joints, that horizontal re-bars carry 51.5 % of the failure load, while diagonal bar is carrying 48.5 %. Moreover, it is highlighted the direct relationship between horizontal and vertical bars, that behave independently from the diagonal bars. In fact, in the case the horizontal reinforcement in the nib is missing, the failure crack is almost vertical, and stirrups in the beam are not exploited. In the case the horizontal reinforcement is placed, the crack width increases but the first stirrups are contributing to the resistance of the joint. Among other achievements, this research highlights two aspects: first, diagonal reinforcement and horizontal reinforcement each contribute for the 50%, and secondly it confirms the subdivision of rebars in one model or the other: in fact when horizontal reinforcement is absent, vertical stirrups (that belong to the same strut and tie scheme) are not exploited.

3.4.2. Trusses superposition assessment

The two models must be independent from each other in the disturbed region. This is not a problem in the nearby of the nib, but an assessment could be necessary towards the B-Region: the first stirrup highlighted in Figure 3.14 could belong to both strut and tie models.

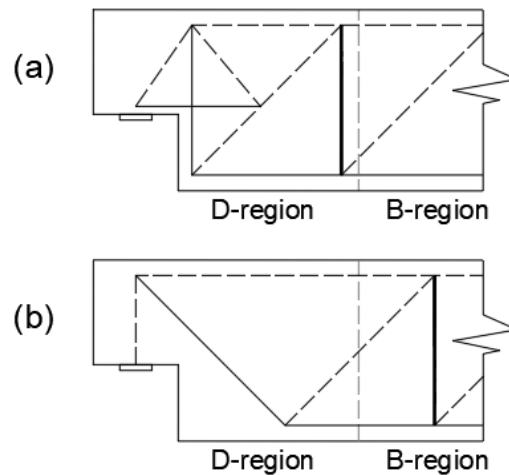


Figure 3.14: common stirrups assessment

Based on simple geometrical properties, it is possible to notice that the first stirrups of model *b* are not even in the disturbed region, but in the part of the beam whose only interest is in shear resistance. This means that no superposition of stirrups is happening in the disturbed region, and that consequently no steel elements are belonging to both models. Regarding struts elements, compression paths are repeated only once nearby the nib, and the only strut present in both models is the longitudinal compression strut, which must withstand to even higher loads, coming from flexural stress of the beam.

3.4.3. Stirrups concurring to a single tie

In model *a*, the first vertical tie is usually the critical element that defines the resistance of the truss and its evaluation is highly affecting the overall resistance. The geometry of the truss is a simplification of reality: more than one row of stirrups must be considered, but this evaluation is not immediate. According to the AASHTO review by Mitchell and Collins⁸⁴ of Figure 3.16, it is possible to define the geometry of diagonal concrete strut. It will give indications about the geometry of the node in Figure 3.15 and this will define the number of stirrups used.

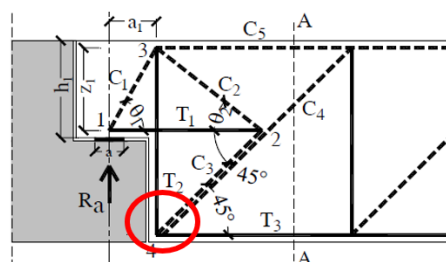


Figure 3.15: node under examination

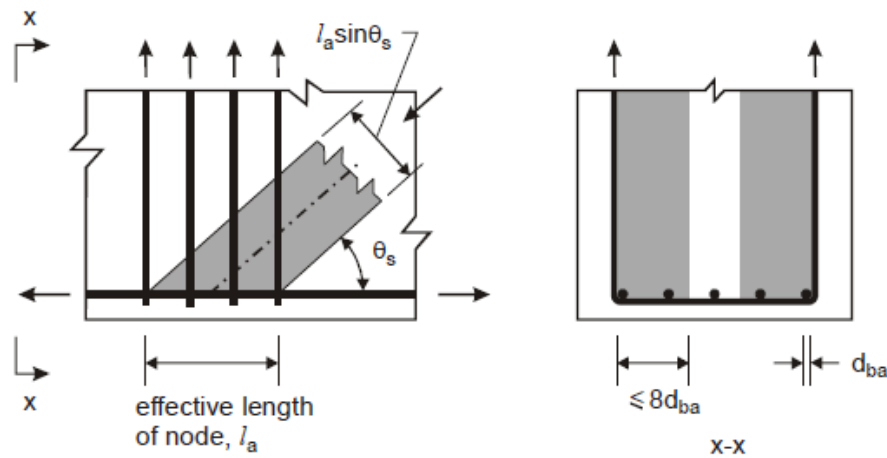


Figure 3.16: schematization of the geometry of the strut⁸⁴

The concrete struts C_3 and C_4 will define the geometry of the node 4.

An iterative procedure is necessary to define the right number of stirrups:

1. Assume the number of stirrups of T_2 tie;
2. Solve the truss and find the values of C_3 and C_4 struts;
3. Define a collaborative width of the strut equal to $6d$ on both arms of the stirrups;
4. Calculate the length l_a of the node, known the acting force and the width $6d$;
5. Check that all the stirrups hypothesised are distant l_a at maximum from the first stirrup nearby the nib.
6. If point 5 is verified, the number of stirrups hypothesised is equal or lower to the correct one, so the calculation is correct or on the safe side;
7. If point 5 is not verified, the number of elements is overestimated, and it must be reduced.

3.4.4. Prestressing aspect

The prestressing strands role has been limited to a reduction of the acting shear due to the inclination of the prestressing tendons. The inclination is usually very small (around 3° - 4°) so this contribution is rather limited.

With regards to the truss elements (highlight in Figure 3.17), prestressing strands have been considered able to carry part of the tension ties load, with a reduction factor that considers the partial exploitation of prestressing forces: prestressing steel is considered to be used in the strut and tie model as tie, with some limitations.

$$F_{tie,Rd} = f_{yd} \cdot A_{tie,r} + \alpha \cdot f_{pd} \cdot A_{tie,p}$$

The coefficient α is usually taken equal to 0.5, considering prestressing losses and the impossibility to check prestressing strands health, the exploitation of 50% of the maximum strength achievable is on the safe side.

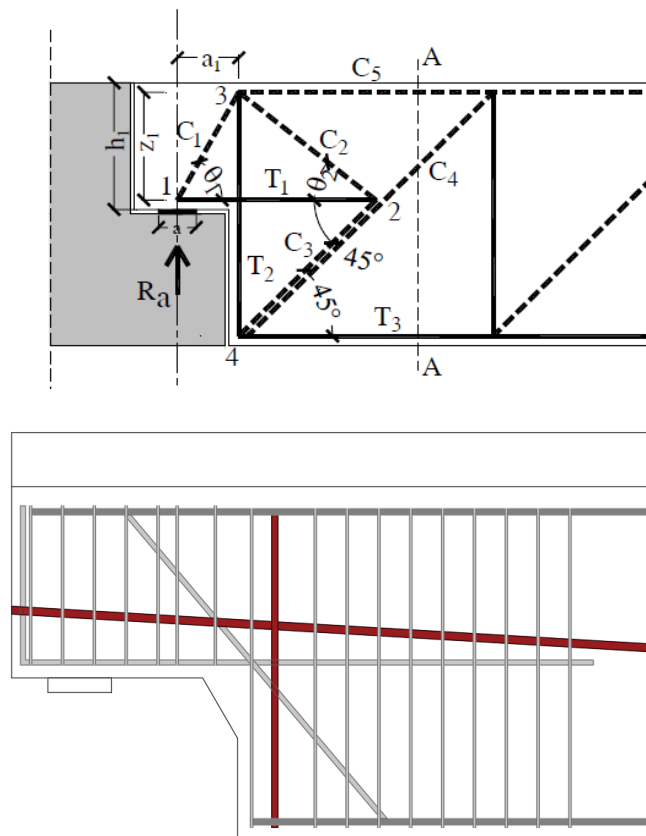


Figure 3.17: highlight on prestressing strands

Prestressing strands are usually longitudinal (with a limited inclination) but also vertical strands can be present. Both configurations influence model α , contributing to the horizontal and vertical steel ties (T_1 and T_2).

The contribution of compressive stress in struts' and nodes' strength is neglected, although it is of beneficial effect.

4. KINEMATIC METHOD: AN UPPER BOUND

Starting from an arbitrary mechanism, the corresponding equilibrium equation provides an upper bound solution. In the case of a half-joint, the most likely failure mechanism is a crack forming in the inner nib of the cross section, that develops with an inclination ϑ until it meets the neutral axis and the upper concrete strut, as shown in Figure 4.1.

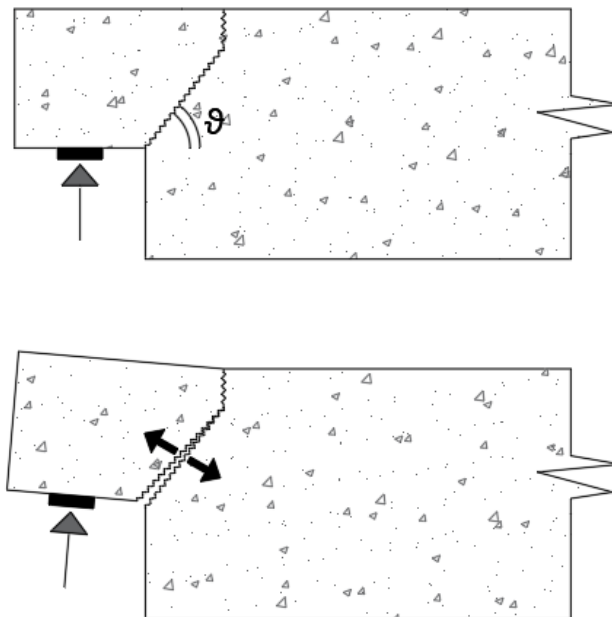


Figure 4.1: general fracture schematization

An initial value of ϑ is hypothesized, and in function of it all the steel elements crossing the crack are considered to fulfil the rotational equilibrium where the crack meets the neutral axis.

The crack is closed by several stirrups, longitudinal reinforcement and prestressing bars, that at the ultimate limit state are supposed to yield. With the hypothesis of yielding of all the crossing bars, the resisting moment is computed and it is further equalized to the acting moment due to

the vertical load multiplied to the lever arm that is the distance between the bearing and the crack tip (point A of Figure 4.2).

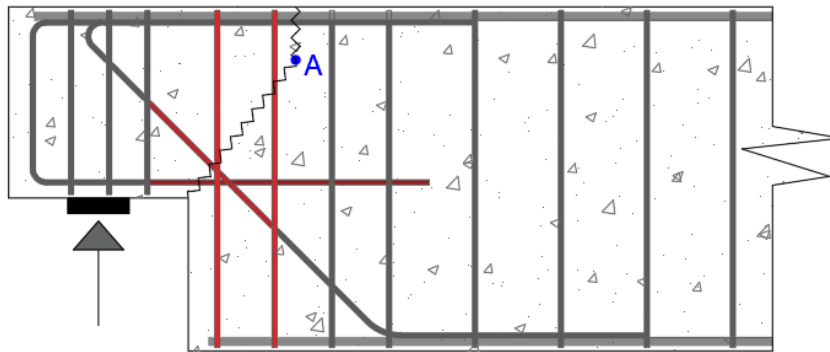


Figure 4.2: rebars contributing to the crack closure

All this procedure is repeated for several values of ϑ and in function of it the minimum (and critical) resistance is identified.

This model has been widely used in the past^{1,51} and even though it is not on the safe side, it usually is more accurate than the lower bound model⁸⁵.

4.1. UPPER BOUND MODEL LIMITS

There are aspects that affect this model and that makes it non reliable, for which a lower bound model should be preferred.

The crack position is hypothesised, it could be in the cross section beyond the nib, its slope is not only affected by the minimum resisting force but it is also a function of the reinforcement layout: in the case of no horizontal reinforcement in the nib it has been experimentally noticed that the crack has almost vertical development⁸.

Precast dapped end beams are often with inverted T shape, so a cast in situ concrete slab is required: performing a mechanism analysis, the reinforcements' lever arm is bigger and so it is the resisting moment. This consideration relies on the assumption of perfect interaction of the two concrete elements (this aspect is usually considered with the presence of steel elements protruding from the precast beam, that are embedded in the cast in situ concrete), nevertheless, relative slip between the two elements is usually not avoided. On the contrary, the lower limit is only depending on the steel reinforcement in the precast beam and is not varying in the

analysis with or without the slab: the positive contribution of the slab is not considered, and the result becomes even more conservative.

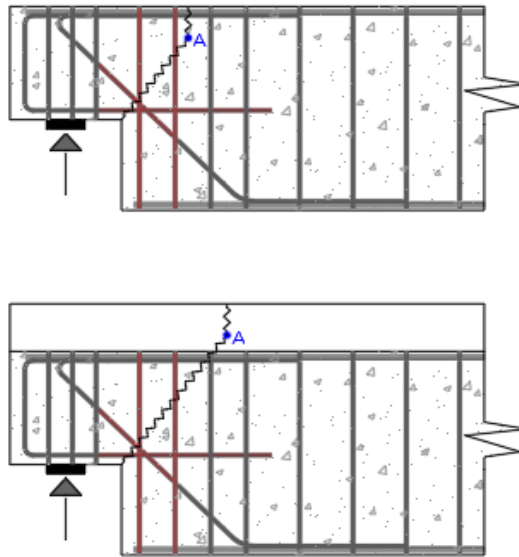


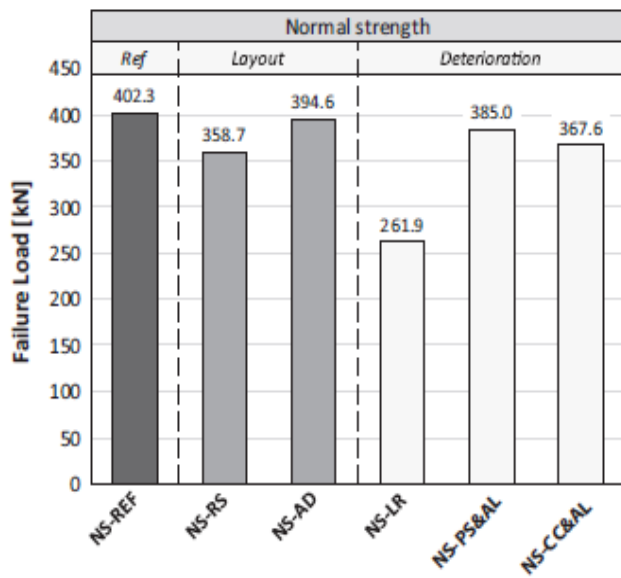
Figure 4.3: slab influence on crack development

Regarding the reliability of data, the lever arm of action of each rebar can be estimated from design indication, that are likely to change in construction phase, and a difference of millimetres can be of impact (maximum length of lever arms of a 90 cm high beam is around 30 cm).

At last, the upper bound is very accurate in defining the limit load of an undisturbed element, whereas it has been proved that the strength of a half-joint subjected to environmental actions can be significantly lower. Desnerck, Lees and Morley⁷ tested half-joints reporting the most likely degradation processes: inner nib reinforcement corrosion and longitudinal rebars corrosion that leads to concrete spalling. In the first case (NS-LR) the corrosion process can be simulated with a diameter reduction of 50% of all the elements (it has been noticed in UK inspections a bar reduction as high as 30-50%⁷⁷) that cause a strength reduction of 35%, while in the second case two different strategies were followed, so the introduction of a thin plastic sheet on top of the longitudinal reinforcement (NS-PS&AL) and concrete cylinders (NS-CC&AL) casted around the anchorage to have a more localized effect. Both specimens showed a strength reduction of maximum 10%, comparing to the reference specimen (NS-REF).

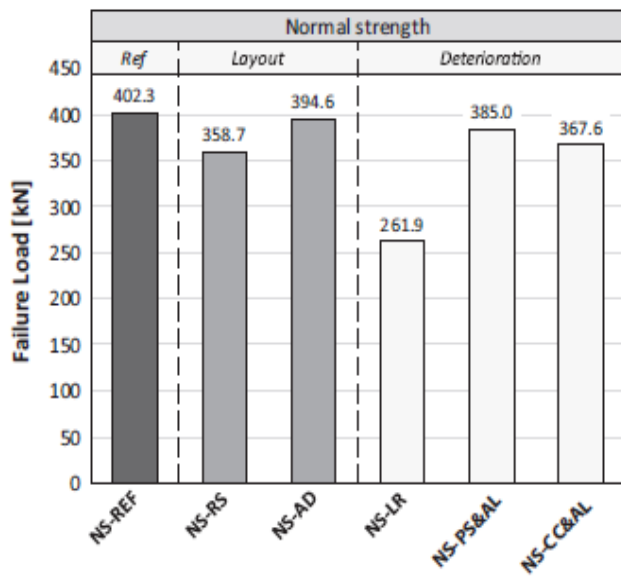
In

NS	Normal Strength
----	-----------------



REF	Reference
RS	Reduced stirrups
AD	Reduced anchorage diagonal
LR	Local reduction
PS&AL	Plastic Sheet
CC&AL	Concrete cylinders

Figure 4.4 the test campaign of Desnerck, Lees and Morley is summarized: several degradation mechanisms are reproduced and the effects on the ultimate resistance are displayed.



NS	Normal Strength
REF	Reference
RS	Reduced stirrups
AD	Reduced anchorage diagonal
LR	Local reduction
PS&AL	Plastic Sheet
CC&AL	Concrete cylinders

Figure 4.4: results of experimental studies carried out by Desnerck et al.⁸

The high sensitivity of the upper bound model to all these factors highlight its non-reliability, since all the reported cases can also happen simultaneously.

5. ANALYTICAL MODEL APPLICATION

This chapter deals with the application of the analytical models to five examples from a database of Gerber beams from existing bridges in the Netherlands, which were originally assessed with an upper-bound method, and for which the shear load acting on the joint is known. All Dutch half-joints are longitudinally prestressed and two of them are also vertically prestressed, reinforcement layouts are various, to have the maximum generalization possible.

A laboratory test carried out by Desnerck et al.¹⁰ which have tested half-joints under normal and deteriorated conditions is also analysed and verified. It is characterised by rebars in the three directions, no prestressing strands and no simulation of deterioration mechanisms (NS-REF), and it is analysed with the purpose of comparing the test results to the numerical analysis results. Moreover, the authors of the research have performed a strut and tie pre-analysis of half-joints with various reinforcement layouts, some of which can be assumed to be complying to the two strut and tie models this thesis is dealing with. This analysis is in paragraph 5.2.

All information regarding geometry, materials and models are in Appendix A.

Material coefficients are applied to concrete and prestressing steel characteristic strengths.

	γ_M	f_d
Concrete	1.5	$f_{cd} = f_{ck}/1.5$
Prestressing steel	$\frac{0.9}{1.1}$	$f_{pd} = f_{pu} \cdot 0.9/1.1$

Concerning the lower bound of strength, each joint reported is schematized according to the reinforcement layout used in the strut and tie truss models of Figure 5.1: orthogonal reinforcement of model *a* and diagonal reinforcement for model *b*. Furthermore, the diagonal strut crossing D- and B- region is showed (C_4 in model *a* and C_3 in model *b*), to show the non-overlapping of the stirrups of the two models in the D-region.

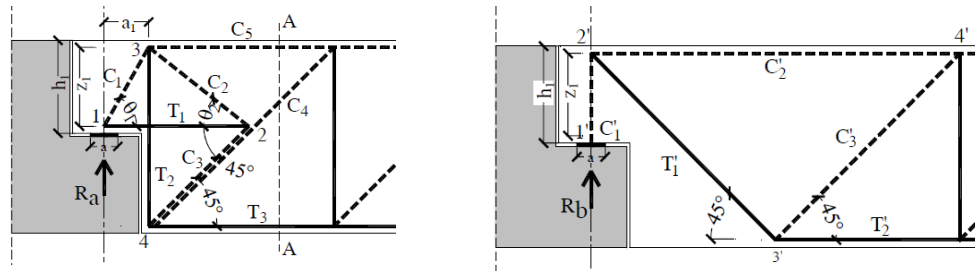


Figure 5.1: strut and tie models a and b

Struts and nodes resistance is assumed according to the Eurocode 2⁷⁴:

	Typical configuration considered	Ultimate resistance
Nodes	C-T-T	$\sigma_{Rd} = 0.75 \cdot v' \cdot f_{cd}$ $v' = 1 - f_{ck}/250$
Struts	With transverse tension	$\sigma_{Rd} = 0.6 \cdot v' \cdot f_{cd}$ $v' = 1 - f_{ck}/250$

Also an upper bound analysis is performed, according to chapter 4 procedures, in order to have an expected range of resistance of each joint. It has been assumed an efficiency coefficient for prestressing cables of 55%, to be applied in the kinematic model.

$$F_p = 0.55 \cdot A_p \cdot f_{pd}$$

5.1. DUTCH BRIDGE PRACTICE: ANALYSIS OF SELECTED EXISTING JOINTS

The Netherlands has the typical landscape that can take maximum advantage from the use of Gerber beams. The flat lands that characterize this country necessitate for bridges and viaducts mainly with the purpose of crossing canals or other roads, therefore costs and construction time can be maximised with a smart design strategy. Since natural embankments are usually missing, artificial embankments are necessary, and their cost impact on construction and material is nearly 50% of the overall. Gerber beams have been often used because they allow a reduction of the overall height of the structure, so a reduction of the embankment volume, and their pre-fabrication was easily introduced in a country where industrial production of structural elements is nearly 90%. Five selected half-joints are investigated and tested with the upper and lower bound models, the scope is to test the models' adaptability and to verify the reliability of the results obtained.

5.1.1. Beam 3

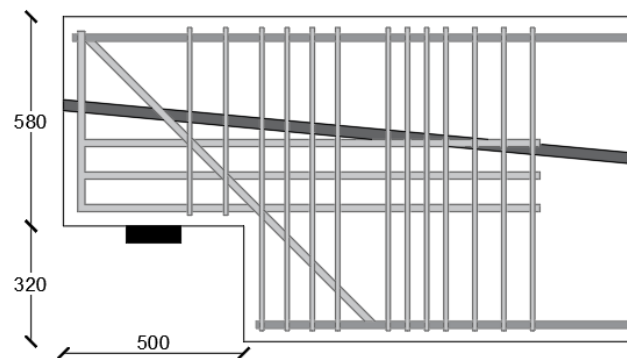


Figure 5.2: Beam 3 half-joint detail

The presented joint is stiff, without a significant height reduction in the dapped end. The beam is longitudinally prestressed, with regular stirrups and horizontal rebars in the nib. Reinforcement information provided are only about the disturbed region, the beam is expected to have enough vertical reinforcement in the deep cross section to bear shear forces. Here are reported the two trusses used as model *a* and model *b*, reinforcement geometry and rebars type, and the resistance computed for each model. The beam shape is box beam, so a cast-in-situ slab is not necessary, and the bridge construction year is 1989.

	Class	Characteristic strength [MPa]	Design Strength [MPa]
Concrete	C 55/67	55	36.67
Steel	FeB500	435	435
Prestressing steel	FeP1860	1860	1522

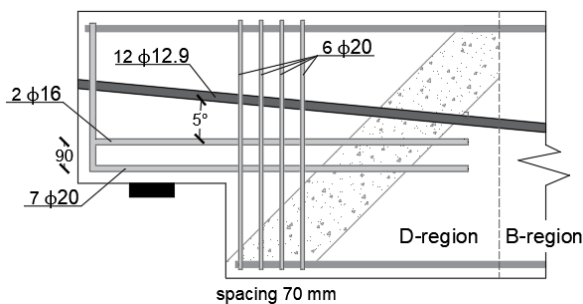


Figure 5.3: beam 3, model a

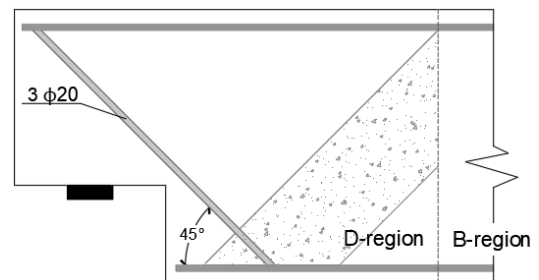


Figure 5.4: beam 3, model b

	Model <i>a</i>	Model <i>b</i>
Failure mode	Concrete crushing	Reinforcement yielding
Failing element	C ₁	T ₁
Failure Load	900 kN	317 kN

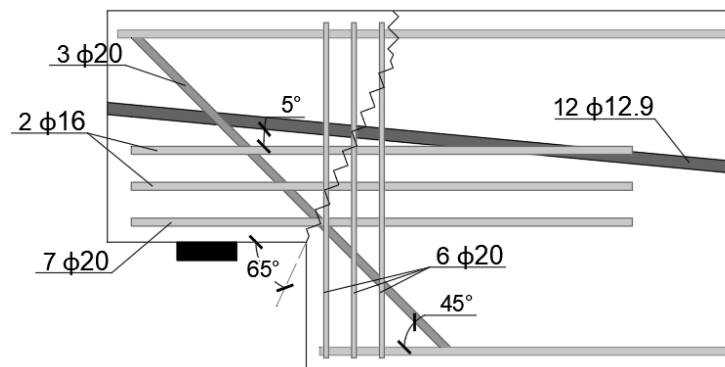


Figure 5.5: Beam 3 kinematic model

Acting Load assumed	980 kN
Upper bound resistance	2786 kN
Lower bound resistance	$R_a + R_b = 900 + 317 = 1216 \text{ kN}$
Prestressing contribution	135.4 kN
Unity check	$\frac{980 - 135.4}{1216} = 0.695$

From this lower bound analysis, the beam appears strong enough to bear the acting load assumed, also considering the prestressing strands contribution in reducing vertical actions.

Model *a* failure mode is caused by the concrete strut C₁ crushing: it is the diagonal strut connecting the steel bearing to the node between upper longitudinal reinforcement and vertical stirrups. This type of failure must be avoided since it is brittle and dangerous, in fact a good reinforcement design should prefer rebars yielding (more ductile) to concrete crushing.

5.1.2. Beam 5

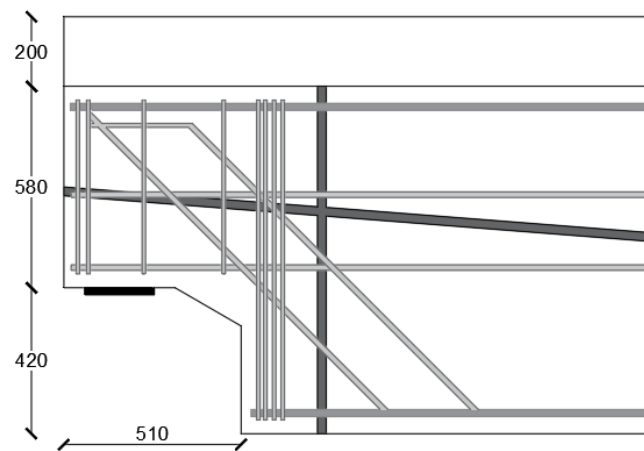


Figure 5.6: beam 5, half-joint detail

This bridge was built in 1968, and the joint has a more complex configuration, with double diagonal reinforcement, several close stirrups in the deep cross section and both vertical and horizontal prestressing. Moreover, the beam has inverted T shape, so a cast-in-situ concrete slab must be applied. The lower bound analysis is not influenced by the slab presence, on the contrary of the kinematic model which produces higher values when a concrete layer on top is considered. Last point to highlight, it has been noticed that the nib geometry of this beam is more useful to prevent and delay crack formation, so it is preferred to the 90° nib geometry.

	Class	Characteristic strength [MPa]	Design Strength [MPa]
Concrete	C 55/67	55	36.67
Steel	QR40	330	330
Prestressing steel	QP105	1030	843

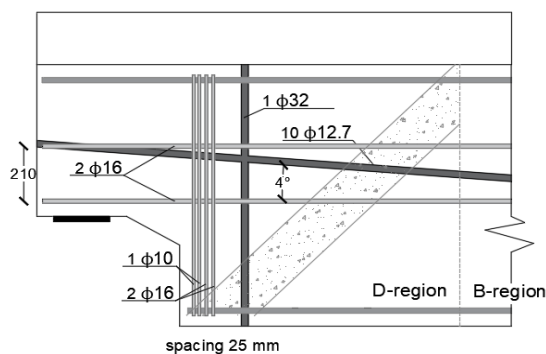


Figure 5.7: beam 5, model a

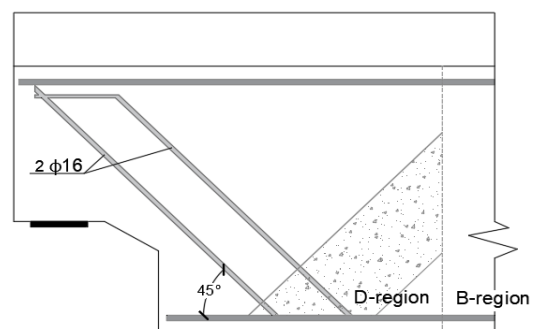


Figure 5.8: beam 5, model b

	Model <i>a</i>	Model <i>b</i>
Failure mode	Reinforcement yielding	Reinforcement yielding
Failing element	T ₂	T ₁
Failure Load	456 kN	188 kN

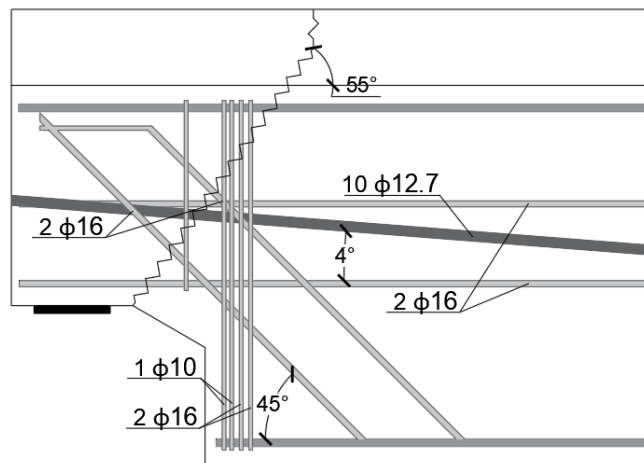


Figure 5.9: Beam 5 kinematic model

Acting Load assumed	693.3 kN
Upper bound resistance	789 kN
Lower bound resistance	$R_a + R_b = 456 + 188 = 643.3 \text{ kN}$
Prestressing contribution	52.2 kN
Unity check	$\frac{693.3 - 52.2}{643.3} = 0.99$

This beam too is expected to bear the acting load supposed. This joint (and all the furthers) has a ductile collapse due to steel yielding in both models, and this is the best failure mode.

5.1.3. Beam 14

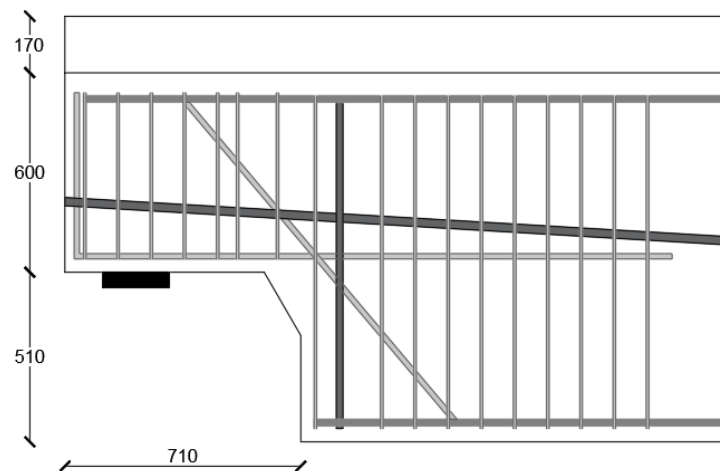


Figure 5.10: Beam 14, half-joint detail

Joint 14 is vertically and longitudinally prestressed, with diagonal, horizontal and vertical steel reinforcement. Although it may look extremely reinforced, it is actually rather weak: vertical rebars in the nib are not considered to be influencing the joint strength and vertical stirrups in the deep cross section are rather weak. Therefore, vertical prestressing has a principal role in the perpendicular model resistance. The bridge was built in 1973.

	Class	Characteristic strength [MPa]	Design Strength [MPa]
Concrete	C 55/67	55	36.67
Steel	QR40	330	330
Prestressing steel	QP190	1864	1525

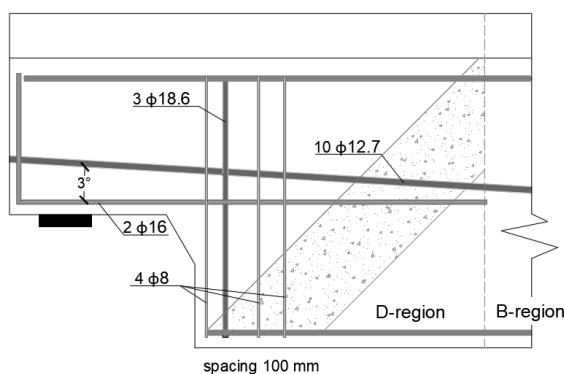


Figure 5.11: Beam 14, model a

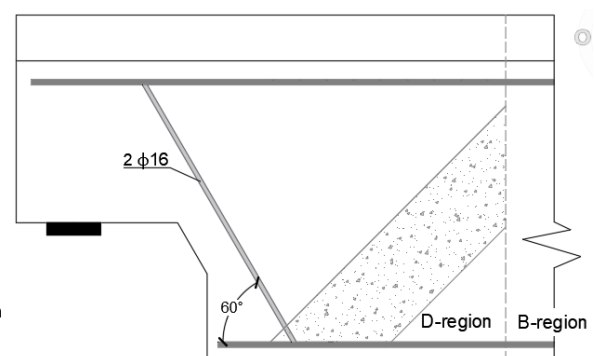


Figure 5.12: beam 14, model b

	Model <i>a</i>	Model <i>b</i>
Failure mode	Reinforcement yielding	Reinforcement yielding
Failing element	T ₂	T ₁
Failure Load	509 kN	115 kN

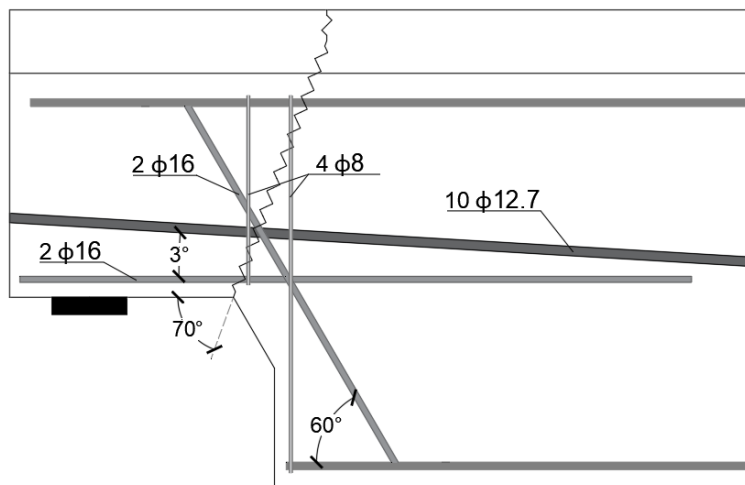


Figure 5.13: Beam 14 kinematic model

Acting Load assumed	1001 kN
Upper bound resistance	920 kN
Lower bound resistance	$R_a + R_b = 509 + 115 = 624 \text{ kN}$
Prestressing contribution	84.4
Unity check	$\frac{1001 - 84.4}{624} = 1.47$

This joint appears not to fulfil resistance requirements, moreover the upper bound analysis shows an ultimate resistance lower than the supposed acting load. Therefore, more accurate investigations are required, to further investigate the results achieved in this preliminary phase.

5.1.4. Beam 27

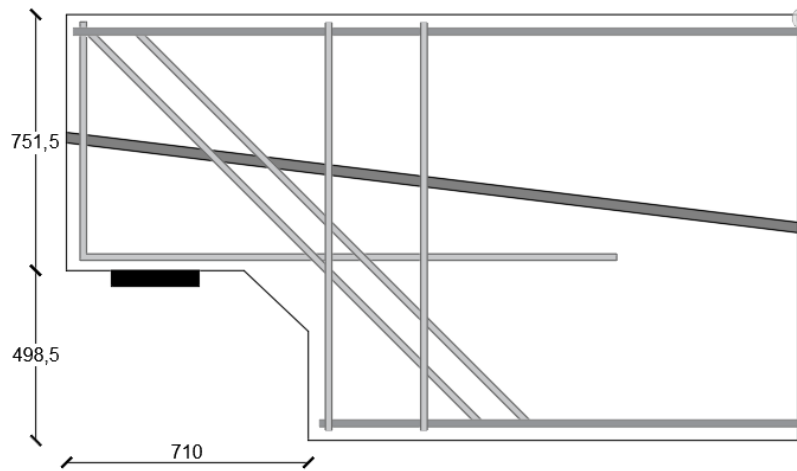


Figure 5.14: Beam 27, half-joint detail

Opposite to beam 14 reinforcement layout, beam 27 shows a simplified rebars configuration, with bigger reinforcement diameter and larger prestressing inclination. The present beam is a box beam, so no concrete slab is necessary.

	Class	Characteristic strength [MPa]	Design Strength [MPa]
Concrete	C 55/67	55	36.67
Steel	QR40	330	435
Prestressing steel	QP170	1670	1366

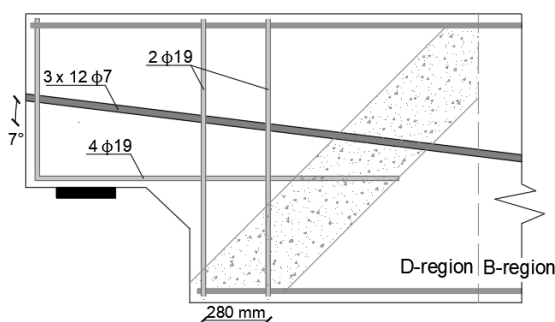


Figure 5.15: beam 27, model a

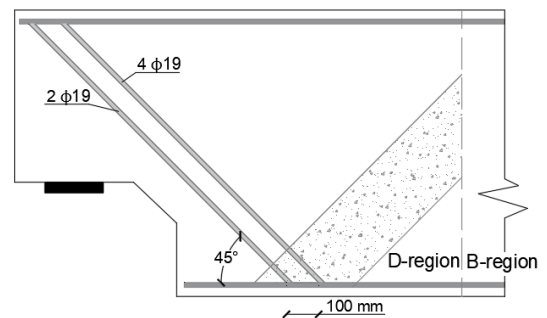


Figure 5.16: beam 27, model b

	Model a	Model b
Failure mode	Reinforcement yielding	Reinforcement yielding
Failing element	T_2	T_1
Failure Load	124 kN	610 kN

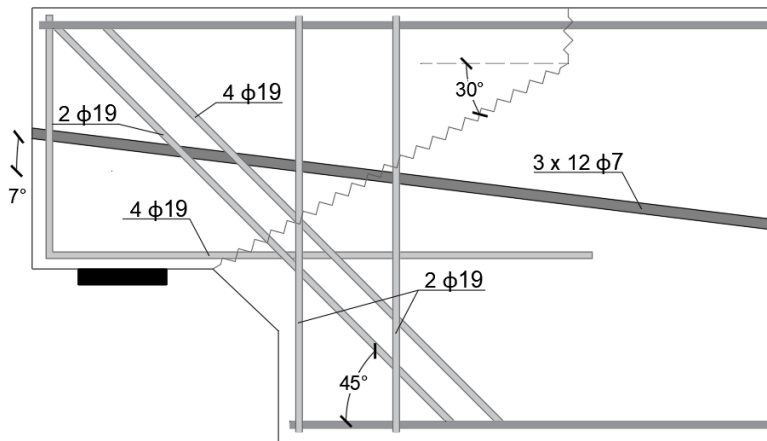


Figure 5.17: Beam 27 kinematic model

Acting Load assumed	946.9 kN
Upper bound resistance	1048 kN
Lower bound resistance	$R_a + R_b = 124 + 610 = 734 \text{ kN}$
Prestressing contribution	116.3 kN
Unity check	$\frac{946.9 - 116.3}{734} = 1.13$

Also beam 27 appears not to fulfil strength requirements, and in modern design requirements are usually present ductility requirements that underline the necessity of smaller reinforcement rebars in a larger number. It is true that in 1963 when the bridge was built those recommendations were not available yet.

5.1.5. Beam 30

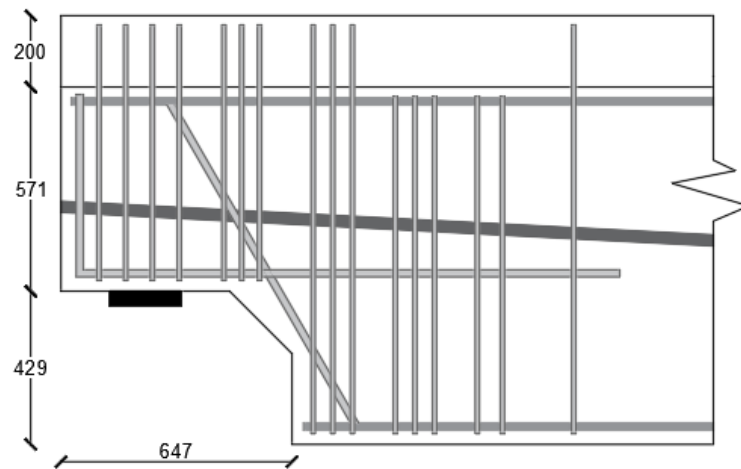


Figure 5.18: Beam 30, half-joint detail

This bridge was built in 1979, and the beams are longitudinally prestressed with an inverted T shape. A cast in situ slab is necessary, and some of the vertical reinforcement in the nib and in the deep cross section is protruding from the precast element to ensure a good stress interaction between the two different concrete layers. This aspect is not considered when dealing with the lower and upper bound analyses.

	Class	Characteristic strength [MPa]	Design Strength [MPa]
Concrete	C 55/67	55	36.67
Steel	QR40	330	330
Prestressing steel	FeP1860	1860	1522

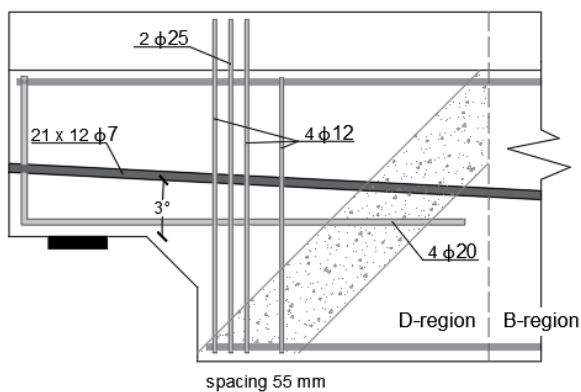


Figure 5.19: beam 30, model a

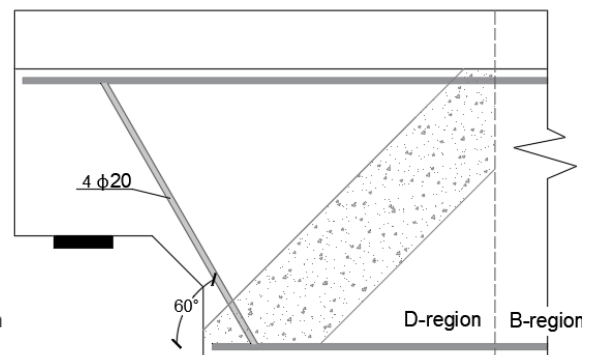


Figure 5.20: beam 30, model b

	Model α	Model b
Failure mode	Reinforcement yielding	Reinforcement yielding
Failing element	T_2	T_1
Failure Load	861 kN	473 kN

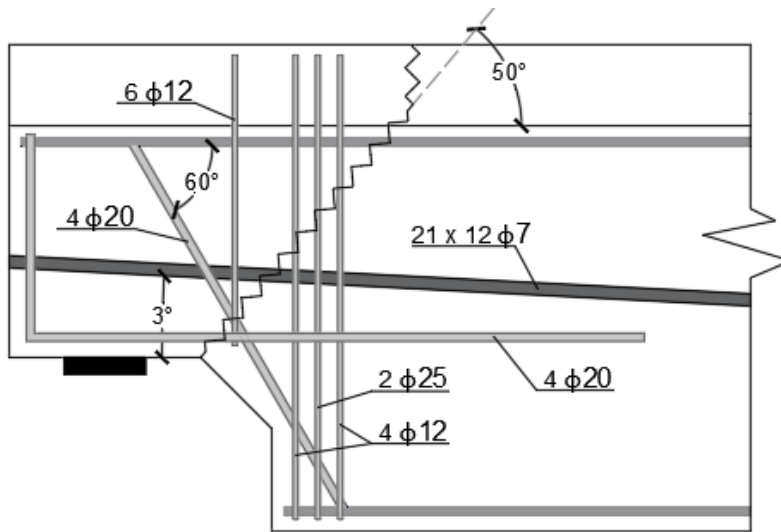


Figure 5.21: Beam 30 kinematic model

Acting Load assumed	823 kN
Upper bound resistance	2369 kN
Lower bound resistance	$R_a + R_b = 861 + 473 = 1334 \text{ kN}$
Prestressing contribution	77.4 kN
Unity check	$\frac{823 - 77.4}{1334} = 0.56$

This last case is strongly verified, with a low unity check and both lower and upper bound showing a high resistance of the beam.

5.2. LABORATORY TEST CARRIED OUT BY DESNERCK ET AL.

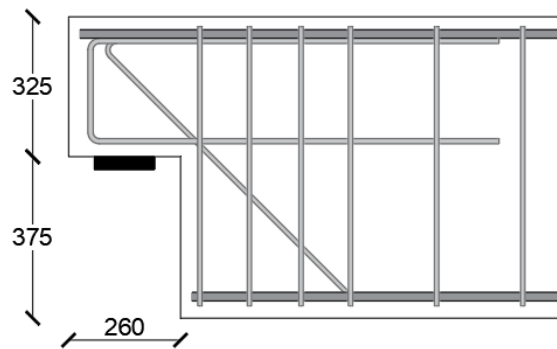


Figure 5.22: Test half-joint

Desnerck, Morley and Lees performed several tests on half-joints in various reinforcement configurations, carrying on a lower bound of strength analysis on each of them. Two reinforcement layouts can be referred to the model *a* and model *b* trusses. In fact, the first is with no diagonal reinforcement (NS-ND of Figure 5.24), and the second is with the horizontal rebar omitted (NS-NU of Figure 5.23).

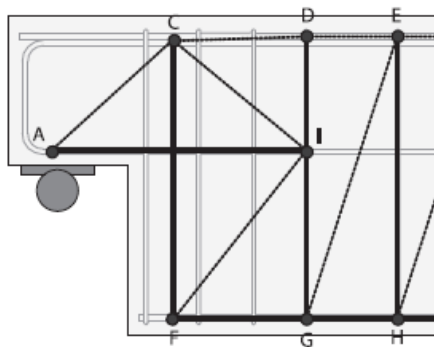


Figure 5.24: strut and tie model for NS-ND test

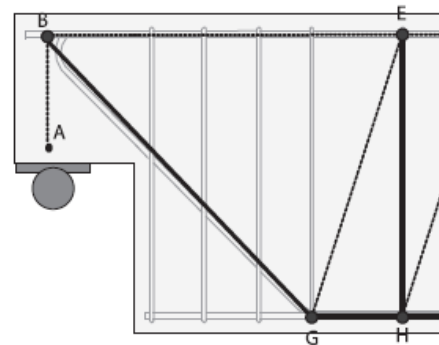


Figure 5.23: strut and tie model for NS-NU test

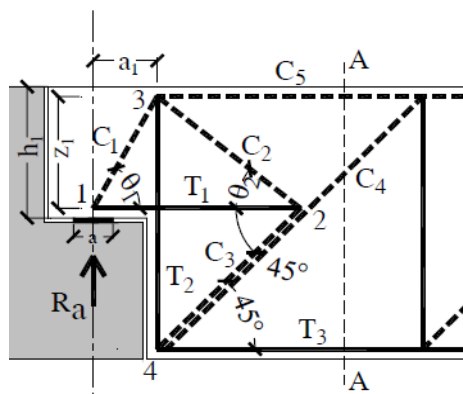


Figure 5.26: model *a*

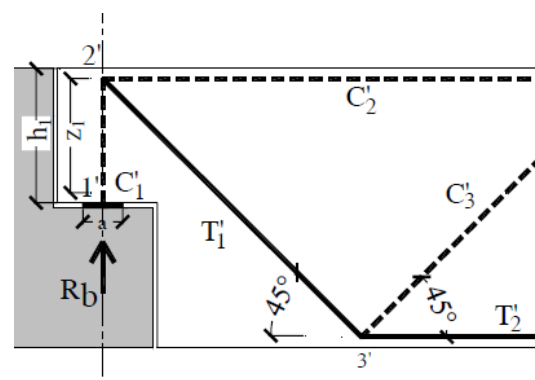


Figure 5.25: model *b*

It is noticeable the similarity between the two reinforcement layouts (and relative strut and tie trusses) used by Desnerck et al. and the two models used in this thesis: NS-ND associated to model *a* and NS-NU to model *b*. Therefore, a direct comparison of the ultimate strength calculated in two different ways will be highlighted. While NS-NU strut and tie model is very similar to model *b*, NS-ND considers the same rebars of model *a*, but the truss model is slightly different: struts connecting the bearing and the first stirrups are symmetrical, while in the model there is more freedom left in defining the shape of the truss. Moreover, NS-ND and NS-NU models are not possible to be superposed, since there are stirrups concurring at both trusses.

A reference reinforcement layout (NS-REF of Figure 5.22), with reinforcement in the three directions is the third laboratory test analysed by the group of researchers: to perform a lower bound analysis of it, a third truss model has been used, with all rebars present. This truss is reported in Figure 5.27 and represents one of the alternative approaches to the present thesis method.

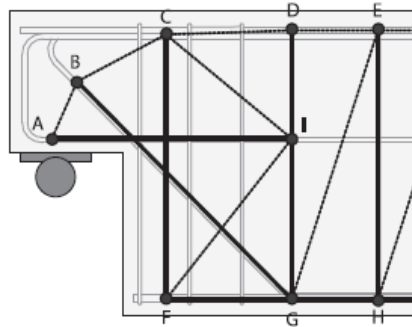


Figure 5.27: Strut and tie model for NS-REF test

Test materials are fulfilling Eurocode requirements in order to be classified as in the following table. All load and safety factors are set to unity, according to Desnerck et al. indications.

	Class	Characteristic strength [MPa]
Concrete	C 30/37	30

	f_y	f_u
Steel ϕ 10	539	596
Steel ϕ 12	529	559
Steel ϕ 25	578	674

Steel constitutive law is assumed to be elastic perfectly plastic, with a constant ultimate strength equal to the yielding stress.

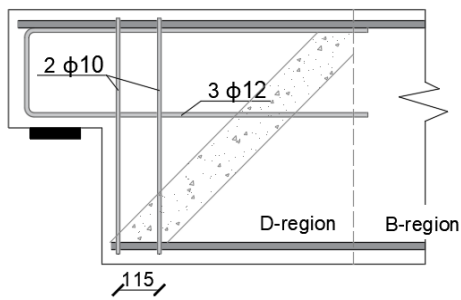


Figure 5.29: Test half-joint, model a

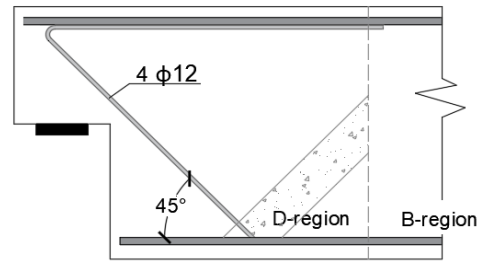


Figure 5.28: Test half-joint, model b

	Model a	Model b
Failure mode	Reinforcement yielding	Reinforcement yielding
Failing element	T ₂	T ₁
Failure Load	124 kN	183 kN
Reference failure load (NS-ND, NS-NU)	149 kN	207 kN

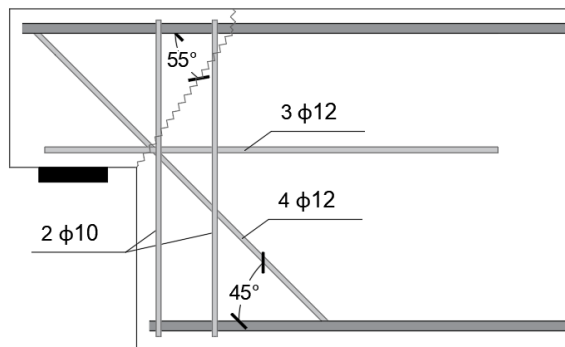


Figure 5.30: Desnerck et al. laboratory test kinematic model

Ultimate resistance NS-REF	337 kN
Upper bound resistance	402 kN
Lower bound resistance	$R_a + R_b = 124 + 183 = 307 \text{ kN}$
Prestressing contribution	0 kN
Unity check	$\frac{337}{307} = 1.1$

Desnerck, Lees and Morley results seem to slightly overestimate the resistance of the joint, when compared to the model results. However, the assumption of summing the two trusses of model *a* and model *b* provides reasonable results when compared to the NS-REF ultimate resistance: the model output is 10% more conservative, but a certain variability in angles and geometries must be considered.

5.3. CONCLUSIONS

The proposed model has been applied to several half-joints. As expected, the possible reinforcement layouts are various, and the model could adapt to all of them, characterized by longitudinal and vertical prestressing strands, vertical, horizontal and diagonal reinforcement. Model *a* and model *b* have been identified in all half-joints, and in all analysed cases except for the beam 3 half-joint, failure of the joint is consequent to rebars yielding.

Considerations relative to the possible superposition of the two models have been confirmed, since each model is applied in the D-region, but it is extended to the B-region, as highlighted by the geometry of each half-joint analysed.

Prestressing strands have been confirmed to provide an important influence on the ultimate resistance of the joint, both in reducing the acting shear force on the joint and in contributing to the ties' resistance in the model *a* trusses.

Based on all information provided by the Dutch database on the load acting on each beam, the application of the strut and tie models is providing conservative results, as expected from a lower bound. In almost all cases, the unity check is close to the unit (or slightly higher) and the upper bound analysis provides coherent results, showing an ultimate resistance higher than the load applied. Beam 14 (par. 5.1.3) is an exception for both models, in fact has a rather high unity check ($\frac{V_{Ed}-V_p}{V_{Rd}} = 1.47$) and the kinematic method provides ultimate values lower than the load applied ($V_{UB} = 922 \text{ kN}$; $V_{Ed} = 1001 \text{ kN}$). This case will be further analysed with the software ATENA to have a better understanding of the obtained results.

The strut and tie model is also applied to a laboratory test carried out by Desnerck et al.¹⁰, which had been analysed with a strut and tie truss that considers all reinforcement rebars in the three directions. The lower bound analysis obtained by the proposed method gives conservative

results when compared to the lower bound proposed by the researchers, but the difference is lower than 10%.

In the next chapter the analytical model will be confirmed by a non-linear numerical analysis, carried out by the software ATENA 2D. The laboratory test will be of fundamental importance to validate the numerical model, through a direct comparison between load-displacement curves obtained by numerical and laboratory analyses. The ATENA model will then be used to analyse the strut and tie model and kinematic model results of beam 14.

6. NUMERICAL ANALYSIS

6.1. INTRODUCTION TO ATENA 2D

The software ATENA 2D is mainly used for non-linear analysis of reinforced and prestressed concrete structures, based on the finite elements method. It provides semi-defined parameters based on the Model Code 2010, but it is also possible to set material's characteristics, bond parameters, load cases, creep, concrete degradation and concrete behaviour under loading. Solution parameters are defined to achieve a solution and to show information about the structure response to the applied load, by means of crack patterns and deformed shape (also magnified displacements). Cracks formation does not interfere with the achievement of a solution.

ATENA 2D is divided in pre-processing and post-processing interfaces, so that the user can have direct contact to all the stages of the process: modify the input parameters and geometry, monitor and visualize all necessary information provided by the analysis.

In the pre-processing stage, all necessary information regarding the structure to be analysed and the analysis characteristics are set:

- Structures' geometry is defined with three elements: joints, lines and macro-elements;
- Reinforcement can be singular or smeared in a certain length, defining bonding characteristics between steel and concrete. It is also possible to set corrosion stages and tension stiffening mechanism;
- Materials' formulation is articulated following strong theoretical fundamentals, detailed in ATENA Program Documentation Part 1 – Theory⁸⁶. Materials' non-linear constitutive law is based on fracture mechanics theory (tensile behaviour) and plasticity theory (compressive behaviour): Rankine failure criterion and Menétrey-Willam failure surface

are combined by means of a developed algorithm. Concrete laws are in Figure 6.1 and Figure 6.2;

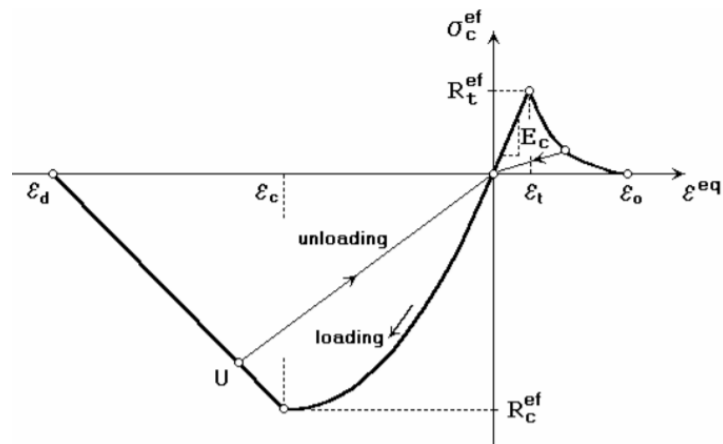


Figure 6.1: Concrete uniaxial constitutive law

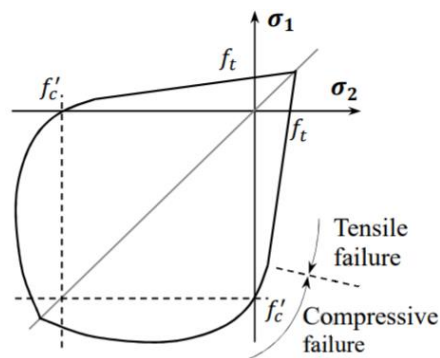


Figure 6.2: Concrete biaxial tension-compression law⁸⁷

- Load cases is a category representing applied loads, applied constant displacements, body forces, imposed thermal variations, supporting reactions, shrinkage and prestressing forces;
- Monitoring points are necessary to elaborate Load/displacement curves and collect every type of information regarding forces development, displacements, strain, stresses, body temperature or slip. They can be placed in nodes or they can integrate information on a surface;
- Mesh is defining the dimensions of the subdivisions of each macro-element and it is automatically produced. It mainly affects the solution accuracy, the process time and the storage required.

ATENA 2D allows to achieve a solution assuming the concrete behaviour in crack propagation: the fixed crack model coefficient rules the residual tensile stress level at which the developing crack direction gets fixed⁸⁶. This coefficient can vary between 0 and 1, and the extreme values define two scenarios:

- Crack coefficient equal to 0 (cc0), the system is a rotated crack model (Figure 6.3) and the direction of the crack changes always with the direction of principal stresses; shear is never present in the crack face.

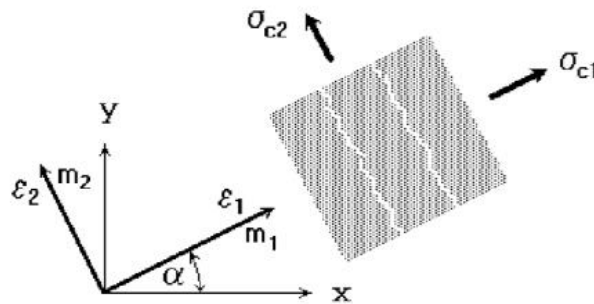


Figure 6.3: Rotated crack model, stress and strain state^{55,88}

- Crack coefficient equal to 1 (cc1), the system is a fixed crack model (Figure 6.4) and the direction of the crack is constant and equal to the one given at crack initiation; shear is present during crack development.

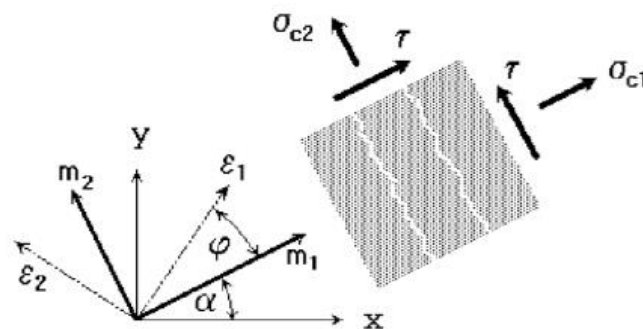


Figure 6.4: Fixed crack model, stress and strain state^{89,90}

The analysis is performed when solution parameters and analysis steps are defined. There are two possible solution methods: Arc-length and Newton-Raphson. Arc-length is widely used in post-peak investigations, providing robust results also when the Newton-Raphson method cannot reach convergence, in fact it fixes loading and displacement conditions at the end of each

step, and allows to study stability problems and non-linear materials with non-smooth or discontinuous stress-strain relationship.

In the current case a non-linear analysis can be performed with the Newton Raphson method, displacement load controlled. The full Newton-Raphson method is based on congruence, equilibrium and constitutive equations, and in the final iterative procedure it appears as follows:

$$K(\bar{p})\Delta\bar{p} = \bar{q} - f(\bar{p}) \quad (6.1)$$

where:

- \bar{q} is the vector of applied joint loads;
- $f(\bar{p})$ is the vector of internal joint forces;
- $\Delta\bar{p}$ is the deformation increment consequent to the load increment;
- \bar{p} are the deformation of the structure prior to load increment;
- $K(\bar{p})$ is the stiffness matrix.

The Newton-Raphson equation is non-linear because of non-linear properties of internal forces, and the non-linearity is proper of the stiffness matrix too. It is less time demanding than the Arc-length method, even though in each iteration it requires the stiffness matrix to be calculated, since it is deformation dependent.

In post-processing it is possible to visualize, elaborate and export all information produced. All information coming from the defined monitoring points can be showed and studied, moreover it is possible to visualize different characteristics of the damaged element in each step of the process. Some of such characteristics are:

- *Cracks*, with different crack width;
- *Bar reinforcement*, showing stresses and strains;
- *Interface*, showing forces and displacements, loads and reaction acting parallel or perpendicular to the interface;
- *Scalars*, showing stress and strain in the selected material.

6.2. DESNERCK ET AL. LABORATORY TEST: VALIDATION OF THE FEM MODEL

First, the ATENA model is validated with Desnerck et al. test with a direct comparison of load/displacement curves and load/crack width curves, all information and results are provided by the authors.

6.2.1. Inputs

The test geometry is reproduced in the program, with material's characteristic and boundary conditions.

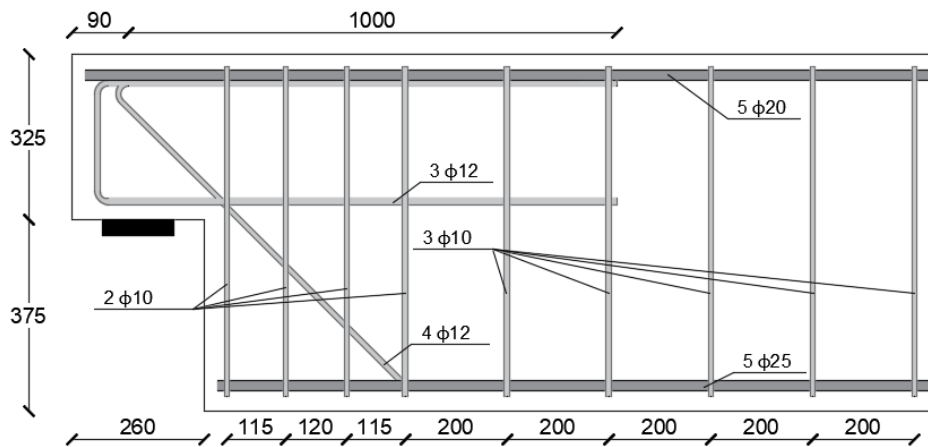


Figure 6.5: geometry and dimensions of experimental half-joint specimen NS-REF [mm]⁹

The beam is a full concrete element, with constant width equal to 0.4 m.

6.2.1.1. MATERIALS

Characteristics of different materials are provided by Desnerck et al.¹⁰.

$f_{c,cub}$	47.6 MPa
$f_{c,cyl}$	33.8 MPa
$f_{ct,fl}$	3.71 MPa
E_c	33.7 GPa

Table 6.1: Concrete properties

$f_y(\phi 10)$	539 MPa
$f_y(\phi 12)$	529 MPa
$f_y(\phi 20 - \phi 25)$	578 MPa
E_s	210 GPa

Table 6.2: Steel reinforcement properties

- Concrete is defined as a Non-Linear cementitious material;

- Poisson’s ratio of concrete has been assumed zero since the cracked condition of concrete is under investigation;
- Sensitivity to fracture energy is further investigated;
- Sensitivity to mesh refinement is further investigated;
- Reinforcement is assumed to be perfectly bonded to concrete, with bilinear constitutive law;
- Ultimate steel elongation is set at 3 mm.

The joint reproduced is representing a three-points bending test, therefore two steel plates are necessary: one to apply the load and the second to apply the supporting reaction. Bearings are therefore defined as *plane stress elastic isotropic* materials, with the following characteristics.

E_s	210 GPa
ν	0.3

Table 6.3: Bearings properties

6.2.1.2. SIMULATION SETUP

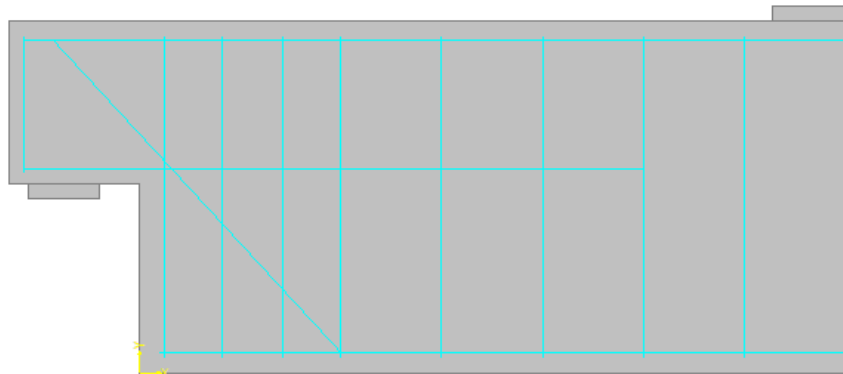


Figure 6.6: Reinforcement layout

Due to the symmetry of the specimen (Figure 6.7) only half beam can be analysed. Boundary conditions ensure the correct representation of reality:

- at the bearing section vertical displacement is avoided, even though rotation is allowed;

- at the half beam cross section, only vertical displacement is allowed.

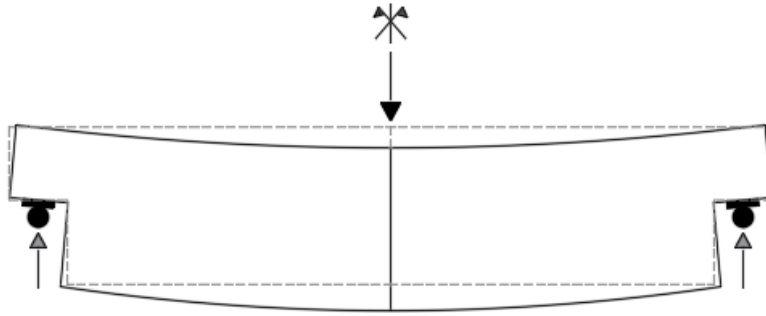


Figure 6.7: static scheme

In ATENA, supporting reactions are set in the *line* elements at midspan and at the *point* element at the bearing.



Figure 6.8: supporting reactions

The applied load is in fact an applied constant displacement of 0.1 mm at the midspan bearing, repeated for each step of the process.

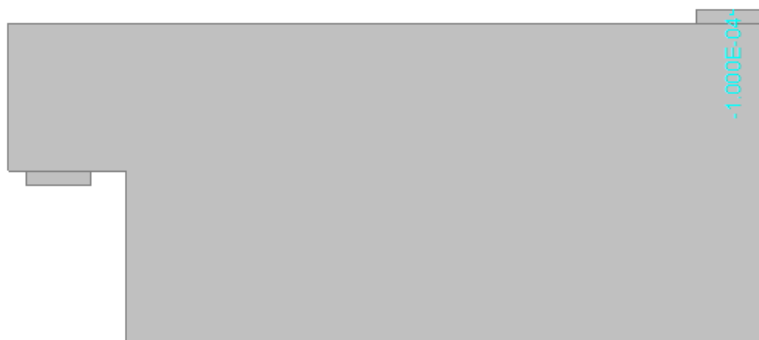


Figure 6.9: applied load

Two monitoring points are placed in order to obtain for every process a Load/Displacement curve. The two points are set:

- To measure the reaction in the upper steel plate where the imposed displacement is applied,
- To measure the vertical displacement in the bottom-right corner, at the cross section where the greatest deflection can be measured.

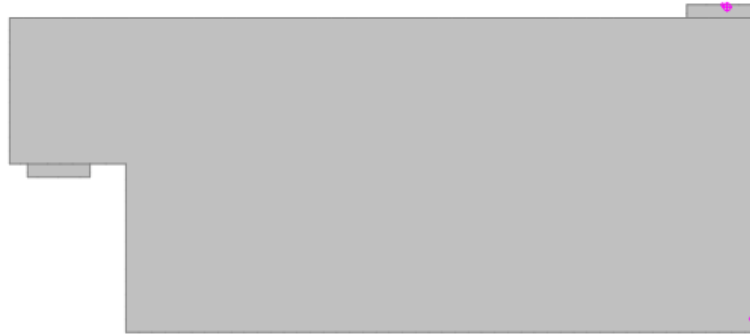


Figure 6.10: Monitoring points

6.2.1.3. SOLUTION PARAMETERS

The solution is achieved with the Newton Raphson method, 150 steps and 60 iterations to reach convergence.

Solution method:	Newton-Raphson	<input checked="" type="checkbox"/> Line search
Optimize node numbers:	Sloan	
Update Stiffness:	Each iteration	
Stiffness Type:	Tangent	
Iteration number limit:	60	
Displacement error tolerance:	0.010000	[-]
Residual error tolerance:	0.010000	[-]
Absolute residual error tolerance:	0.010000	[-]
Energy error tolerance:	0.000100	[-]

General	Line Search	Conditional Break Criteria
Solution method:	With iterations	
Unbalanced energy limit:	0.800	[-]
Limit of line search iterations:	3	
Line search limit - min.:	0.010	[-]
Line search limit - max.:	1.000	[-]

	Break immediately	Break after step	
Displacement error multiple:	10000.0	10.0	[-]
Residual error multiple:	10000.0	10.0	[-]
Absolute residual error multiple:	10000.0	10.0	[-]
Energy error multiple:	1000000.0	10000.0	[-]

Figure 6.11: solution parameters

6.2.2. Outputs

The non-linear analysis is performed in order to obtain Load/displacement curves that can be compared to the load-displacement curve provided by the researchers and obtained by direct laboratory test. To strengthen the obtained results, L/d curves are compared with the variation of determined parameters, such as mesh dimension and fracture energy.

6.2.2.1. MESH SENSITIVITY

The load-displacement curve obtained by Desnerck et al. by direct testing of the specimen is compared to L/d curves obtained with ATENA in case of fracture energy computed following the Model Code 1990, rotated crack model (cc0) and with different mesh sizes: 3 cm, 8 cm and 15 cm.

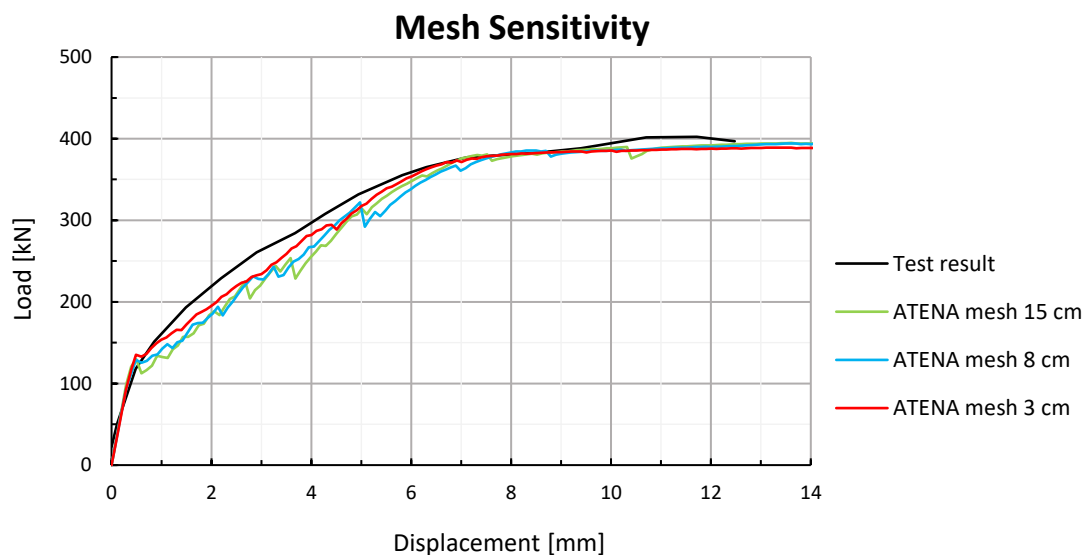


Figure 6.12: load-displacement curve sensitivity to mesh refinement

As expected, the finer mesh is more regular and more coherent to the test output, even though all three curves show a good approximation to the laboratory test curve.

6.2.2.2. FRACTURE ENERGY SENSITIVITY

Fracture energy represents the tensile strength of concrete, it is the integral of the stress/displacement curve when pure tension forces are applied (see Figure 6.13). It can be analytically computed with different formulas, and indications relative to it are provided by the Model Code 1990 and the Model Code 2010. Both cases are referred to the mean bending resistance of concrete, but MC2010 indications are more independent to the concrete type.

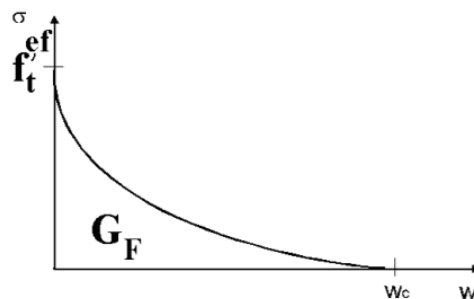


Figure 6.13: Exponential crack opening law, fracture energy

Model Code 1990 and Model Code 2010 indications on fracture energy are compared. In both cases two different analysis are performed with the two extreme values of the fixed crack model coefficient, with a 3 cm mesh.

Model Code 1990: $G_F = a_d \cdot f_{cm}^{0.7} [N/m]$ $G_F = 6 \cdot 44.8^{0.7} = 85.91 N/m$

Model Code 2010: $G_F = 73 f_{cm}^{0.18} [N/m]$ $G_F = 73 \cdot 44.8^{0.18} = 144.73 N/m$

Table 1. Coefficient, a_d , to take into account the effect of maximum aggregate size, d , on fracture energy G_F

d [mm]	a_d
8	4
16	6
32	10

Figure 6.14 coefficient a_d^2

The maximum aggregate size considered is $d = 16 \text{ mm}$.

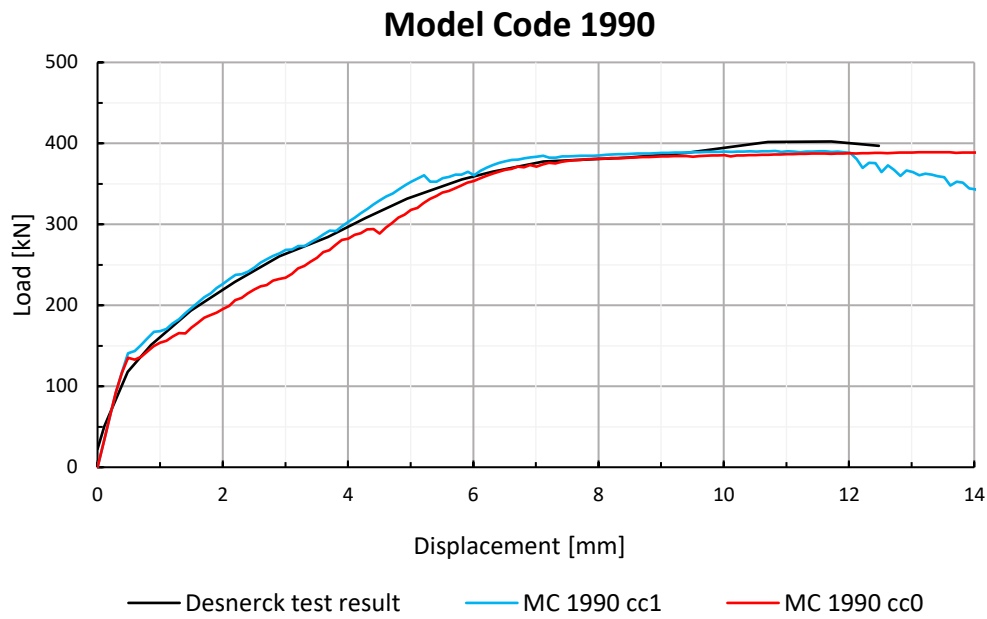


Figure 6.15: Load/ Displacement curves with Model Code 1990

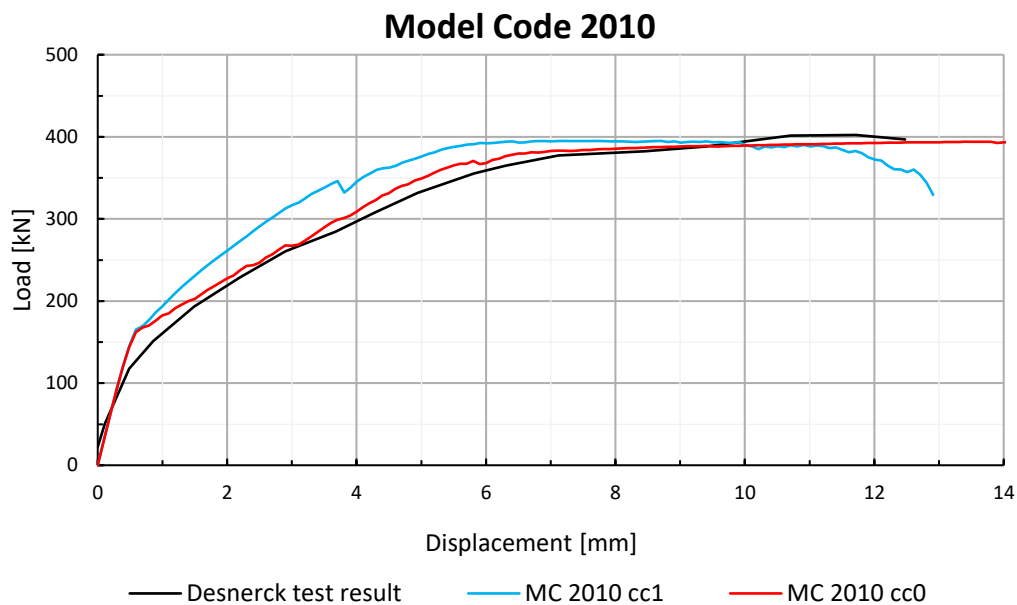


Figure 6.16: Load/ Displacement curves with Model Code 2010

It is possible to notice that the Model Code 1990 has more restrictive output when compared to Model Code 2010, and while the rotated crack model in both cases shows a nearly plastic behaviour, the fixed crack model has a descendent curve after a plateau.

Sensitivity tests have outlined the optimal input parameters in order to have coherent, regular and critical results:

- Mesh size: 3 cm
- Model code 1990, therefore $G_F = a_d \cdot f_{cm}^{0.7} [N/m]$.

6.2.2.3. CRACK WIDTH COMPARISON

Based on the test performed by Desnerck et al. it is possible to compare numerical and laboratory main crack forming at the inner part of the nib.

The four displacement gauges are positioned as referring to Figure 6.18.

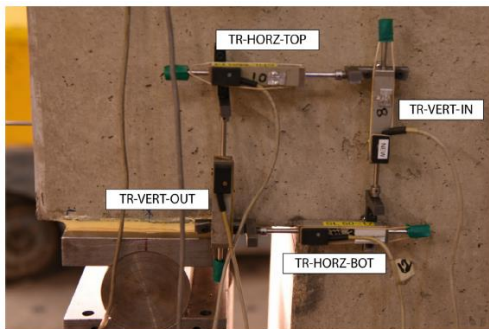


Figure 6.18: transducers positioning in the inner part of the nib¹⁰



Figure 6.17: ATENA model for monitoring points

Four monitoring points are placed in correspondence to the closest mesh nodes to the test transducers. Then, the load displacement curves are compared, in both cases of fixed and rotated crack models.

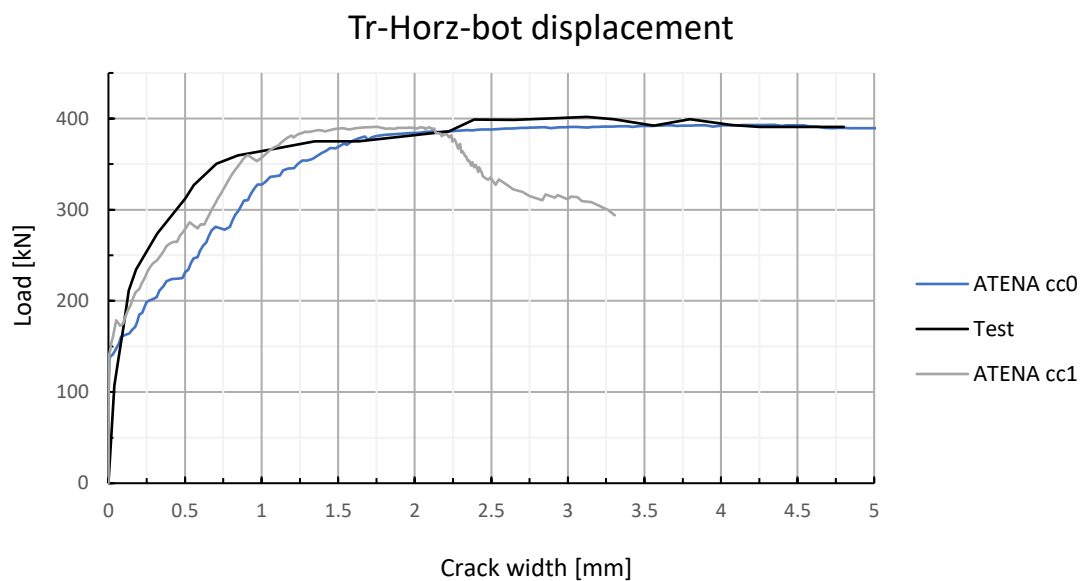


Figure 6.19: horizontal displacement

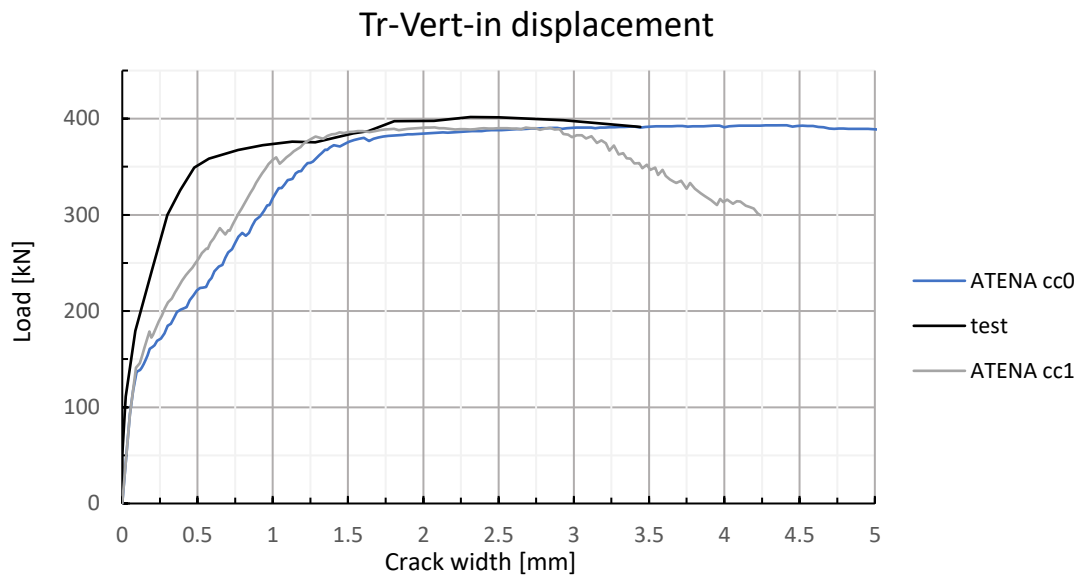


Figure 6.20: Vertical displacement

Fixed crack model provides less ductile results, as expected also from previous analyses. The initial part of the curves is corresponding to the elastic field where almost no cracks are developed, and the first crack is forming at a load level between 20% and 33% of the failure load, also according to Barton test campaign on half-joints². Crack width below 0.1 mm is assumed to be stable and relatively safe. When cracks are larger than 0.1 mm, they start to be unstable and dangerous, also because of the higher probability of environmental attacks, water seepage and consequent corrosion mechanism.

In the elastic field, numerical and laboratory tests show a good superposition, but as cracks formation mechanism starts, accuracy decreases. However, there is a good agreement between laboratory and numerical tests, both regarding ultimate bearing capacity and stiffness of the joint.

6.2.2.4. RENDERINGS

In this paragraph different steps and different characteristics are shown: crack width, concrete strain and reinforcement stress are displayed at crack initiation, development and failure. Only rotated crack model is displayed.

First, crack width is shown. Cracks initiate at the inner nib and develop in the whole cross section. Critical cracks that cause the failure of the half-joints are at the inner nib, going through the cross section, towards the upper layer of the beam.

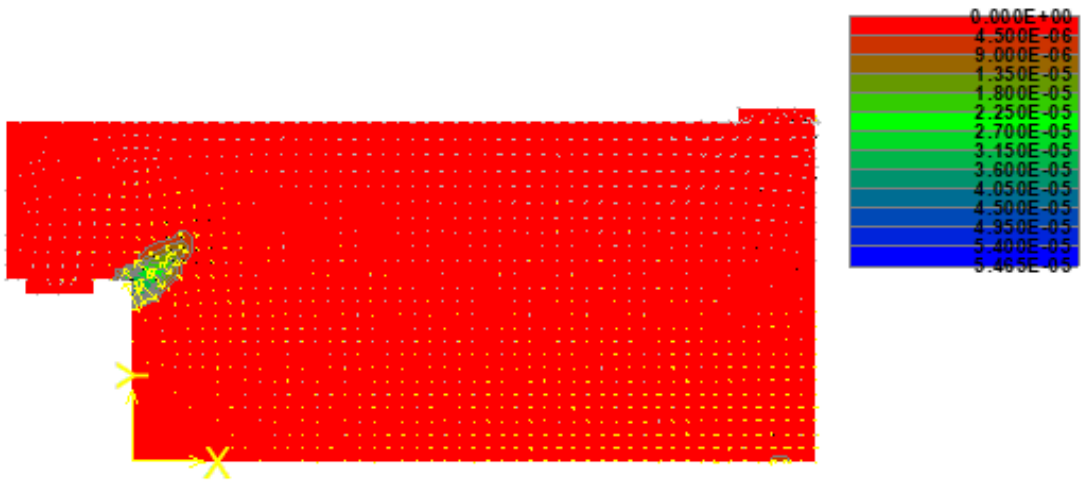


Figure 6.21: step 5, crack initiation

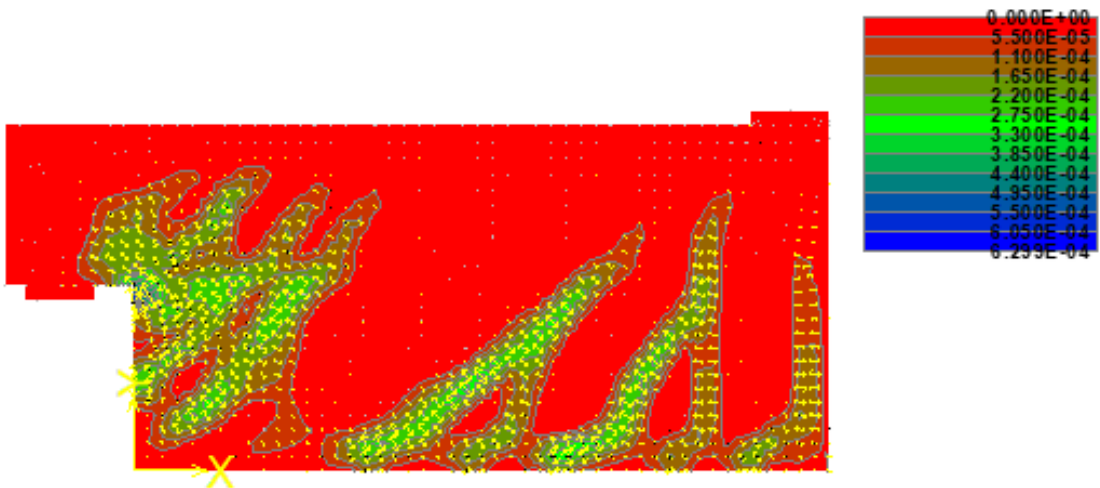


Figure 6.22: step 60, crack development

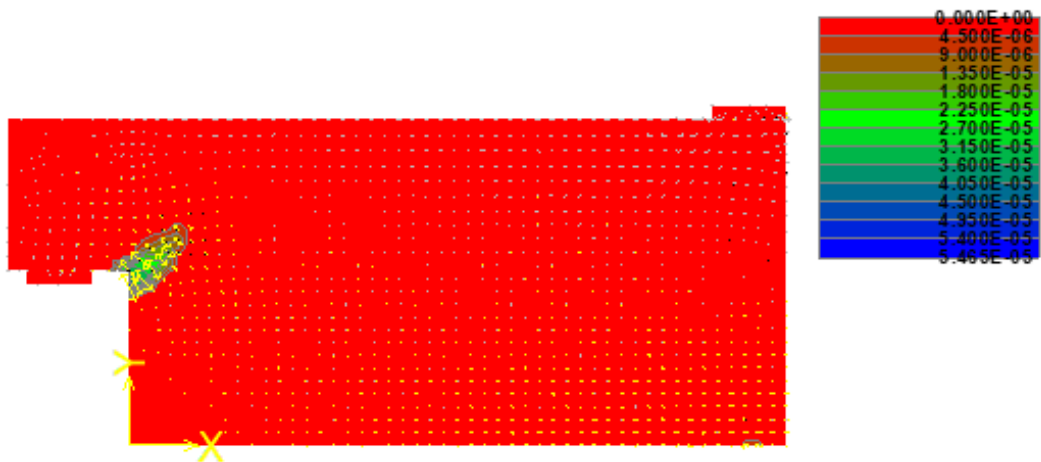


Figure 6.23: step 110, peak resistance

Secondly, the minimum concrete strain is shown. This is an important indication of the failure mode, that is not caused by concrete crushing but steel yielding. Concrete is compressed in the upper part of the beam and it is subjected to tension in the lower part: it is important to check that the minimum strain of concrete does not exceed its critical value (0.35%), since concrete crushing is a brittle failure mode, while steel rebars yielding is more ductile. Moreover, from the analytical model it is possible to deduce that the first elements to fail are diagonal and the vertical stirrups, and this is confirmed from the renders at step 110, where concrete strain is below the critical threshold.

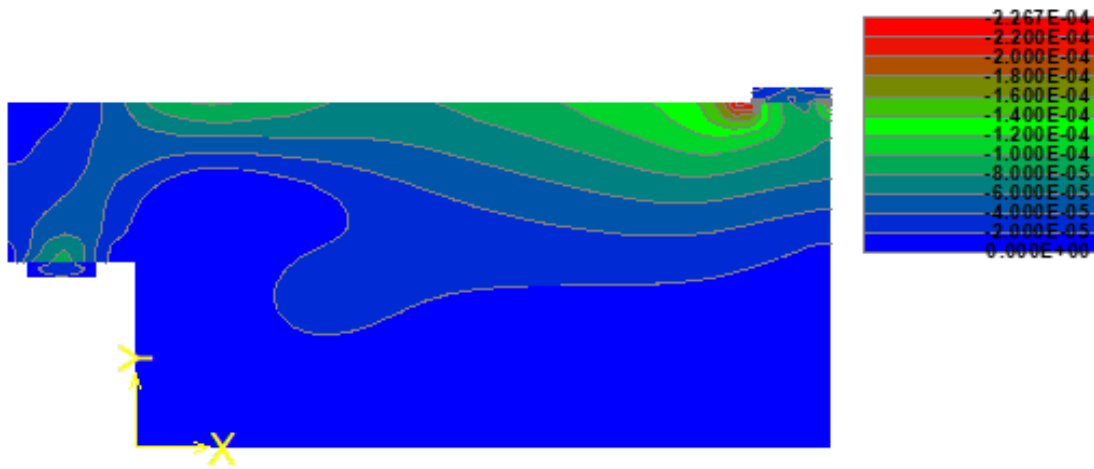


Figure 6.24: step 5, crack formation

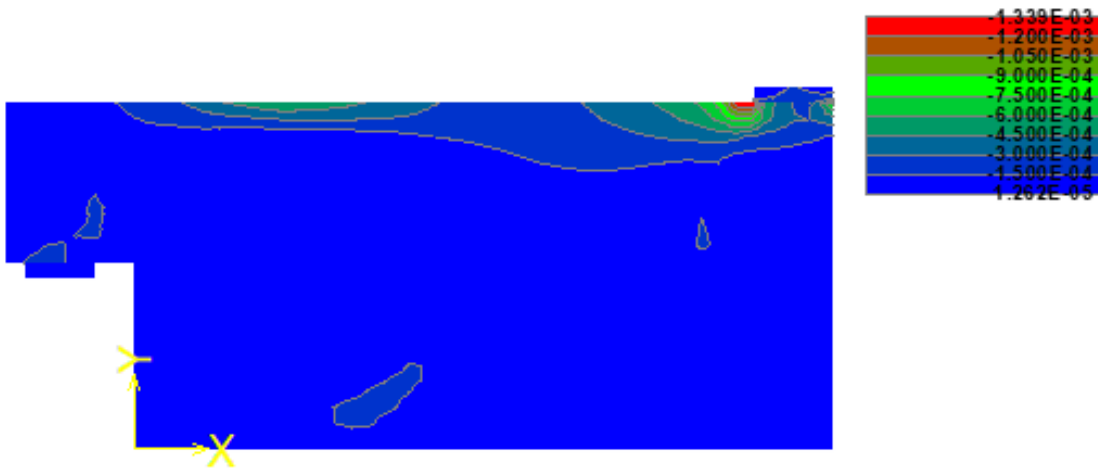


Figure 6.25: step 60, crack development

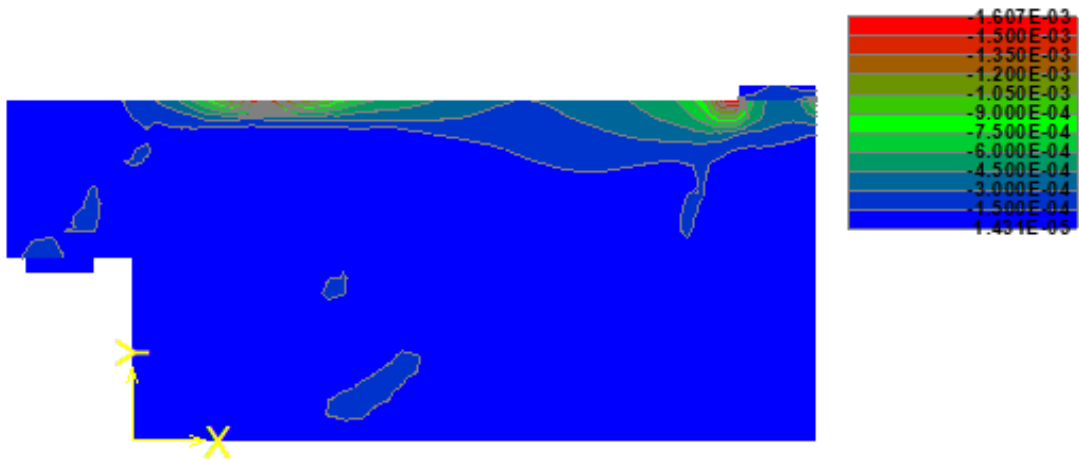


Figure 6.26: step 110, peak resistance

At last, reinforcement internal stresses are shown. This last point is necessary to highlight the failure mode and the number of stirrups hypothesised in the model *a* (chapter 3.4.3). In fact, at crack formation (Figure 6.27) the first rebars to yield are at the nib, then stresses start to increase and at the peak resistance (Figure 6.29), horizontal, diagonal reinforcements and the first two stirrups are totally yielded. This confirms the steel failure and the number of stirrups concurring to the vertical steel tie (2 stirrups). Moreover, longitudinal reinforcement is developing internal stresses because of bending, but at failure of the joint it is still in elastic phase.

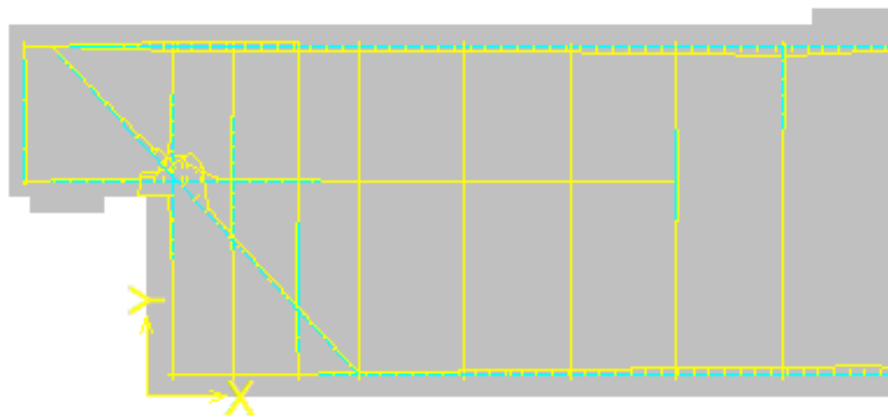


Figure 6.27: step 5, crack initiation

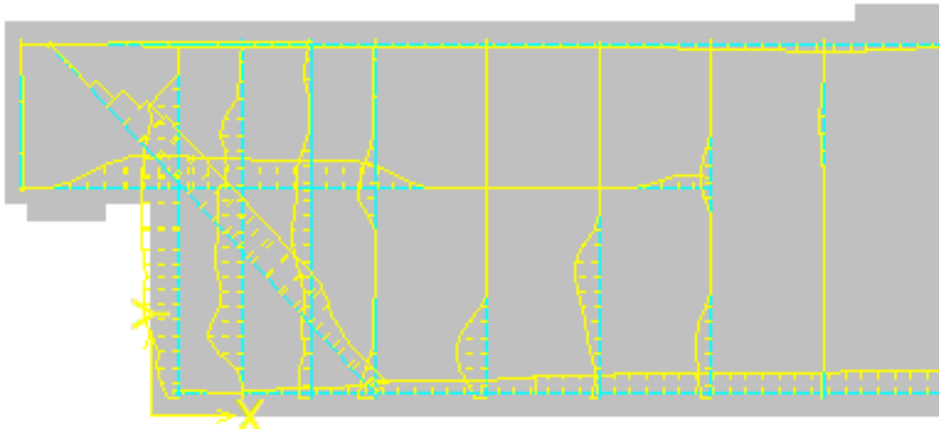


Figure 6.28: step 60, crack development

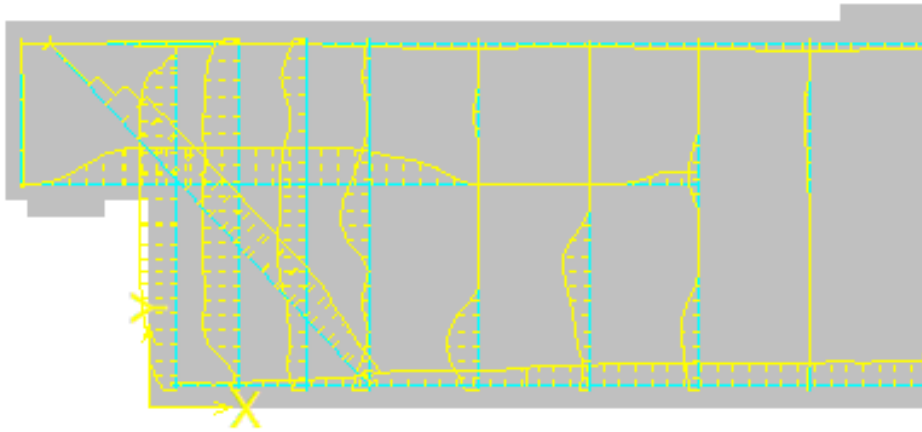


Figure 6.29: step 110, peak resistance

6.3. SELECTED DATABASE JOINT: VALIDATION OF THE ANALYTICAL MODELS

One joint is selected from the Dutch database: it does not fulfil the strength requirements according to the strut and tie and the kinematic models. It is the joint of beam 14, an inverted T, precast, prestressed beam with a layer of cast in situ concrete on top. The numerical analysis is performed with and without cast in situ slab.

6.3.1. Inputs

The beam geometry and reinforcement layout are reported below in Figure 6.30.

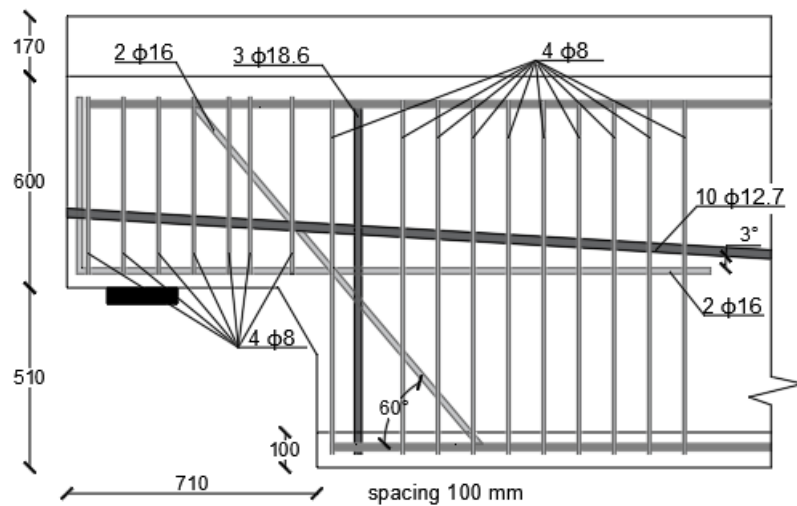


Figure 6.30: Beam 14 reinforcement layout and geometry

The beam is schematized in three concrete macro-elements, and two steel plates for supporting and loading conditions. The three concrete elements are representing the bottom flange, the web and the cast in situ slab.

The beam thickness varies in the cross section: the bottom flange and concrete slab are 1.25 m thick, while the beam web is 0.4 m. The flange of the precast beam is 0.1 m high.

6.3.1.1. MATERIALS

The materials used have been specified according to Eurocode classes. Therefore, the characteristic properties are identified.

C 25/30	
$f_{c,cub}$	30 MPa
$f_{c,cyl}$	25 MPa
$f_{ct,fl}$	2.2 MPa
E_c	31 GPa

Table 6.4: concrete slab properties

C 55/67	
$f_{c,cub}$	67 MPa
$f_{c,cyl}$	55 MPa
$f_{ct,fl}$	4.2 MPa
E_c	38 GPa

Table 6.5: precast beam concrete properties

Reinforcement QR40	
f_{yk}	330 MPa
E_s	210 MPa

Table 6.6: Reinforcing steel properties

Prestressing Steel QP190	
f_{pk}	1691 MPa
E_s	195 MPa

Table 6.7: Prestressing steel properties

- Concrete is defined as a Non-Linear cementitious material;
- Poisson's ratio of concrete has been assumed zero since the cracked condition of concrete is under investigation;
- Fracture energy is calculated according to the Model Code 1990:

$$G_{F,beam} = 6 \cdot f_{cm}^{0.7} = 6 \cdot 63^{0.7} = 109.1 \text{ N/m}$$

$$G_{F,slab} = 6 \cdot f_{cm}^{0.7} = 6 \cdot 33^{0.7} = 69.4 \text{ N/m}$$

- Mesh is defined with quadrilateral elements, size 3 cm;
- Reinforcement is assumed to be perfectly bonded to concrete, with bilinear constitutive law;
- Ultimate reinforcing and prestressing steel elongation is set at 3 mm.

The joint reproduced is representing a three-points bending test, therefore two steel plates are necessary: one to apply the load and the second to apply the supporting reaction. Bearings are therefore defined as *plane stress elastic isotropic* materials, with the following characteristics:

E_s	210 GPa
ν	0.3

Table 6.8: Bearings properties

In all the numerical models produced with ATENA, the interface between steel plates and concrete beam is assumed to behave as perfect connection, so no slip is occurring. However, in case of two concrete layers cast in two different moments an interface material is necessary and must be modelled. In the present case there is a precast beam of C55/67 with on top a cast-in-situ

slab C25/30 and the interface between those two must not be considered as a perfect connection.

ATENA models interfaces materials following Mohr-Coulomb failure criteria (see Figure 6.31), so tensile strength f_t , cohesion c and friction coefficient ϕ must be defined. The choice of these three parameters is not arbitrary, it must fulfil the following rules:

$$f_t \leq \frac{c}{\phi}; f_t \leq c$$

$$c > 0; f_t > 0; \phi > 0$$

In addition to f_t, c, ϕ , also normal and tangential stiffnesses in their initial and residual value are to be fixed in order to define the surface slip (Figure 6.32 and Figure 6.33):

$$\begin{Bmatrix} \sigma \\ \tau \end{Bmatrix} = \begin{pmatrix} K_{nn} & 0 \\ 0 & K_{tt} \end{pmatrix} \cdot \begin{Bmatrix} \Delta u \\ \Delta v \end{Bmatrix} \quad (6.2)$$

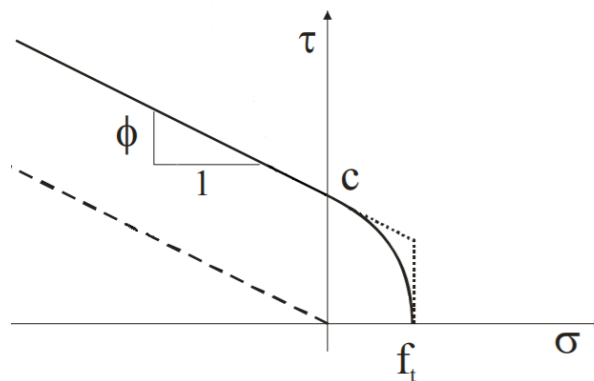


Figure 6.31: Mohr-Coulomb failure criterion

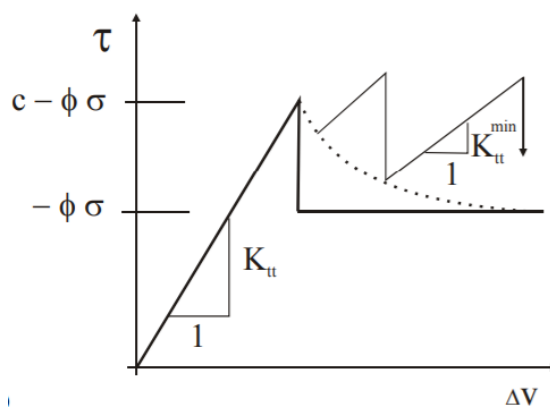


Figure 6.32: Typical interface model behaviour in shear

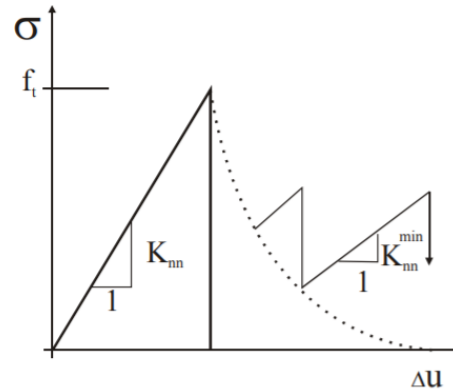


Figure 6.33: Typical interface model behaviour in tension

All these parameters are evaluated according to ATENA manual, that gives some generical indications related to the weakest material at the interface:

- Tensile strength must be lower of the tensile strength of the weakest material, from 25% to 50% of its value:

$$f_t = 0.5 \cdot f_t(C25/30) = 0.5 \cdot 2.6 \text{ MPa} = 1.3 \text{ MPa}$$

- Cohesion is usually greater than the tensile strength and a recommended value is set to 100% to 200% of the interface tensile strength:

$$c = 2 \text{ MPa}$$

- Friction angle is hardly lower than 0.1 and usually has values between 0.3 and 0.5. Two analyses will be performed with variation of the friction coefficient
- Both initial stiffnesses can be referred to the interface thickness t and less stiff neighbouring material:

$$t = 0.01 \text{ m}$$

$$K_{nn} = K_{tt} = 10 \cdot \frac{E_{25/30}}{t} = 3.1 \cdot 10^7 \text{ MPa}$$

- Residual stiffness is taken as a fraction of the initial one:

$$K_{nn,res} = K_{tt,res} = \frac{K_{initial}}{100} = 3.1 \cdot 10^5 \text{ MPa}$$

6.3.1.2. SIMULATION SETUP

All reinforcement information provided is regarding the precast element, but for a correct stress propagation between precast beam and cast in situ slab, a number of steel rebars are placed ($4 \phi 10/10 \text{ cm}$).

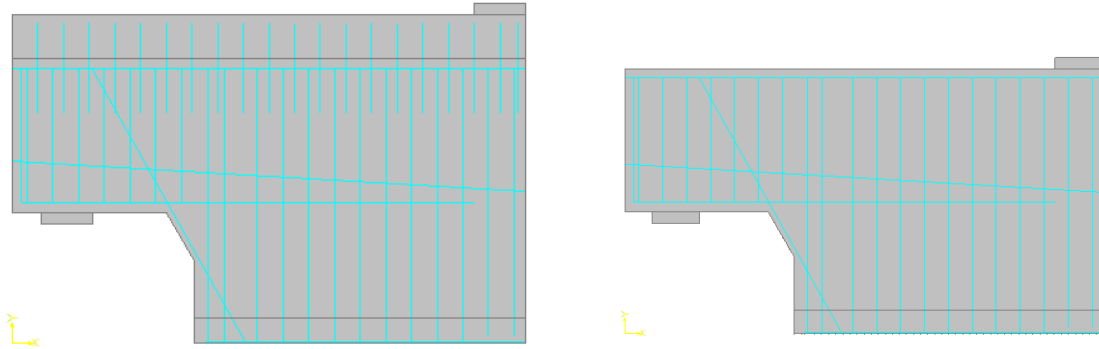


Figure 6.34: reinforcement layout

Due to the symmetry of the specimen, only half beam can be analysed, and the boundary conditions provided ensure the correct representation of reality.

Supporting reactions simulate half of a simply supported beam (Figure 6.7):

- at the bearing section vertical displacement is avoided, even though rotation is allowed;
- at the half beam cross section, only vertical displacements are allowed.

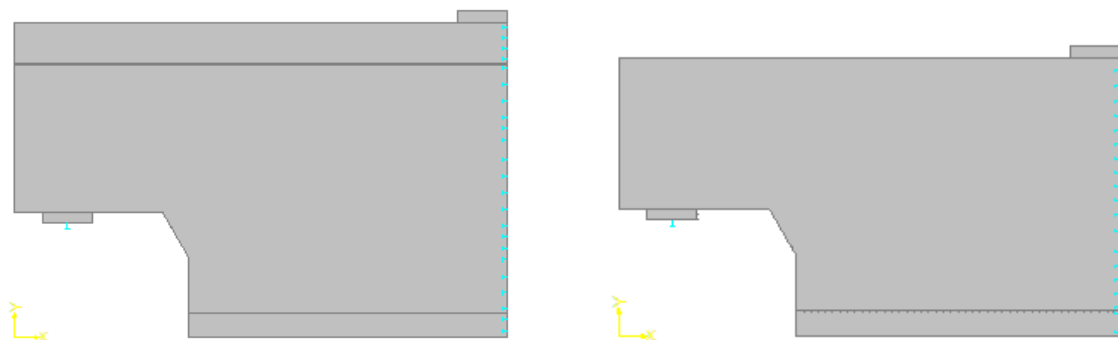


Figure 6.35: supporting reactions

The applied load is in fact a constant displacement of 0.1 mm , repeated for each step of the process.

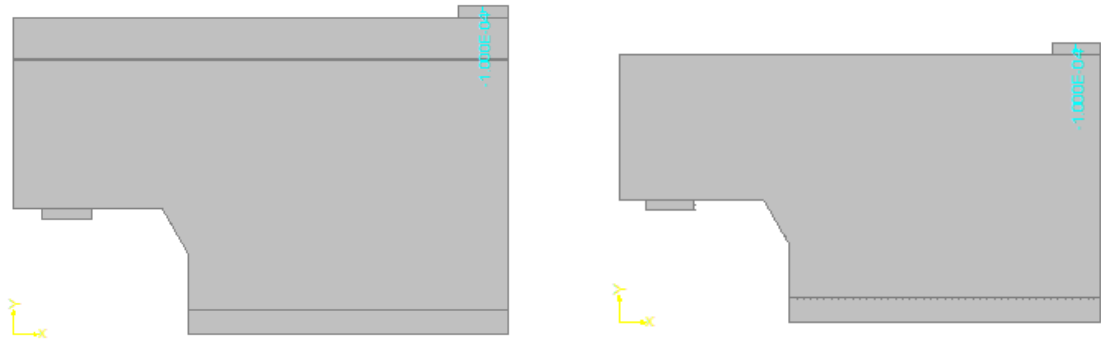


Figure 6.36: applied load

Two monitoring points are placed in order to obtain for every process a Load/Displacement curve. The two points are set: one in the upper steel plate where the imposed deformation is applied, and the other one in the bottom-right corner where the midspan displacement can be measured.

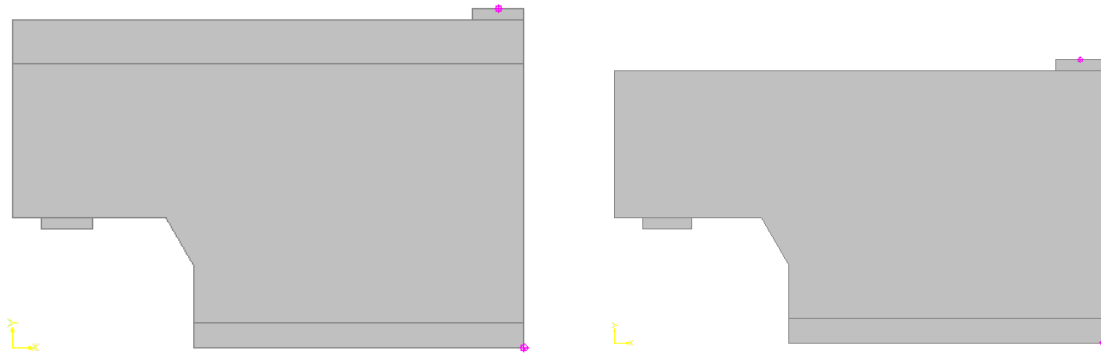


Figure 6.37: Monitoring points

6.3.1.3. SOLUTION PARAMETERS

The solution is achieved with the Newton Raphson method, at least 130 steps. The number of iterations varies from 60 to 140, to achieve convergence criteria.

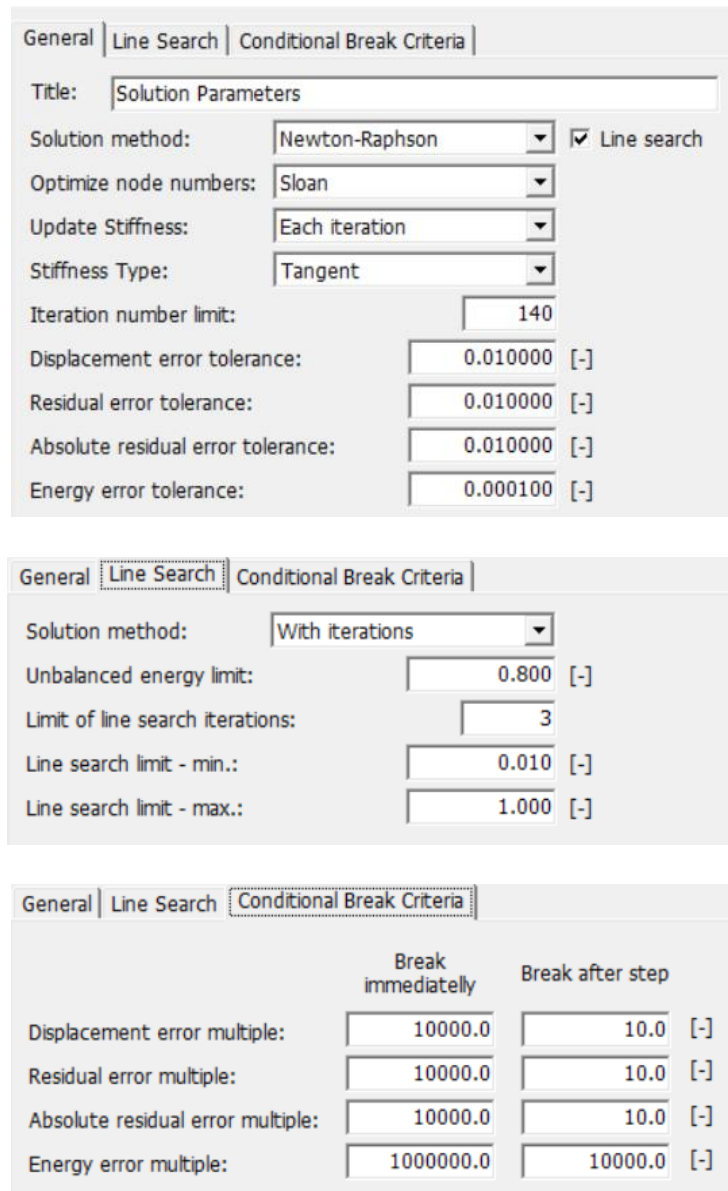


Figure 6.38: solution parameters

All analyses are performed in the two limit configurations of fixed crack and rotated crack models.

6.3.2. Outputs

Half-joint of beam 14 is analysed in its two configurations (precast beam with or without slab), with the two limit crack models (rotated and fixed). The output is compared to the results coming from the lower and upper bound analyses.

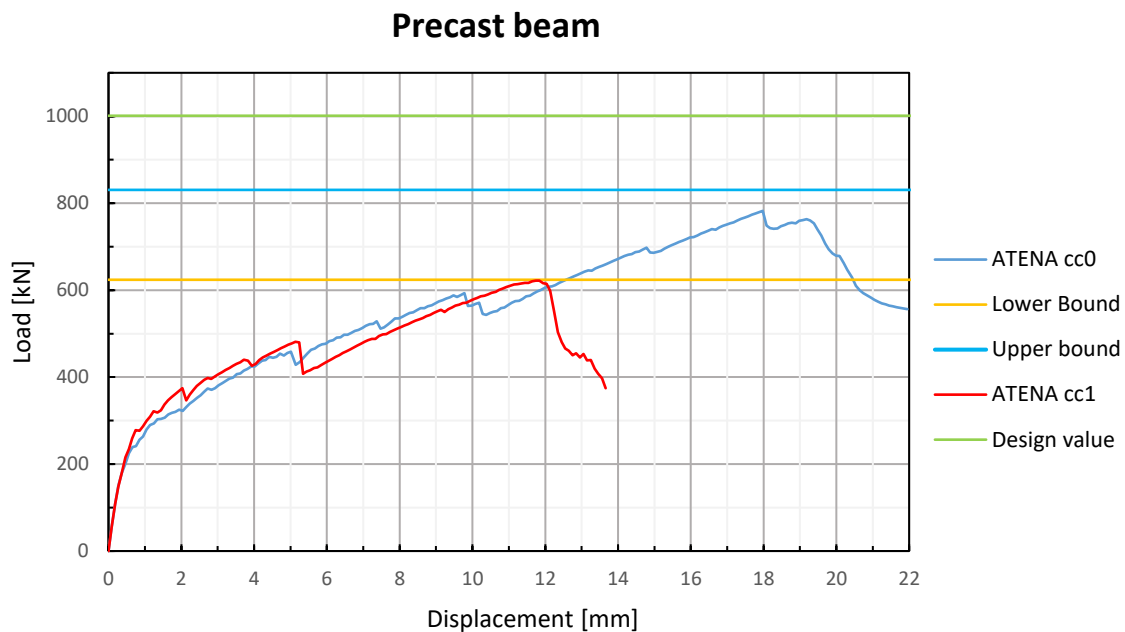


Figure 6.39: Load/displacement curve of the inverted T precast beam

The precast inverted T beam in displacement load controlled non-linear analysis shows three stages:

- An initial uncracked phase, with a constant stiffness and elastic behaviour. The duration of this phase is not deeply affected by the choice of fixed or rotated crack model: the first crack is forming is at a load of 200 kN, and this is in the correct range of 20% and 33% of the failure load, also according to Barton test campaign on half-joints² and Desnerck laboratory tests¹⁰;
- The second phase is characterized by crack propagation until failure. It is a hardening phase with a variable stiffness which is lower than the uncracked joint stiffness: when the tensile strength of concrete is exceeded, there is an inevitable formation of cracks, that cause a progressive reduction of the concrete cross section, hence a reduction of the overall stiffness.
- The third phase is the softening part after the peak, when the cross section bearing capacity is reached and overcome.
- The local peaks at steps 20, 50 and 120 (2 mm, 5 mm and 12mm displacement) are witnessing the yielding of diagonal, vertical and horizontal reinforcement as the load increases.

The rotated crack model shows a ductile behaviour, with a critical displacement of around 18 mm, whereas the fixed crack model has peak resistance at 12 mm displacement.

When the concrete slab is hardened, the beam is expected to increase stiffness and strength. The beam is then a *double T* or *I* beam, with the upper flange of a lower concrete class and the interface highly affecting the good interaction between the two concrete layers.

The fixed crack model shows less ductile behaviour, with a maximum displacement of 16 mm while the rotated crack model is until 22 mm.

The interface material depends on several parameters, among which the friction coefficient, which values are suggested to be between 0.3 and 0.5. The analysis is performed with two different friction coefficients, to show the sensitivity to this parameter.

Precast beam and cast in situ slab, $\phi=0.5$

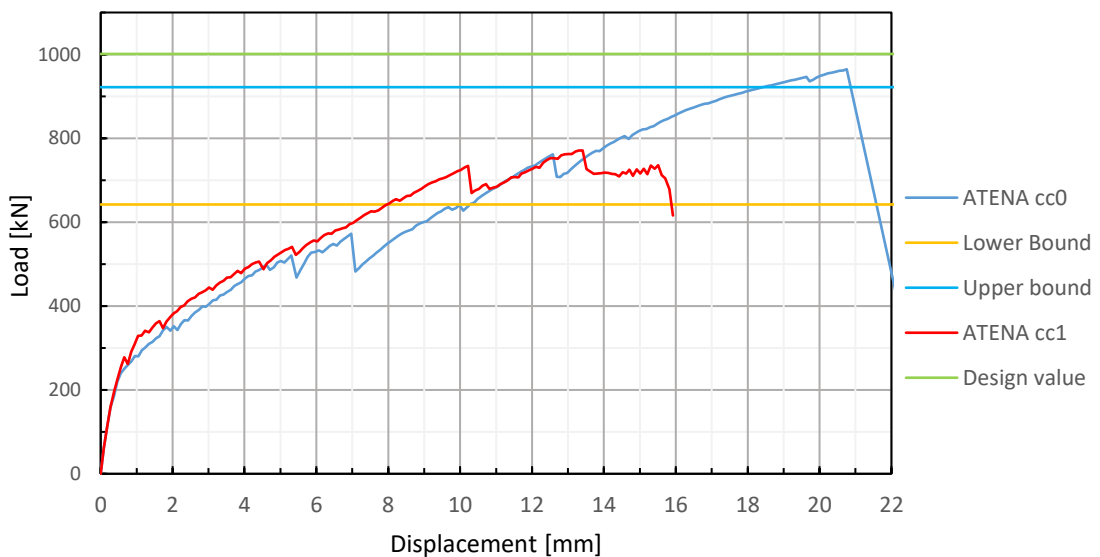


Figure 6.40: Load/displacement curve of the inverted T beam and concrete slab, $\phi=0.5$

Precast beam and cast in situ slab, $\phi=0.4$

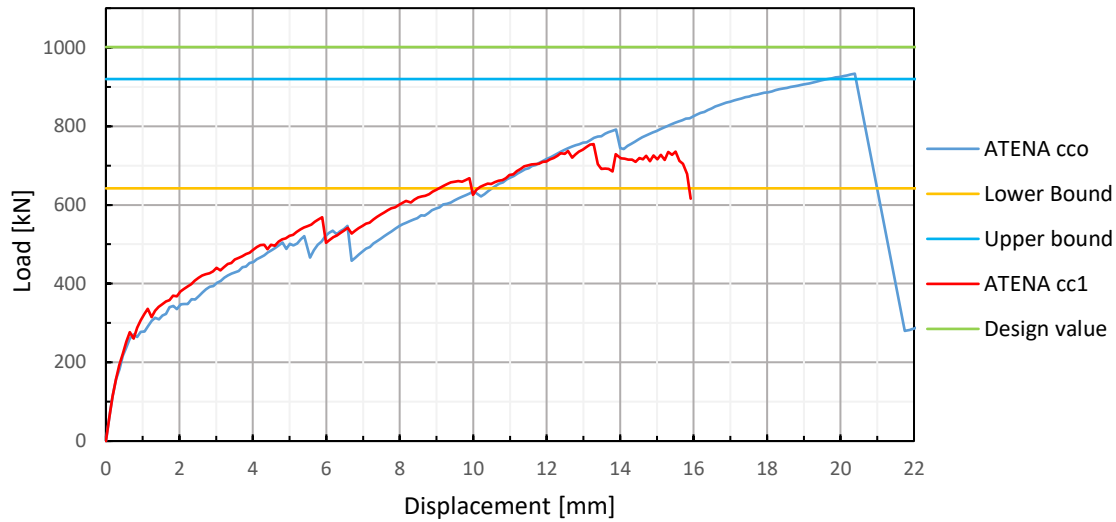


Figure 6.41: Load/displacement curve of the inverted T beam and concrete slab, $\phi=0.4$

Friction coefficient influence, rotated crack model (cc0)

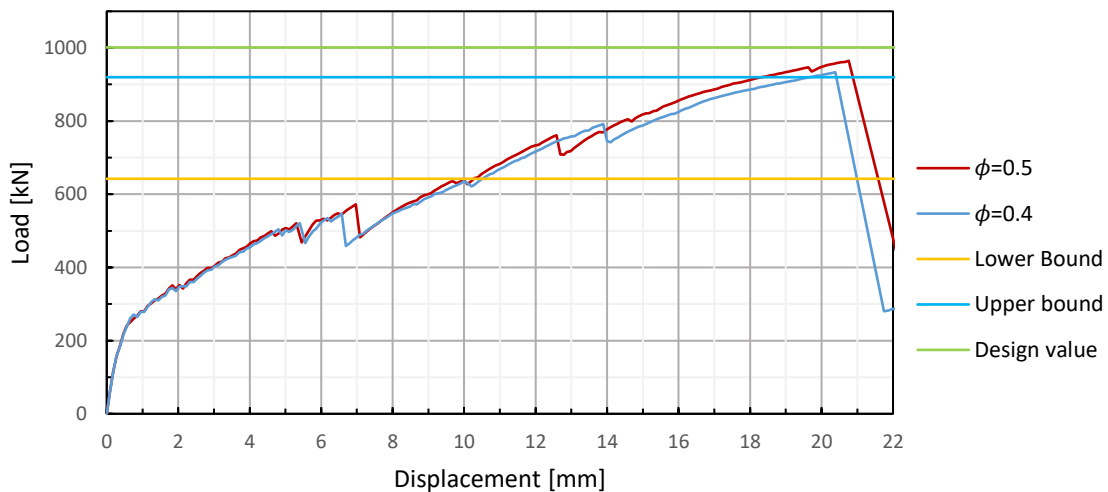


Figure 6.42: Load/displacement of the inverted T beam and cast in situ slab at the variation of the friction coefficient.

The reduction of the friction coefficient causes a loss of strength and rigidity of the joint, and the difference is highlighted in the plastic phase of the load/displacement curve. A good adhesion and stress propagation between the precast beam and the slab must be ensured, and it is usually obtained by steel rebars protruding from the precast element and then embedded in the concrete slab, during casting. The influence of the friction coefficient in determining the limit

resistance shows how the upper bound model is inappropriate to define the maximum strength of the joint: it relies on the assumption of perfect bond between precast and cast in situ concrete layers, and this could not be reflecting the reality.

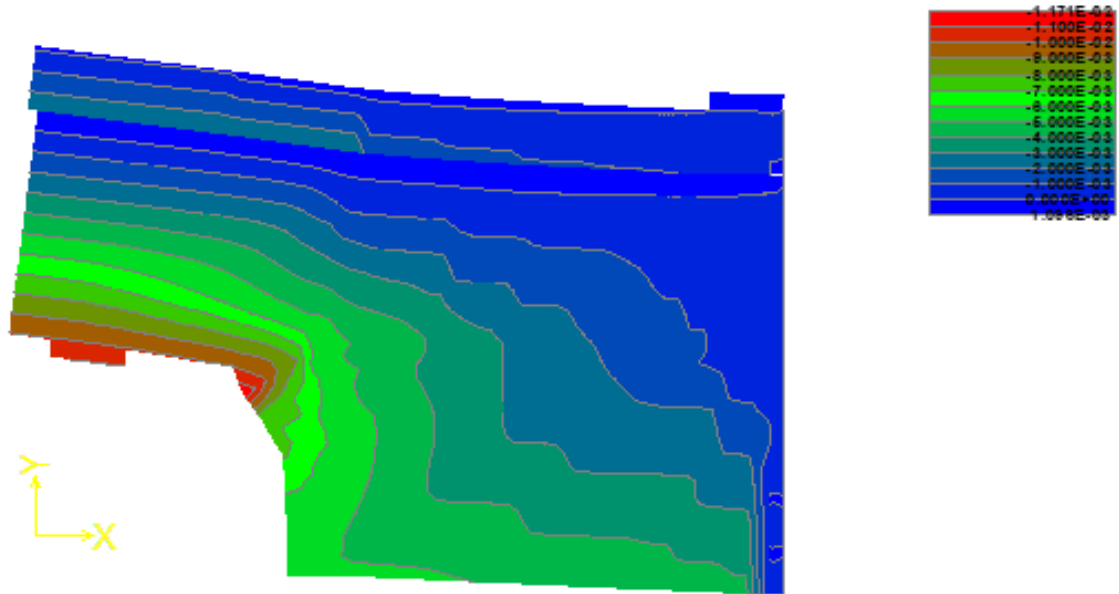


Figure 6.43: magnified displacement of beam 14, peak resistance

In Figure 6.43 the highlight of the relative slip between precast beam and cast in situ slab of the half-joint of beam 14 is displayed.

6.3.2.1. RENDERINGS

Here are shown some steps and some characteristics of the rotated crack model analysis performed on the precast beam with and without cast in situ slab. Such as for Desnerck et al. numerical model, crack width, concrete minimum strain and steel reinforcement internal stresses are displayed at crack initiation, propagation, peak resistance and failure.

First, the precast beam without cast in situ slab is shown. When crack width is displayed, the first cracks develop in the beam nib, with a load approximately 30% of the maximum resistance.

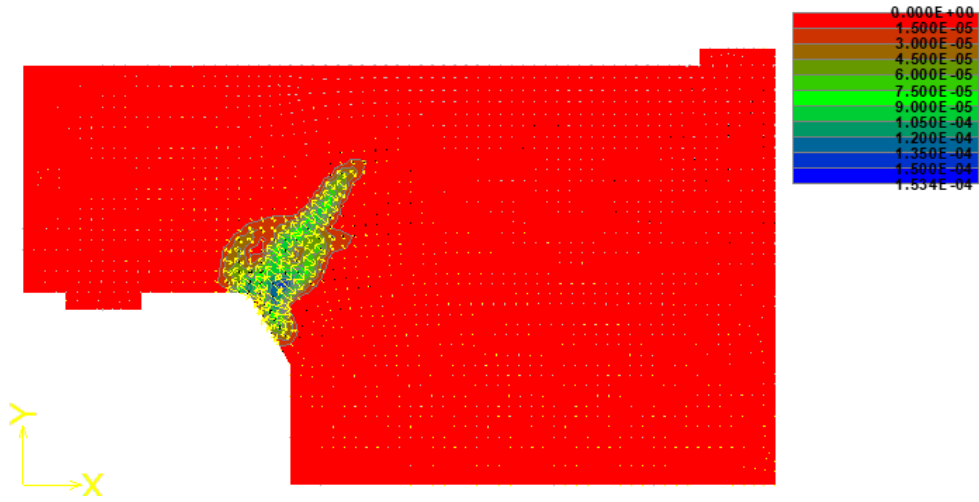


Figure 6.44: step 8, crack width at crack initiation

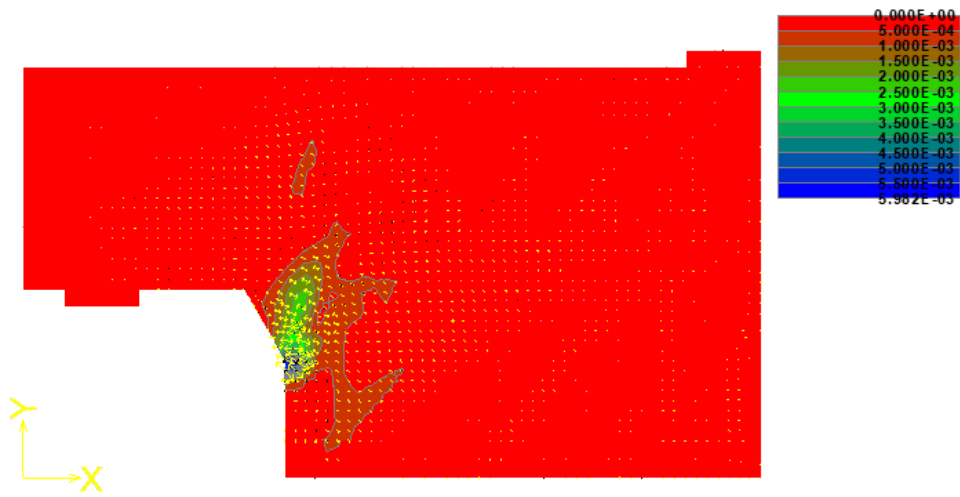


Figure 6.45: step 140, crack width at crack development step

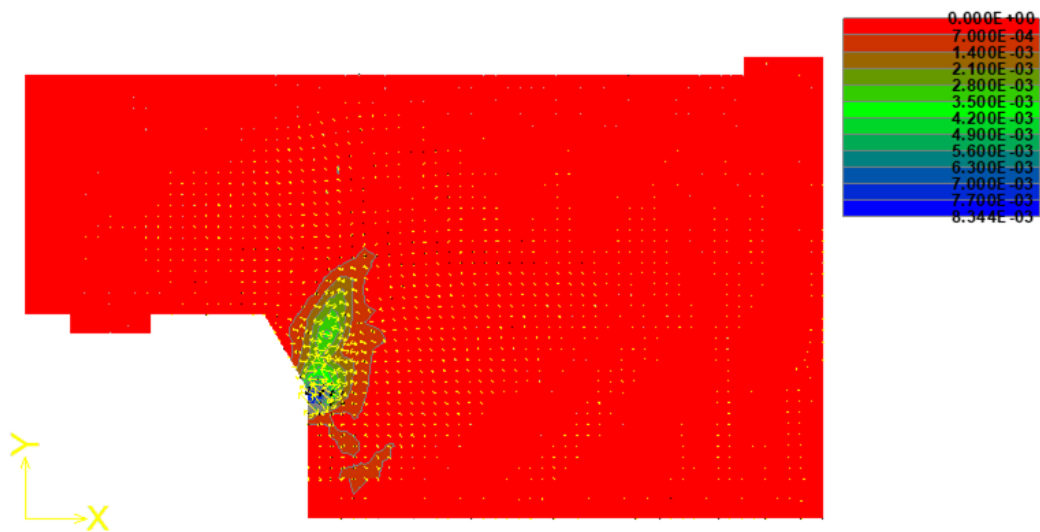


Figure 6.46: step 179, crack width at peak resistance

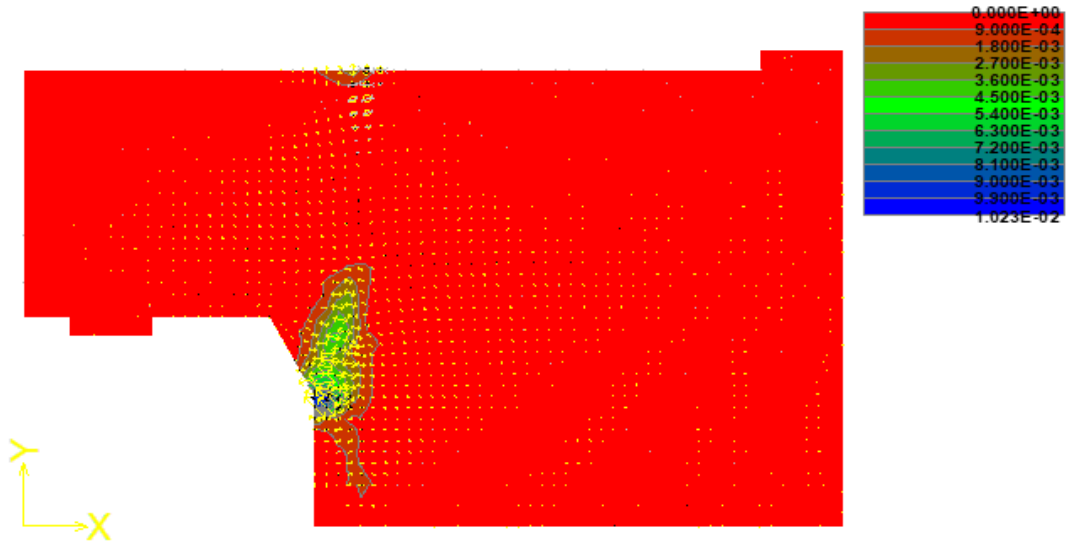


Figure 6.47: step 220, crack width at beam failure

After failure, the residual resistance of the beam is reduced of about the 30%. Minimum concrete strain confirms that the failure of the beam is not caused by concrete crushing, in fact at the peak load step the concrete strain is not reaching the critical value.

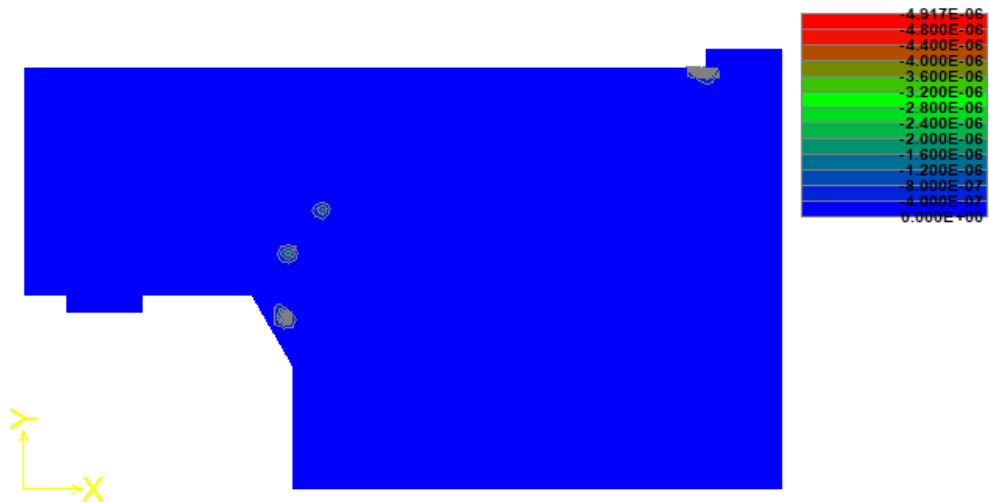


Figure 6.48: step 8, concrete minimum strain at crack initiation

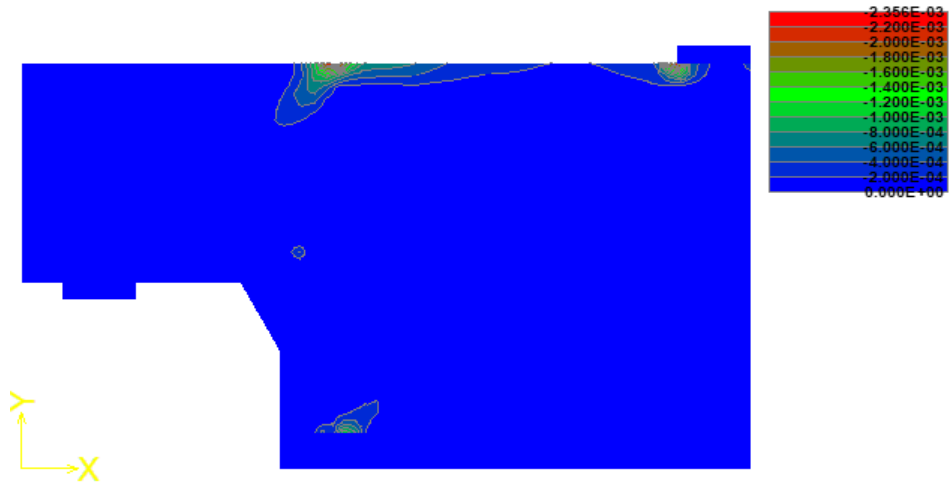


Figure 6.49: step 140, concrete minimum strain at crack development

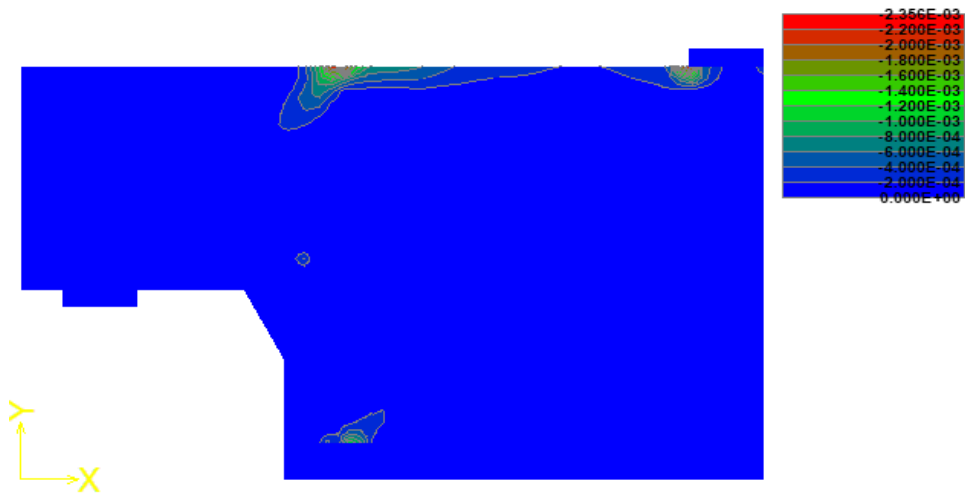


Figure 6.50: step 179, concrete minimum strain at peak resistance



Figure 6.51: step 220, concrete minimum strain at beam failure

When reinforcement internal stresses are displayed, it is possible to confirm the failure mode, the influence of prestressing strands, and the number of vertical stirrups exploited in the model α . It is easy to notice the contribute of vertical and longitudinal prestressing strands.

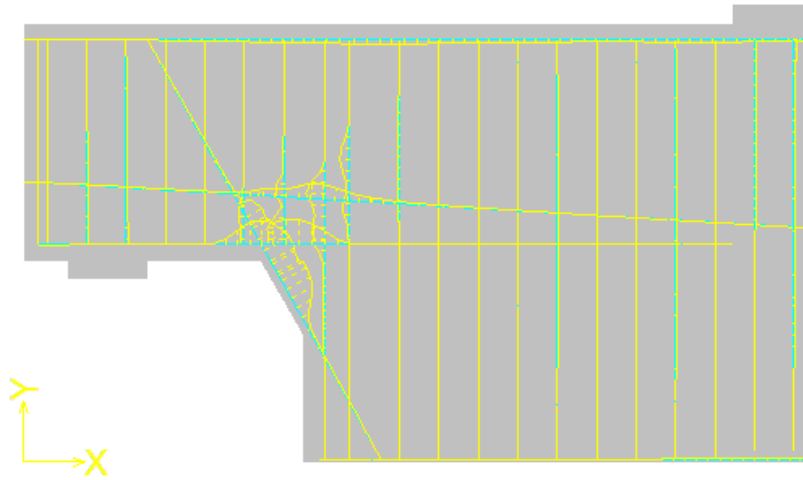


Figure 6.52: step 8, reinforcement internal stresses at crack initiation

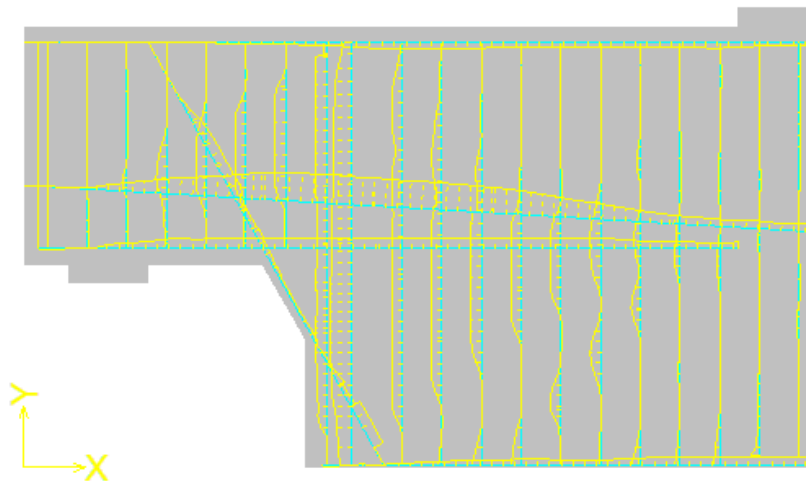


Figure 6.53: step 140, reinforcement internal stresses at crack development

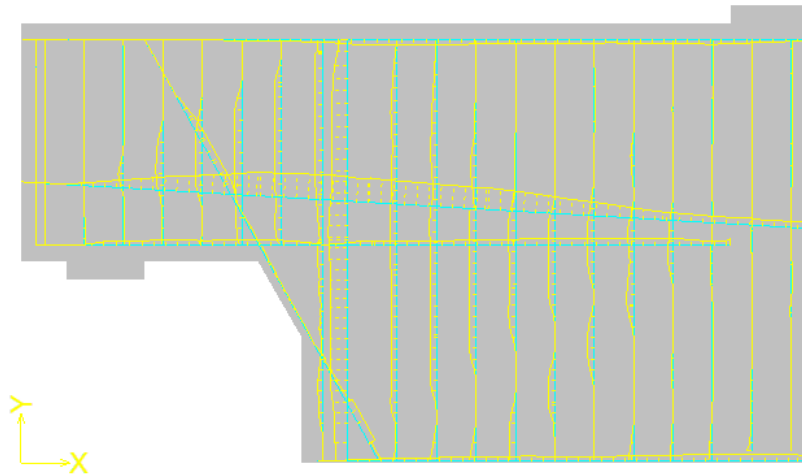


Figure 6.54: step 179, reinforcement internal stresses at peak resistance

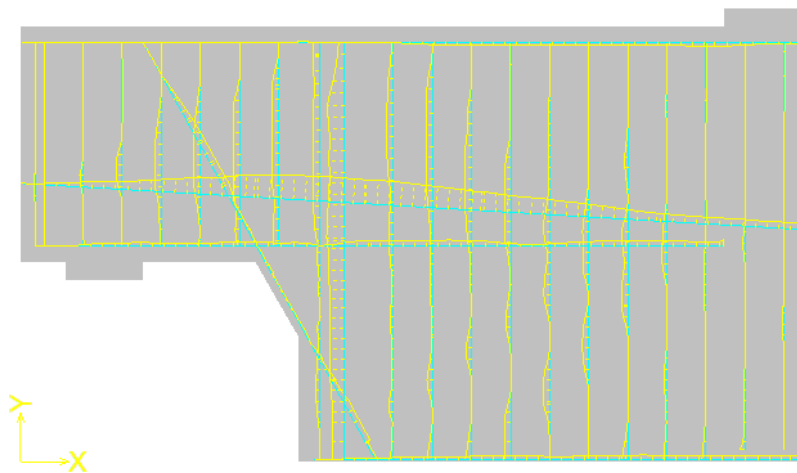


Figure 6.55: step 220, reinforcement internal stresses at beam failure

After the peak, rebars internal stress is reduced.

Secondly, the precast beam and concrete slab is shown. It is possible to notice some discontinuities at the interface, and that rebars connecting the two concrete elements are subjected to higher stresses as they are closer to the nib. Beam failure mode is not changing, such as cracks formation and propagation.

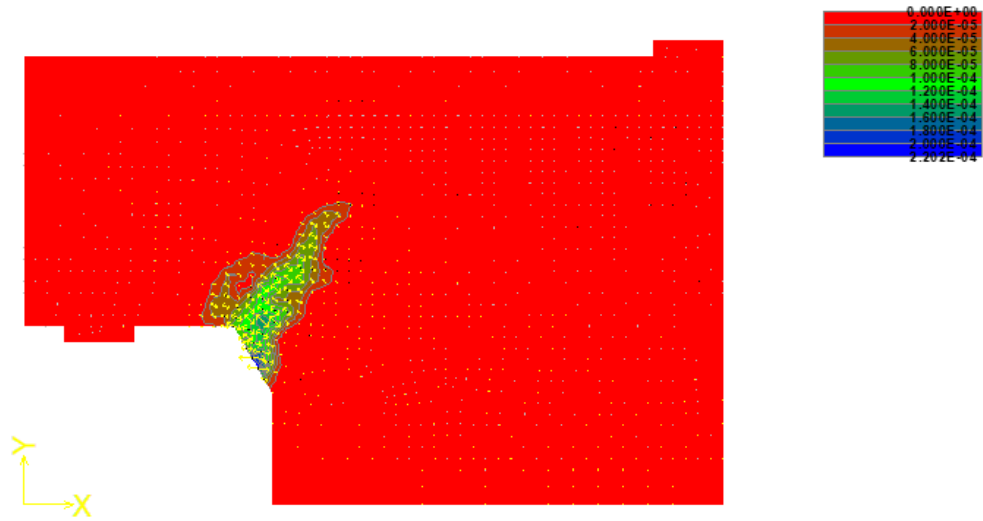


Figure 6.56: step 8, crack width at crack initiation

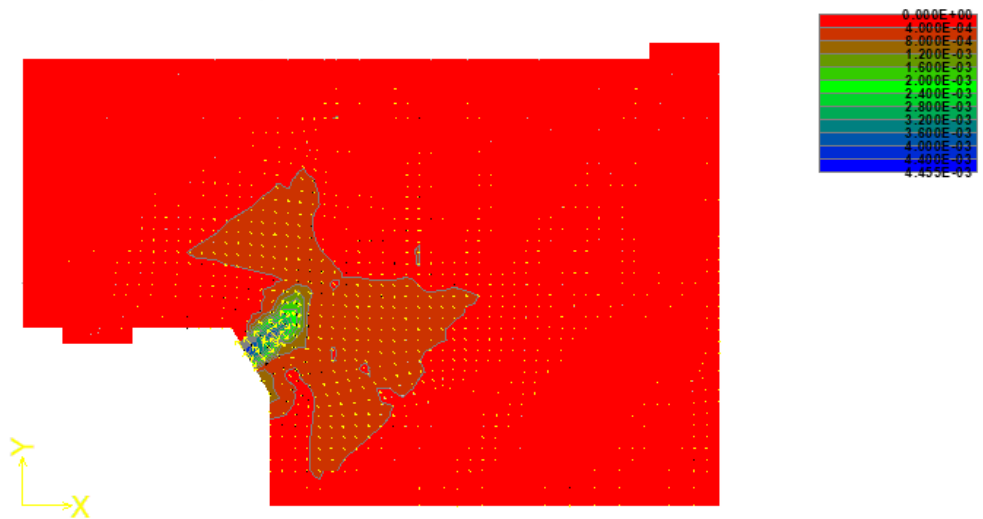


Figure 6.57: step 140, crack width at crack development

When the slab is applied, crack width is reduced as a consequence of the stiffness increase.

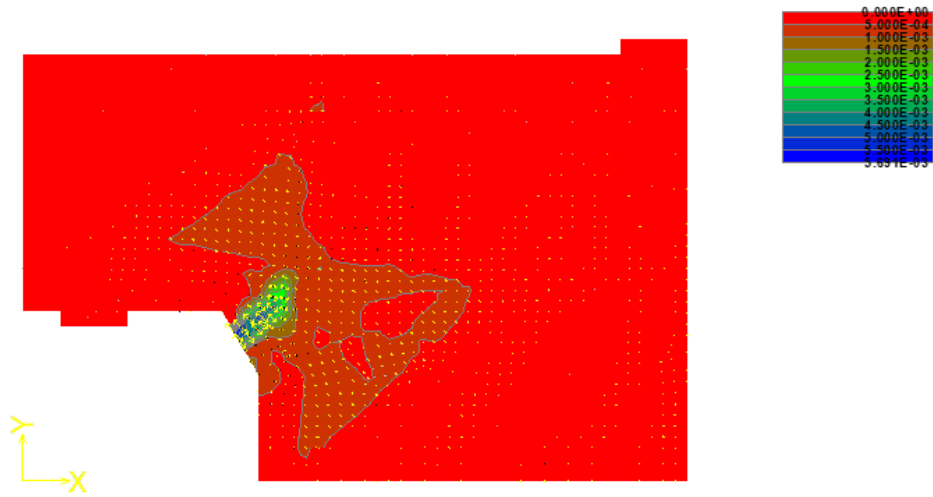


Figure 6.58: step 179, crack width at peak resistance

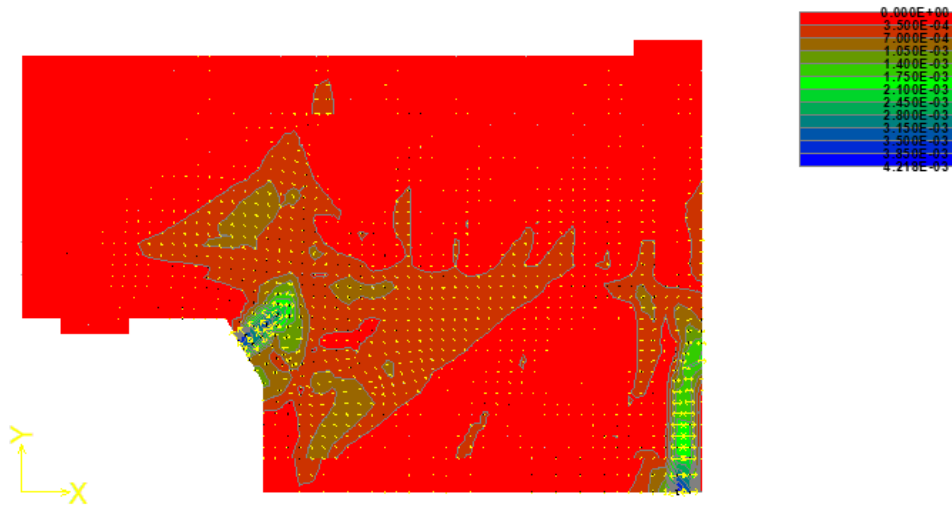


Figure 6.59: step 220, crack width at beam failure

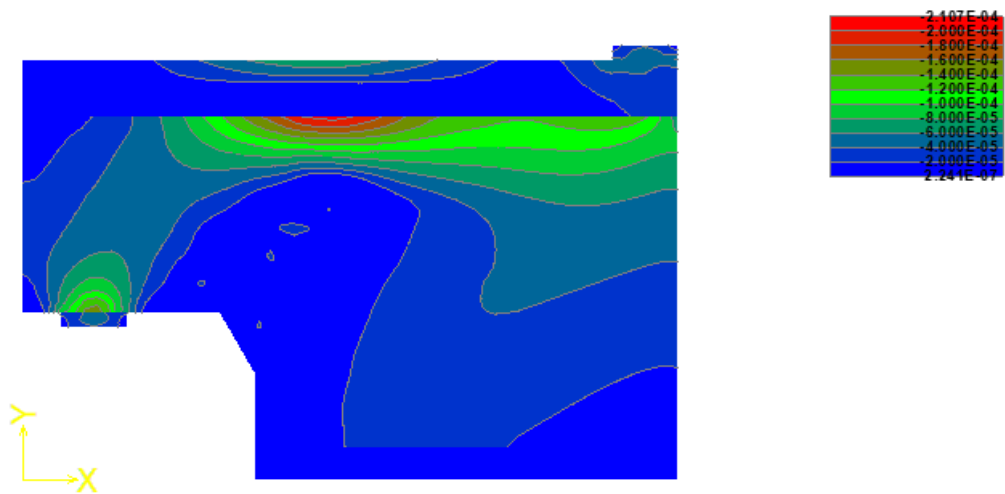


Figure 6.60: step 8, concrete strain at crack initiation

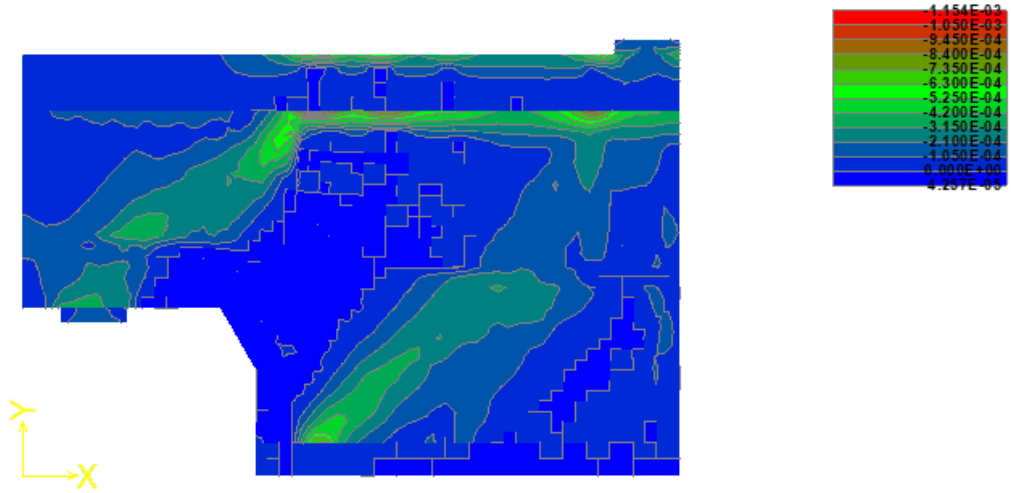


Figure 6.61: step 140, concrete strain at crack development

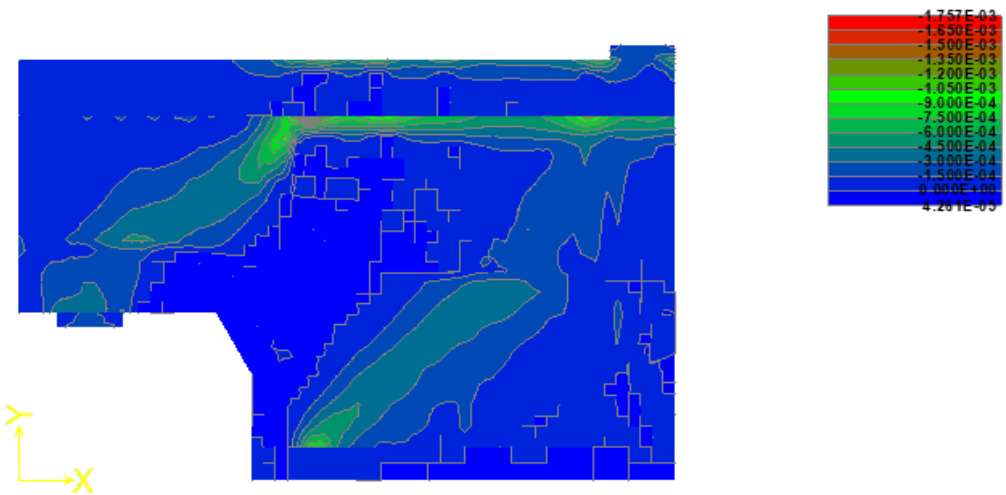


Figure 6.62: step 179, concrete strain at peak load

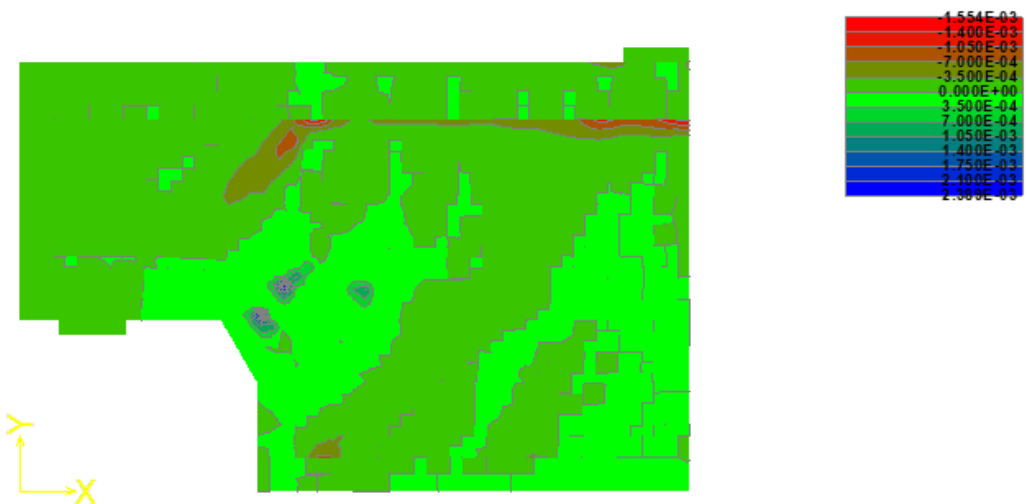


Figure 6.63: step 220, concrete strain at beam failure

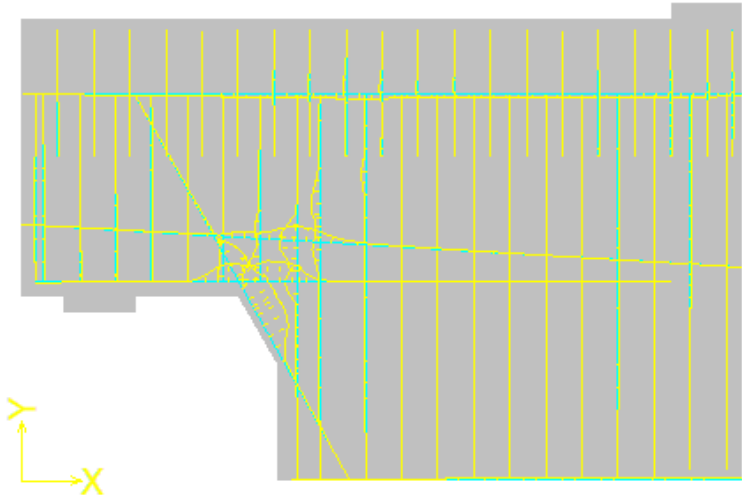


Figure 6.64: step 8, reinforcement internal stresses at crack initiation

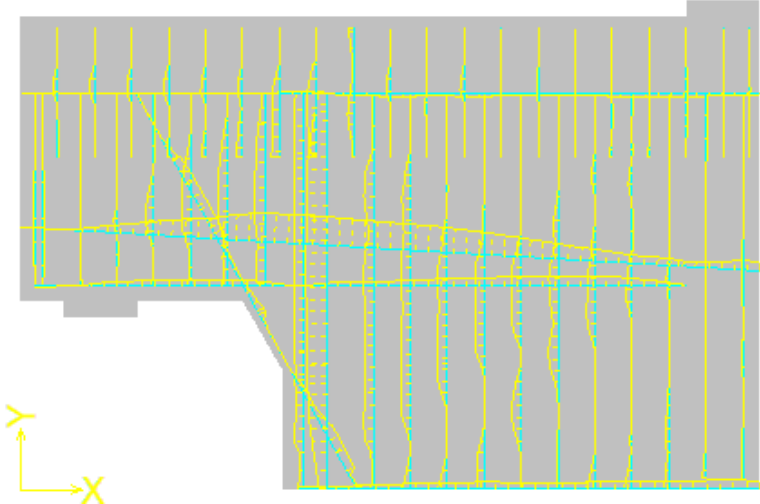


Figure 6.65: : step 140, reinforcement internal stresses at crack development

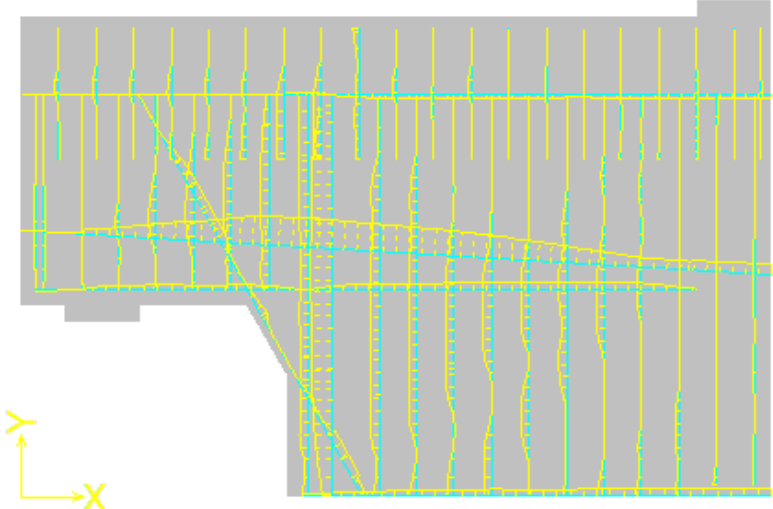


Figure 6.66: step 179, reinforcement internal stresses at peak resistance

At the peak resistance (Figure 6.66) of the half-joint the number of stirrups hypothesised to yield in model *a* vertical tie is confirmed (3 stirrups).

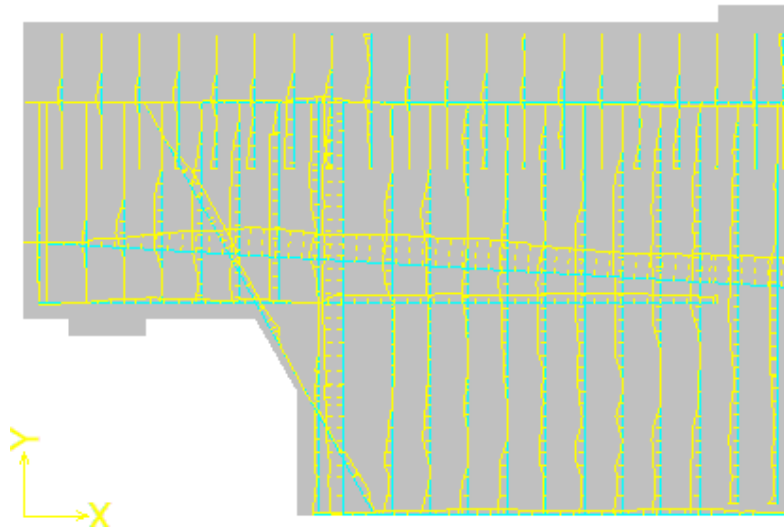


Figure 6.67: step 220, reinforcement internal stresses at beam failure

6.4. DISCUSSION OF OBTAINED RESULTS

The analytical models (strut and tie and kinematic) are applied to five elements coming from a database of the Dutch bridge practice and to a laboratory test.

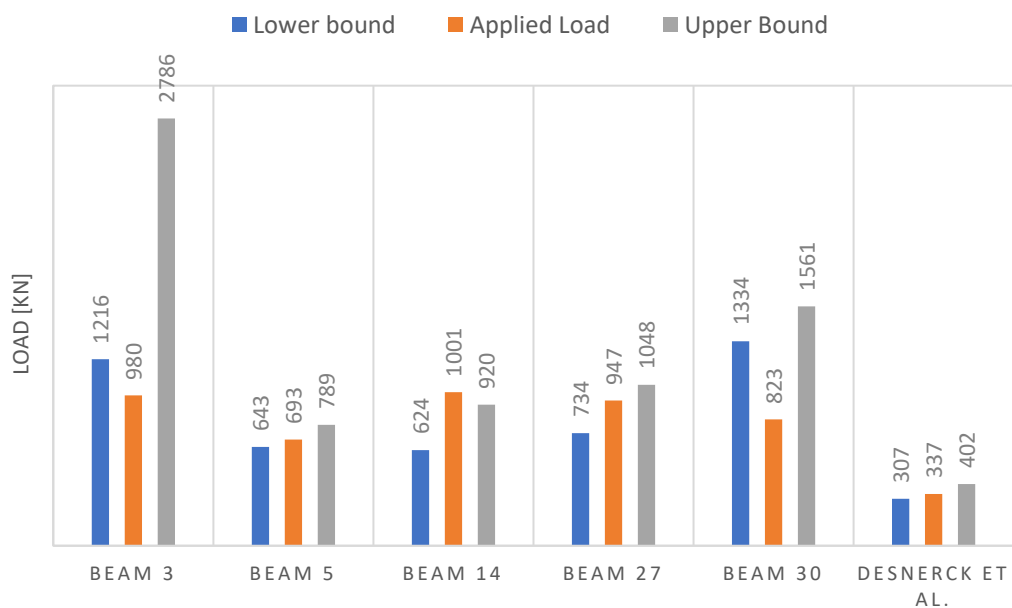


Figure 6.68: analytical model outputs

Results obtained have a generally good agreement with the indications of loads applied, referring to Figure 6.68:

- Two cases (beam 3 and beam 30) have the ideal output with both upper and lower bound values bigger than the acting load;
- Two cases (beam 5 and beam 27) show a less conservative output, but still coherent with the definition of upper and lower bound, in fact the acting load is of a value in between of the two boundaries.
- One case is providing non-coherent results in term of ultimate resistance, and this is beam 14. Both boundaries are smaller than the acting load value.

Hence, a numerical analysis is performed on the joint that is providing controversial results, but it is first validated and calibrated with Desnerck et al. laboratory test. The load displacement curve obtained by the ATENA analysis has a good agreement with the laboratory outputs, considering a 3 cm quadrilateral mesh and fracture energy computed following the Model Code 1990. Initial stiffness, reduced stiffness after cracking, bearing capacity and ductility of the joint are accurately reproduced in the ATENA 2D model results. Moreover, when the load/displacement curve is compared to the results obtained in the analytical model application, it is possible to notice a good fitting of the curve between the two extreme values computed with the lower and upper bound methods.

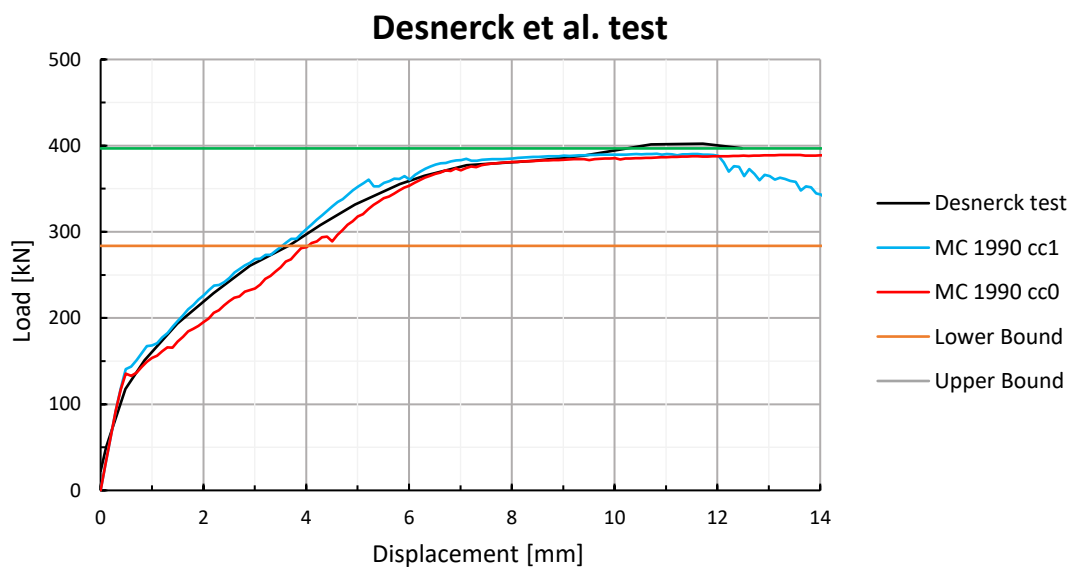


Figure 6.69: Desnerck et al. L/d curve

As previously mentioned in chapter 4.1, the upper bound is unsafe for several reasons but it is usually more accurate than the lower bound. This aspect is highlighted in Figure 6.69, where the upper bound line is almost coincident to the peak of the L/d curve. The lower bound provides conservative results, in all cases it gives ultimate strength values smaller than the resistance outlined by the numerical analyses.

The case of beam 14 half-joint is analysed because the analytical model shows contradictory results when compared to the design value of the joint: both the upper and lower bound are smaller than the assumed applied load. A deeper analysis with the ATENA software was necessary, therefore numerical analyses have been carried on beam 14 with and without the concrete slab on top of the precast inverted T beam and the output here shown is referred to the precast beam and cast in situ slab, with a friction coefficient $\phi=0.5$.

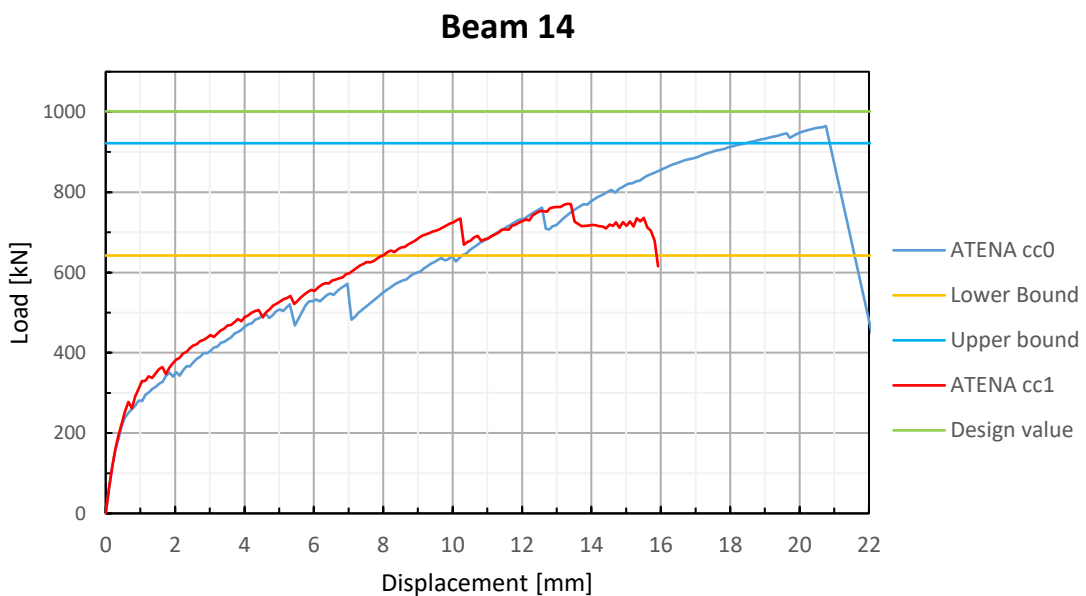
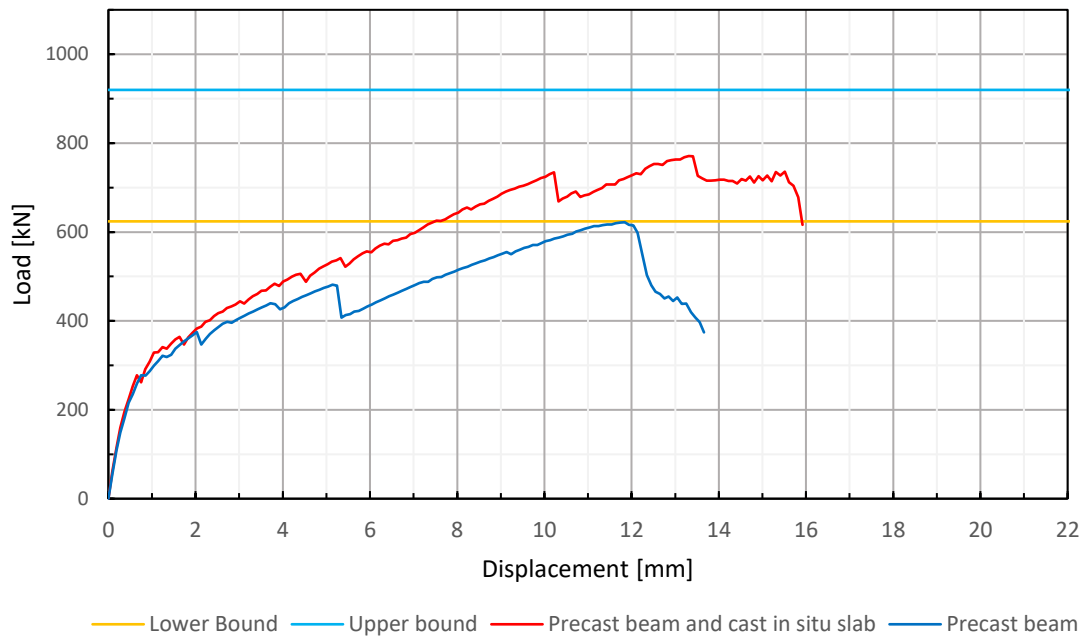


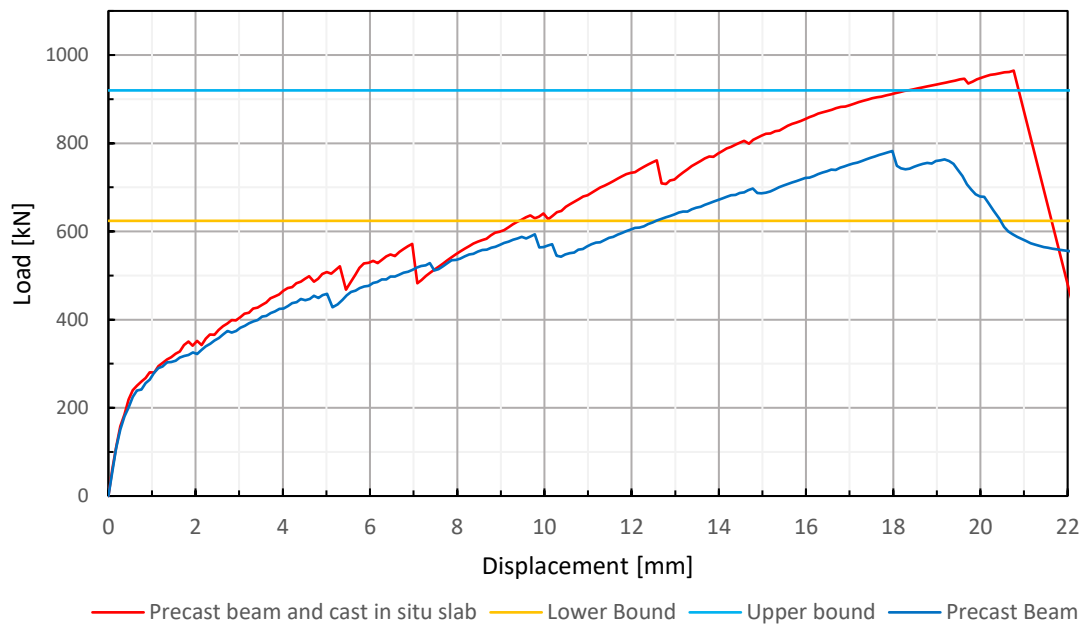
Figure 6.70: Beam 14 L/d curve, precast beam and cast in situ slab

The Load/displacement curve is fitting between the two extreme values of the upper and lower bound analyses, thus confirming the analytical model results. Slab influence is highlighted with a direct comparison between the two Load/displacement curves.

Beam 14, Fixed crack model



Beam 14, Rotated crack model



When the cast in situ slab is applied and hardened on top of the inverted precast T beam, both fixed and rotated crack models show an increase in strength and stiffness: the peak load is larger and so it is the ultimate displacement. It is possible to notice in both fixed and rotated crack

models that when concrete tensile strength is exceeded, the cross section is cracking and therefore entering in the plastic field, the beam with concrete slab is less sensitive to the cross section weakening caused by cracks formation and propagation. Cracks are in fact smaller and more distributed, thus less impacting. It is also true that the failure is more brittle and dangerous.

ATENA renderings confirm several aspects:

- Cracks formation is at the nib;
- Failure of the analysed half-joint is due to reinforcement yielding and not concrete crushing;
- The number of considered stirrups in the model a is confirmed;
- Longitudinal reinforcement does not yield;
- Vertical reinforcement is mainly exploited when close to the nib;
- Interface between cast in situ slab and precast beam is affecting the peak resistance and maximum displacement;
- Concrete strain at crack development (Figure 6.61) and peak resistance (Figure 6.62) clearly shows the inclined concrete struts of model a truss.

6.5. CONCLUSIONS

The proposed strut and tie model has been applied to several half-joints in chapter 5, and in this chapter a numerical analysis with ATENA 2D has been performed in order to strengthen the results coming from the analytical analyses of two selected half-joints.

First, the program ATENA 2D is introduced and explained in its principal characteristics and technical aspects: pre-processing and post-processing interface, solution parameters and theoretical background are shown.

Then, the numerical model is validated with Desnerck, Lees and Morley's laboratory test carried on a half-joint, showing a good compliance between the Load/displacement and Load/crack width curves obtained by direct testing and the ones coming from the numerical analysis. Different results are obtained with the variation of the fixed crack coefficient, mesh size and

fracture energy to check the model sensitivity to those parameters and to obtain a strong compromise that could be considered of good agreement to Desnerck et al. laboratory test. ATENA 2D post-processing could highlight the assumptions made in the analytical analyses, such as crack location, failure mode and stirrups concurring at the model trusses. The lower bound is proven to be a safe estimation of the joint resistance, while the upper bound is providing an unsafe but more accurate indication of it.

Finally, the numerical model is applied to beam 14 half-joint of the Dutch database, whose analysis had contradictory results with the analytical models. The analysis is performed on the precast beam with and without applied slab, to outline the influence of the concrete layer on the ultimate resistance, ductility and stiffness. To have a congruent simulation, the interface between the precast beam and the concrete slab is modelled following ATENA manual indications and vertical steel elements are set to allow a proper connection. ATENA 2D shows a good agreement to the models proposed by the thesis, since the load/displacement curve is in between the two boundaries highlighted by the upper and lower bounds.

In the following chapter, a general guideline outlining each step of the model application is provided and explained. It is a fundamental aspect of the proposed thesis work since its accessibility is one of its principal goals.

7. GENERAL GUIDELINE

When a half-joint necessitates to be assessed in its load bearing capacity, a standard procedure can be highlighted and followed. Here, a brief schematization of all passages is reported.

Known the half-joint geometry, reinforcement and concrete classes, work separately on model *a* and model *b* trusses.

1. Model a truss (refer to Figure 7.1 and Table 7.1):

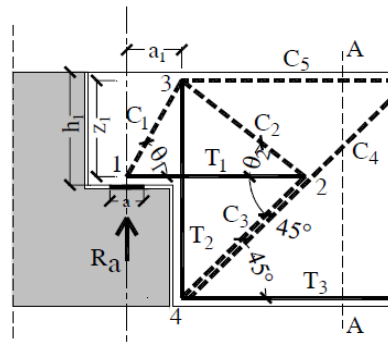


Figure 7.1: model a truss

- a1. Hypothesise the number of stirrups concurring at T_2 steel tie (n_i);
- a2. Compute T_1 and T_2 yielding forces;

$$T_1 = A_{s,h} \cdot f_{yk} + 0.5 f_{pd} \cdot A_{p,l} \quad (7.1)$$

$$T_2 = n_i \cdot A_{s,v} \cdot f_{yk} + 0.5 f_{pd} \cdot A_{p,v} \quad (7.2)$$

- a3. Define the resistance of the joint in function of the two steel elements (see Table 7.1) and identify the weakest:

$$R_a(T) = \min (R_a(T_1); R_a(T_2)) \quad (7.3)$$

- a4. Decide a standard to follow (Eurocodes, ACI, national standards etc.) to define struts' and nodes' strength;
- a5. Calculate all struts compressive strenghts, based on point a4 (see chapter 3.3.1);
- a6. Verify that the concrete struts can withstand the stresses caused by the force $R_a(T)$, referring to Table 7.1;
- a7. If point a5 is verified, the resistance of the joint is function of the steel elements:

$$R_a = R_a(T) \quad (7.4)$$

- a8. If point a5 is not verified, define the resistance of the joint in function of the weakest concrete member (Table 7.1):

$$R_a = R_a(C) = \min (R_a(C_1); R_a(C_2)) \quad (7.5)$$

- a9. Calculate the load acting in each element of the truss, function of R_a ;
- a10. Sum all concrete struts loads concurring to node 4 and check the geometry of the node (refer to chapter 3.4.3), and verify the number of stirrups concurring to that node as follows:

- a10.1. Define a collaborative width of the struts concurring to node 4 equal to $6d$ on both arms of the stirrups;

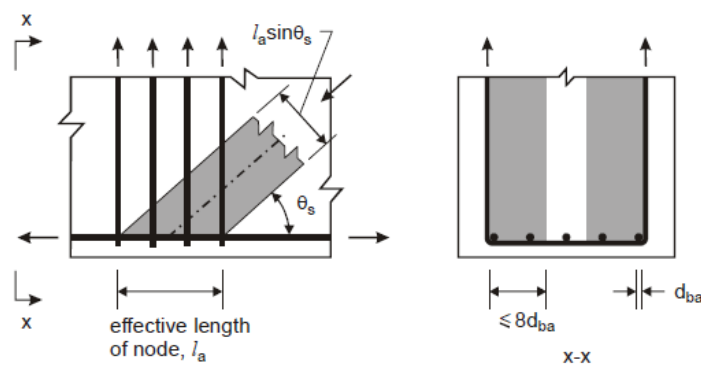


Figure 7.2: schematization of the geometry of the strut (chapter 3.4.3)

- a10.2. Calculate the length l_a of the node, known the acting force and the width $6d$;
- a10.3. Check that all the stirrups hypothesised are distant l_a at maximum from the first stirrup nearby the nib.

- a11. If point a10.3 is not verified the number of stirrups concurring to node 4 is not correct: go back to point a1 and reduce the number of stirrups in the steel tie T_1 ($n_{i+1} < n_i$);
- a12. If point a10.3 is verified, the number of stirrups is correct, the resistance of the joint is defined as R_a .

Model a internal truss forces			
$C_{1,Ed}$	$R_a / \sin\theta_1$	$R_a(C_1)$	$C_1 \cdot \sin\theta_1$
$C_{2,Ed}$	$\frac{R_a}{[\tan\theta_1 \cdot (\sin\theta_2 + \cos\theta_2)]}$	$R_a(C_2)$	$C_2 \cdot [\tan\theta_1 \cdot (\sin\theta_2 + \cos\theta_2)]$
$C_{3,Ed}$	$\sqrt{2} \frac{R_a}{[\tan\theta_1 \cdot (1 + \cot\theta_2)]}$	$R_a(C_3)$	$C_3 \cdot \frac{[\tan\theta_1 \cdot (1 + \cot\theta_2)]}{\sqrt{2}}$
$C_{4,Ed}$	$\sqrt{2} R_a$	$R_a(C_4)$	$C_4 / \sqrt{2}$
$T_{1,Ed}$	$R_a / \tan\theta_1$	$R_a(T_1)$	$\tan\theta_1 \cdot T_1$
$T_{2,Ed}$	$R_a + \frac{R_a}{[\tan\theta_1 \cdot (1 + \cot\theta_2)]}$	$R_a(T_2)$	$\frac{[\tan\theta_1 \cdot (1 + \cot\theta_2)]}{[1 + \tan\theta_1 \cdot (1 + \cot\theta_2)]} \cdot T_2$

Table 7.1: model a truss internal forces

2. Model b truss (refer to Figure 7.3 and Table 7.2):

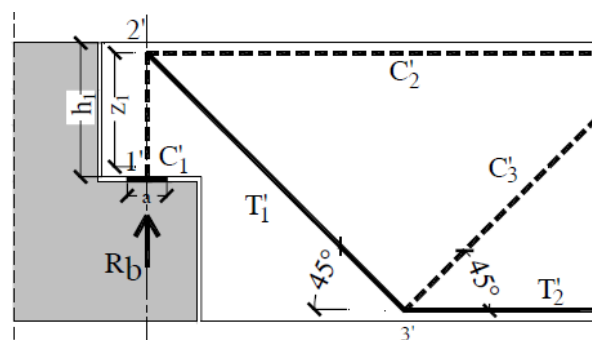


Figure 7.3: model b truss

b1. Compute T_1 yielding force;

$$T_1 = A_{s,d} \cdot f_{yk} \quad (7.6)$$

b2. Define the resistance of the joint in function of T_1 ;

$$R_b(T) = R_b(T_1) \quad (7.7)$$

b3. Calculate all struts compressive strenght, based on point a4 (see chapter 3.3.1);

b4. Verify that the concrete struts can withstand the stresses caused by the force $R_b(T)$, referring to Table 7.2;

b5. If point b4 is verified, the resistance of the joint is function of the steel element:

$$R_b = R_b(T) \quad (7.8)$$

b6. If point b4 is not verified, define the resistance of the joint in function of the weakest concrete member:

$$R_b = R_b(C) = R_b(C_1) \quad (7.9)$$

Model <i>b</i> internal truss forces			
$C_{1,Ed}$	R_b	$R_b(C_1)$	C_1
$C_{2,Ed}$	$R_b/\tan\theta$	$R_b(C_2)$	$\tan\theta \cdot C_2$
$T_{1,Ed}$	$R_b/\sin\theta$	$R_b(T_1)$	$\sin\theta \cdot T_1$
$T_{2,Ed}$	$R_b/\tan\theta$	$R_b(T_2)$	$\tan\theta \cdot T_2$

Table 7.2: model *b* truss internal forces

3. Define the resistance of the joint as the sum of the two components

$$R = R_a + R_b$$

8. FURTHER RESEARCH

This thesis provides a deep analysis of half-joints lower bound resistance: based on the strut and tie method. However, the author is aware that the topic is wide, with several aspects that can be the object of future research. Therefore in this chapter possible topics of future studies are suggested.

Slab influence

When an inverted T beam is positioned, it is necessary to place a cast in situ slab on top of the precast elements. This concrete slab is influencing the structure behaviour, as highlighted from the numerical simulations in chapter 6.3.

Of course, several parameters are influencing the performance and its improvement, such as the slab geometry and material class, the type of interface and type of connecting elements. Further investigation of these parameters could provide interesting results, also considering issues of strengthening or repairing.

Concrete protection

Concrete is highly sensitive to environmental attacks, that lead to strength loss, plastic shrinkage, decrease of service life. Research went through the direction of defining new tools to protect the concrete surface from direct contact with the environment, and strong results have been provided by material and concrete researchers⁹¹. However, de-icing salt coming from the road surface is often the cause of further concrete deterioration, enhancing sulphate attacks that cause physical and chemical degradation, and in this case too, surface treatments or some considerations about w/c in design can provide good results⁹².

De-icing salt seepage is a dangerous mechanism that easily induces reinforcement corrosion, and it is also more effective when concrete is cracked. For this purpose, it can be interesting to test the influence of the application of self-healing concrete. This technique exploits living

bacteria, that can survive to concrete mixing and casting, and which are responsible of calcium carbonate formation and oxygen consumption: as concrete cracks, oxygen seeps inside the concrete activating such bacteria, whose digestion mechanism causes micro-cracks filling and an oxygen barrier that protects steel reinforcement⁹³.

These examples come from current research efforts, that could be of interesting application in half-joint strengthening and maintenance procedures.

Rebars corrosion: loss of ductility and strength

It has been proved that the rebars corrosion can be associated to cross section or steel strength reduction. It is one of the most severe half-joint deterioration mechanisms, since inspections to the most critical parts is not possible (Desnerck et al.⁹ simulation proved that a nib reinforcement reduction of 50% due to corrosion leads to a strength loss). Corrosion of the steel rebars in concrete is correlated to several effects⁷⁰: further concrete cracking (rust occupies a larger volume than steel), reduction of steel strength and ductility, reduction of bond between steel and concrete are just a few examples.

Further research on half-joints can investigate the influence of various stages of reinforcement corrosion, and its effect in ductility of the element.

Guidelines for field inspections

Field inspections usually provide qualitative indications on the structural health, with poor technical aspects. Unfortunately, it is not possible to perform extensive load tests on existing structures, because of technical and management limitations, therefore it can be interesting and significantly impacting to include field inspections qualitative results into a model, to deal with deteriorated elements in a quantitative point of view. The main problem when dealing with half-joints is that most of the critical parts are not accessible, but with a snake-eye camera it is usually possible to have a visual inspection of the remote areas too⁹⁴.

Geometry of the beam influence

The geometry of the beam and of the nib directly affects the crack formation and strength of the joint. As mentioned before, the cast in situ slab causes a stiffness and resistance increase in the precast element, and other elements such as the beam shape (inverted T, box beam or full-concrete beam), web (or webs) thickness, nib angle and concrete cover can be investigated in order to prove their influence on the half-joint failure.

External prestressing strengthening

Most of Gerber beams are prestressed, because the introduction of a compression stress in the element could allow the achievement of longer spans. The use of external prestressing has proved to be a powerful tool^{95,96} when dealing with bridge rehabilitation and it could be tested in case of half-joints, simply reinforced and prestressed.

Stop criteria calibration

Half-joints monitoring is a topic not properly studied. Yet, investigation in this direction can provide original research and useful tools, since most of these structures are getting to the end of their lifetime. Stop criteria rely on crack control and are mainly used in combination to proof load tests, to determine the threshold that indicates if the bridge passes the test or not.

While the original application of such criteria is for flexural cracks⁹⁷, in the recent years there have been a first recalibration to shear cracks^{98,99}. It can be interesting to investigate a possible application of stop criteria also to Gerber joints, mainly for two reasons:

- They can provide early warning of the failure, so they can be applied also in case of critical failure modes (shear failures are brittle);
- There is usually one main crack developing in the half-joints, so the critical crack width is not distributed in several cracks.

9. CONCLUSIONS

Half-joints are structural elements widely used in the 1960s-1980s, and that now are getting at the end of their service life, after years of environmental attacks, some repairing and some damages. Literature review has shown an extensive research activity carried on during the 1970s and 1980s focussed on reinforcement layout optimization, crack control and ultimate resistance enhancement, while in the recent years the focus moved towards strengthening solutions and deterioration processes simulation. Nowadays, there are inheriting structures that are subjected to years of environmental attacks, sometimes with small damages and repairing, sometimes strengthened or apparently in a perfect conservation state of their materials and functionality. Hence, while on one side there is a non-conformity to nowadays standards and a questionable design and construction, on the other side there are problems that affect all structures, also the ones with non-arguable design aspects: traffic loads have increased substantially, many existing structures are about to reach their end-of-life and environmental events cause inevitable degradation on materials.

The purpose of this thesis is then to develop a model that can easily and safely define the limit resistance of a half-joint: it is based on the strut and tie method, which is representing an application of the lower bound plasticity theorem, providing conservative indication of the ultimate resistance of the joint. For the sake of completeness, an alternative and complementary method is introduced and exploited to define an upper bound of strength: the kinematic method was widely used in the past to deal with half-joints or similar elements but it provides unsafe results, even if more accurate. Assumptions have been made to consider all possible elements concurring to the models, regarding the prestressing aspect, the geometry of the trusses and the inclination of the crack forming at the nib.

Both models have been applied to several half-joints example of existing structures and laboratory tests: they could adapt to several reinforcement layouts, beam and joints geometry, materials, prestressing strands.

Among the analytical applications, one case provided non-congruent results (half-joint of beam 14), since both lower and upper bounds were smaller than the acting load indicated: a numerical analysis was then performed to study this incongruence.

After a brief introduction to the ATENA 2D finite element programme, the numerical model has been calibrated on Desnerck, Lees and Morley laboratory test, showing an excellent agreement in terms of load/displacement curves and load/crack width curves, after a calibration on mesh size, fracture energy and crack propagation in concrete. Afterwards, the numerical analysis is performed on the half-joint of the Dutch practice, confirming the analytical models' achievements: the load/displacement curves develop in between the boundaries calculated, validating the S&T and kinematic models.

The analysis on beam 14 half-joint has been performed with and without cast in situ concrete slab, to highlight its influence on the overall strength, stiffness and failure mode: the interface material influence on the overall strength and stiffness, showing the non-reliability of the kinematic method compared to the strut and tie. In fact, the kinematic method is relying on several hypothesis, among which the perfect bond between precast and cast in situ concrete elements. This is an idealization of reality, in fact even though there are connecting elements between the two concrete layers, and the concrete cast in situ is bonding to the precast concrete, some slip is inevitable (also shown in the numerical simulation), causing a decrease of the ultimate resistance.

In conclusion, the analytical models could perfectly adapt to all half-joints analysed, providing safe results and accurate indications of the ultimate strength of such elements. The numerical analysis is validated with Desnerck et al. laboratory tests and confirms the achievements of the strut and tie and kinematic models, such as crack location, stirrups concurring to a single tie, models superpositions and prestressing strands contribution.

10. REFERENCES

1. Mattock AH, Chan TC. Design and behaviour of dapped end beams. *PCI Journal*. 1979;18:37-49.
2. Barton DL, Anderson RB, Bouadi A, Jirsa JO, Breen JE. *Investigation of Strut-and-Tie Models for Dapped Beam Details*. Texas Univ. at Austin. Center for Transportation Research; 1991.
3. Bossio A, Lignola GP, Prota A. An overview of assessment and retrofit of corroded reinforced concrete structures. In: *Procedia Structural Integrity*. Vol 11. Elsevier B.V.; 2018:394-401. doi:10.1016/j.prostr.2018.11.051
4. Werner MP, Dilger WH. Shear Design of prestressed concrete stepped beams. *J Prestressed Concr Inst*. 1973;18(4):37-49. doi:10.15554/pcij.07011973.37.49
5. Taher SE-DMF. Strengthening of critically designed girders with dapped ends. *Proceedings of the Institution of Civil Engineers - Structures and Buildings*. 2005;158(2):141-152. doi:10.1680/stbu.2005.158.2.141
6. Sas G, Dăescu C, Popescu C, Nagy-György T. Numerical optimization of strengthening disturbed regions of dapped-end beams using NSM and EBR CFRP. *Composites Part B: Engineering*. 2014;67:381-390. doi:10.1016/j.compositesb.2014.07.013
7. Desnerck P, Lees JM, Morley C. Assessment of Reinforced Concrete Half-Joint Structures: Dealing with Deterioration. Published online 2014.
8. Desnerck P, Lees JM, Morley CT. The effect of local reinforcing bar reductions and anchorage zone cracking on the load capacity of RC half-joints. *Engineering Structures*. 2017;152:865-877. doi:10.1016/j.engstruct.2017.09.021

-
9. Desnerck P, Lees JM, Morley CT. Strut-and-tie models for deteriorated reinforced concrete half-joints. *Engineering Structures*. 2018;161:41-54. doi:10.1016/j.engstruct.2018.01.013
 10. Desnerck P, Lees JM, Morley CT. Impact of the reinforcement layout on the load capacity of reinforced concrete half-joints. *Engineering Structures*. 2016;127:227-239. doi:10.1016/j.engstruct.2016.08.061
 11. Temple, Jonathan. Structural Change and Europe's Golden Age. *CEPR Discussion Papers*. Published online 2001.
 12. Alvarez-Cuadrado F, Pinteá MI. A quantitative exploration of the Golden Age of European growth. *Journal of Economic Dynamics and Control*. 2009;33(7):1437-1450. doi:10.1016/j.jedc.2009.02.004
 13. Roads in the Netherlands - Wikipedia. Accessed June 6, 2020. https://en.wikipedia.org/wiki/Roads_in_the_Netherlands#History
 14. di Prisco M. Critical infrastructures in Italy: state of the art, case studies, rational approaches to select the intervention priorities. In: *Fib Symposium*. ; 2019.
 15. Gasparini D. The prestressing of structures: a historical review. In: *Second International Congress on Construction History*. ; 2006:1221-1232.
 16. Menduni Enrico. *L'Autostrada Del Sole*. Il Mulino; 1999.
 17. autostrade.it. Accessed May 13, 2020. https://www.autostrade.it/comunicazione-e-media/mediateca/archivio-storico/-/media-items/image/playlist/storico-a1-Milano-Napoli?p_p_state=pop_up&controlPanelCategory=portlet_media_WAR_mediaportlet
 18. Iori T. L'Autostrada del Sole. In: Cuzzolin, ed. *Primo Convegno Nazionale*. ; 2006:1111-1120.
 19. Morandi R. *The Long-Term Behaviour of Viaducts Subjected to Heavy Traffic and Situated in an Aggressive Environment: The Viaduct on the Polcevera in Genoa*.; 1979.
 20. Gonzalez JA, Algaba S, Andrade C. Corrosion: Of reinforcing bars in carbonated concrete. *British Corrosion Journal*. 1980;15(3):135-139. doi:10.1179/bcj.1980.15.3.135

21. Snyder MJ. *Protective Coatings to Prevent Deterioration of Concrete by Deicing Chemicals.*; 1965.
22. COLLEPARDI M, MARCIALIS A, TURRIZIANI R. Penetration of Chloride Ions into Cement Pastes and Concretes. *Journal of the American Ceramic Society.* 1972;55(10):534-535. doi:10.1111/j.1151-2916.1972.tb13424.x
23. Otsuki N, Miyazato S, Yodsudjai W. Influence of Recycled Aggregate on Interfacial Transition Zone, Strength, Chloride Penetration and Carbonation of Concrete. *Journal of Materials in Civil Engineering.* 2003;15(5):443-451. doi:10.1061/(ASCE)0899-1561(2003)15:5(443)
24. Šauman Z. Carbonization of porous concrete and its main binding components. *Cement and Concrete Research.* 1971;1(6):645-662. doi:10.1016/0008-8846(71)90019-6
25. Ministero delle Infrastrutture e dei Trasporti, Consiglio superiore dei Lavori Pubblici. *Linee Guida per La Classificazione e Gestione Del Rischio, La Valutazione Della Sicurezza Ed Il Monitoraggio Dei Ponti Esistenti.*; 2020.
26. Matthews S, Bigaj-van Vliet A, Walraven J, Mancini G, Dieteren G. fib Model Code 2020: Towards a general code for both new and existing concrete structures. *Structural Concrete.* 2018;19(4):969-979. doi:10.1002/suco.201700198
27. Heinrich Gottfried Gerber - Wikipedia. Accessed June 10, 2020. https://it.wikipedia.org/wiki/Heinrich_Gottfried_Gerber
28. Bazzucchi F, Restuccia L, Ferro GA. Considerations over the Italian road bridge infrastructure safety after the polcevera viaduct collapse: Past errors and future perspectives. *Frat-tura ed Integrità Strutturale.* 2018;12(46):400-421. doi:10.3221/IGF-ESIS.46.37
29. Morandi R. Il viadotto sul Polcevera per l'autostrada Genova-Savona. *L'industria italiana del Cemento.* 1967;XXXVII:849-872.
30. Ponti articolati e continui: 150 anni di esperienze – prima parte - Pagina 2 di 7 - Strade & Autostrade Online. Accessed May 13, 2020. <https://www.stradeeautostrade.it/ponti-e-viadotti/ponti-articolati-e-continui-150-anni-di-esperienze-prima-parte/2/>
31. Mathivat Jacques. *The Cantilever Construction of Prestressed Concrete Bridges.* J. Wiley; 1983.

-
32. di Prisco M, Colombo M, Martinelli P, Coronelli D. The technical causes of the collapse of Annone overpass on SS.36. Published online 2018:1-16.
 33. Mitchell D, Marchand J, Croteau P, Cook WD. Concorde overpass collapse: Structural aspects. *Journal of Performance of Constructed Facilities*. 2011;25(6):545-553. doi:10.1061/(ASCE)CF.1943-5509.0000183
 34. Ghosn M, Moses F, Frangopol DM. Redundancy and robustness of highway bridge superstructures and substructures. *Structure and Infrastructure Engineering*. 2010;6(1-2):257-278. doi:10.1080/15732470802664498
 35. Ministero delle infrastrutture e dei trasporti - Commissione ispettiva ministeriale. Accessed September 9, 2020. <https://www.lavoripubblici.it/normativa/20180914/Ministero-delle-infrastrutture-e-dei-trasporti-Commissione-ispettiva-ministeriale-18245.html>
 36. Domaneschi M, Pellicchia C, de Iulius E, et al. Collapse analysis of the Polcevera viaduct by the applied element method. *Engineering Structures*. 2020;214. doi:10.1016/j.engstruct.2020.110659
 37. Collins MP, Mitchell D. A Rational Approach to shear design - The 1984 Canadian code provisions. *Journal of the American Concrete Institute*. 1986;83.
 38. De la Concorde overpass: Before and after the collapse | CBC News. Accessed May 13, 2020. <https://www.cbc.ca/news/canada/montreal/de-la-concorde-overpass-collapse-timeline-1.3784265>
 39. Collins MP. Towards a Rational Theory for RC Members in Shear. Published online 1978.
 40. Ritter W. Die Bauweise Hennebique. *Schweizerische Bauzeitung*. 1899;33(7):49-52. doi:10.3931/e-rara-20036
 41. Morsch E. *Concrete-Steel Construction (Der Eisenbetonbau)*. The Engineering News Pub. Co.; 1909.
 42. Kupfer H. GENERALIZATION OF MORSCH'S TRUSS ANALOGY USING THE PRINCIPLE OF MINIMUM STRAIN ENERGY. Published online 1964.
 43. Leonardt F. Reducing the shear reinforcement in reinforced concrete beams and slabs. *Magazine of Concrete Research*. 1965;17(53):187-198. doi:10.1680/mac.1965.17.53.187

44. Collins MP, Mitchell D. SHEAR AND TORSION DESIGN OF PRESTRESSED AND NON-PRESTRESSED CONCRETE BEAMS. *Journal - Prestressed Concrete Institute*. 1980;25(5):32-100. doi:10.15554/pcij.09011980.32.100
45. Marti P. BASIC TOOLS OF REINFORCED CONCRETE BEAM DESIGN. *Journal of the American Concrete Institute*. 1985;82(1):46-56. doi:10.14359/10314
46. Lampert P, Thürlimann B. *Ultimate Strength and Design of Reinforced Concrete Beams in Torsion and Bending*. Birkhäuser Basel; 1972. doi:10.1007/978-3-0348-5954-7_1
47. Wagner H, Flugtechn Z. Motorluftschiffahrt 20. Published online 1929.
48. Schlaich J, Schafer K, Jennewein M. Towards a Consistent Design of Structural Concrete. *PCI Journal*. 1987;32:74-150.
49. Muttoni A, Schwartz J, Thürlimann B. *Design of Concrete Structures with Stress Fields*. Birkhäuser Basel; 1996.
50. Ruiz M, Muttoni A. *On Development of Suitable Stress Fields for Structural Concrete*. Accessed May 15, 2020. <http://i-concrete.epfl.ch/>
51. Reynolds GC, Cement and Concrete Association. *The Strength of Half-Joints in Reinforced Concrete Beams*. Cement and Concrete Association; 1969.
52. Mattock AH. Design Proposals for Reinforced Concrete Corbels. *J Prestressed Concr Inst*. 1976;21(3):18-42. doi:10.15554/pcij.05011976.18.42
53. Liem SK. Maximum shear strength of dapped-end or corbel. Published online 1983.
54. Moreno-Martínez JY, Meli R. Experimental study on the structural behavior of concrete dapped-end beams. *Engineering Structures*. 2014;75:152-163. doi:10.1016/j.engstruct.2014.05.051
55. Vecchio FJ, Collins MP. MODIFIED COMPRESSION-FIELD THEORY FOR REINFORCED CONCRETE ELEMENTS SUBJECTED TO SHEAR. *Journal of the American Concrete Institute*. 1986;83(2):219-231. doi:10.14359/10416
56. Cook WD, Mitchell D. Studies of disturbed regions near discontinuities in reinforced concrete members. *ACI Struct Journal*. 1988;85.

-
57. Clark L, Thorogood P. Serviceability behaviour of reinforced concrete half-joints. *Struct Eng.* 1988;66:295-302.
 58. Nanni A, Huang PC. Validation of an alternative reinforcing detail for the dapped ends of prestressed double tees. *PCI Journal.* 2002;47(1):38-49. doi:10.15554/pcij.01012002.38.49
 59. Mattock AH, Theryo TS. STRENGTH OF PRECAST PRESTRESSED CONCRETE MEMBRANES WITH DAPPED ENDS. *Journal - Prestressed Concrete Institute.* 1986;31(5):58-75. doi:10.15554/pcij.09011986.58.75
 60. Aswin M, Mohammed B, ... ML-A in M, 2015 undefined. Shear failure of RC dapped-end beams. *hindawi.com.* Accessed May 13, 2020. <https://www.hindawi.com/journals/amse/aa/309135/abs/>
 61. Mattock. Strut-and-Tie Models for Dapped-End Beams. *Concrete International.* 2012;34(2):35-40.
 62. Nagrodzka-Godycka K, Piotrkowski P, Windisch A. Experimental study of dapped-end beams subjected to inclined load. *ACI Structural Journal.* 2012;109(6):901-902. doi:10.14359/51683489
 63. Lu WY, Chen TC, Lin IJ. Shear strength of reinforced concrete dapped-end beams with shear span-to-depth ratios larger than unity. *Journal of Marine Science and Technology (Taiwan).* 2015;23(4):431-442. doi:10.6119/JMST-015-0511-1
 64. Abdul-Jawad HM. Modelling of dapped-end beams using Abaqus software. *IJCIET.* Published online 2018.
 65. Ajina J. Effect of Steel Fibers on Precast Dapped-End Beam Connections. Published online 1986.
 66. Lu WY, Lin IJ, Hwang SJ, Lin YH. Shear strength of high-strength concrete dapped-end beams. *Journal of the Chinese Institute of Engineers, Transactions of the Chinese Institute of Engineers, Series A/Chung-kuo Kung Ch'eng Hsueh K'an.* 2003;26(5):671-680. doi:10.1080/02533839.2003.9670820
 67. Mohamed R, Elliott K. Shear strength of short recess precast dapped end beams made of steel fibre self-compacting concrete.

68. Apostolopoulos CA, Papadakis VG. Consequences of steel corrosion on the ductility properties of reinforcement bar. *Construction and Building Materials*. 2008;22(12):2316-2324. doi:10.1016/j.conbuildmat.2007.10.006
69. Corrosion of Embedded Materials. Accessed June 10, 2020. <https://www.cement.org/learn/concrete-technology/durability/corrosion-of-embedded-materials>
70. Mak MWT, Desnerck P, Lees J. Correlation between surface crack width and steel corrosion in reinforced concrete. In: *MATEC Web of Conferences*. ; 2018. <https://doi.org/10.1051/matecconf/201819904009>
71. Hamoudi AA, Phang MKS, Bierweiler RA. DIAGONAL SHEAR IN PRESTRESSED CONCRETE DAPPED-BEAMS. *J Am Concr Inst*. 1975;72(7):347-350. doi:10.14359/11140
72. ACI Committee. Building code requirements for structural concrete. Published online 2014.
73. Gergely P, Publication LL-S, 1968 undefined. Maximum crack width in reinforced concrete flexural members. *concrete.org*. Accessed June 10, 2020. <https://www.concrete.org/publications/internationalconcreteabstractsportal/m/details/id/17348>
74. European Committee for Standardization. EN 1992-1-1 Eurocode 2: Design of concrete structures - Part 1-1: General rules and rules for buildings. In: ; 2005.
75. Comité Euro-International du Béton. *CEB-FIP Model Code 1990*.; 1993.
76. Herzinger R, Elbadry M. Alternative reinforcing details in dapped ends of precast concrete bridge girders: Experimental investigation. *Transportation Research Record*. 2007;(2028):111-121. doi:10.3141/2028-13
77. Desnerck P, Lees JM, Valerio P, Loudon N, Morley CT. Inspection of RC half-joint bridges in England: Analysis of current practice. *Proceedings of the Institution of Civil Engineers: Bridge Engineering*. 2018;171(4):290-302. doi:10.1680/jbren.18.00004
78. Saint-Venant B de. *Memoire Sur La Torsion Des Prismes*. [S.l.]; 1853. Accessed May 18, 2020. <http://hdl.handle.net/2027/hvd.32044091959866>
79. Schlaich M, Anagnostou G. Stress fields for nodes of strut-and-tie models. *Journal of Structural Engineering (United States)*. 1990;116(1):13-23. doi:10.1061/(ASCE)0733-9445(1990)116:1(13)

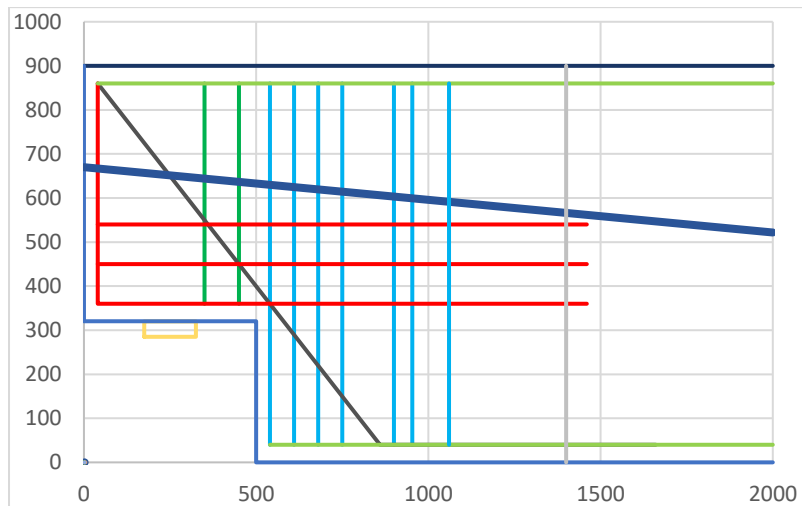
-
80. Schlaich J, Schiifer K. *Design and Detailing of Structural Concrete Using Strut-and-Tie Models*. Accessed May 18, 2020. http://www.pgmecc.ime.br/~webde2/prof/ethomaz/bloco_sobre_estacas/biela_tirante.pdf
81. Fédération internationale du béton. *Fib Model Code for Concrete Structures 2010.*; 2013.
82. Ramirez J. REEVALUATION OF AASHTO DESIGN PROCEDURES FOR SHEAR AND TORSION IN REINFORCED AND PRESTRESSED CONCRETE BEAMS. Published online 1985. Accessed June 12, 2020. <https://elibrary.ru/item.asp?id=7419087>
83. Angiotti F, Guiglia M, Marro P, Orlando M. *Progetto Delle Strutture in Calcestruzzo Armato: Con l'eurocodice UNI-EN 1992-1-1 e Le Norme Tecniche per Le Costruzioni*. Hoepli; 2011.
84. Mitchell D, Collins M. *Revision of Strut-and-Tie Provisions in the AASHTO LRFD Bridge Design Specifications – Final Report.*; 2013.
85. Baker J, Baker L, Heyman J. Plastic design of frames 1 fundamentals. Published online 1980. Accessed October 5, 2020. <https://books.google.com/books?hl=it&lr=&id=Iac5AAAAI-AAJ&oi=fnd&pg=PR7&ots=QjgugRIC6Y&sig=yZ52bC1jSsXRzPQZIk8AonRQiaY>
86. Cervenka V, Jendele L, Consulting JC-C, Prague undefined, 2007 undefined. ATENA program documentation part 1 theory.
87. Kupfer H, Hilsdorf H, Proceedings HR-J, 1969 undefined. Behavior of concrete under biaxial stresses. *concrete.org*. Accessed September 2, 2020. <https://www.concrete.org/publications/internationalconcreteabstractsportal.aspx?m=details&ID=7388>
88. Crisfield MA, Wills J. Analysis Of R/C Panels Using Different Concrete Models. *Journal of Engineering Mechanics*. 1989;115(3):578-597. doi:10.1061/(ASCE)0733-9399(1989)115:3(578)
89. Cervenka V. Constitutive Model for Cracked Reinforced Concrete. *ACI*. 1985;82:877-882.
90. Darwin D, Pecknold DAW. *INELASTIC MODEL FOR CYCLIC BIAXIAL LOADING OF REINFORCED CONCRETE*. University of Illinois Engineering Experiment Station. College of

- Engineering. University of Illinois at Urbana-Champaign.; 1974. Accessed September 3, 2020. <https://www.ideals.illinois.edu/handle/2142/13822>
91. Aguiar J, Camões A, Moreira P. Performance of concrete in aggressive environment. Published online 2008. Accessed September 7, 2020. <https://repositorium.sdum.uminho.pt/handle/1822/12904>
 92. Suleiman AR, Soliman AM, Nehdi ML. Effect of surface treatment on durability of concrete exposed to physical sulfate attack. *Construction and Building Materials*. 2014;73:674-681. doi:10.1016/j.conbuildmat.2014.10.006
 93. Wiktor V, Jonkers HM. Quantification of crack-healing in novel bacteria-based self-healing concrete. *Cement and Concrete Composites*. 2011;33(7):763-770. doi:10.1016/j.cemconcomp.2011.03.012
 94. Santhanam BS, Shah P bt M. Concrete half joint bridges in New South Wales: challenges in risk management. *undefined*. Published online 2011.
 95. Petrangeli MP. *External Prestressing for Bridge Rehabilitation in Italy*. Accessed September 14, 2020. <http://onlinepubs.trb.org/Onlinepubs/conf/1995/cp7/cp7v2-022.pdf>
 96. Harajli MH. *Strengthening of Concrete Beams by External Prestressing*. Accessed September 14, 2020. https://www.pci.org/PCI_Docs/Publications/PCI%20Journal/1993/November/Strengthening%20of%20Concrete%20Beams%20by%20External%20Prestressing.pdf
 97. Lantsoght EOL, Yang Y, van der Veen C, Hordijk DA, de Boer A. Stop criteria for flexure for proof load testing of reinforced concrete structures. *Frontiers in Built Environment*. 2019;5. doi:10.3389/fbuil.2019.00047
 98. Benitez K, Lantsoght E, Yang Y. Development of a stop criterion for load tests based on the critical shear displacement theory. In: *IALCCE 2018*. ; 2018.
 99. Yang Y, Zarate GI, Lantsoght E, Hordijk DA. Calibration of the shear stop criteria based on crack kinematics of reinforced concrete beams without shear reinforcement. In: *Fib Congress*. ; 2018.

APPENDIX

A. ANALYTICAL MODELS: LOWER AND UPPER BOUNDS

A.1 Beam 3



Geometry

height slab	0	mm
height precast	900	mm
height nib	580	mm
length nib	500	mm
eccentricity of support reaction	250	mm
bearing	2 x	rectangular
bearing width	150	mm
width in the other direction or diameter	200	mm
bearing thickness	35	mm
working width	280	mm
slope edge with vertical	90	°

Material

concrete	C55/67	reinforcing steel	FeB500	prestressing steel	FeP1860			
f_{ck}	55	MPa	f_s (A)	435	MPa	f_{pk}	1860	MPa
f_{cd}	36.67	MPa	c	40	mm	f_{pd}	1522	MPa
			f_s (B)	435	MPa	σ_p	761	MPa
						anchor	670	mm

Reinforcement layout

1 vertical reinforcement in the nib								
Quantity	4	x	$\phi 12$	Area	452.3893	mm ²		
Positioning		x1	350 mm	x2	350	mm		
		y1	360 mm	y2	860	mm		
2 vertical reinforcement in the nib								
Quantity	4	x	$\phi 12$	Area	452.3893	mm ²		
Spacing	100	mm						
Positioning		x1	450 mm	x2	450	mm		
		y1	360 mm	y2	860	mm		
1 stirrups in the beam								
Quantity	6	x	$\phi 20$	Area	1884.956	mm ²		
Positioning		x1	540 mm	x2	540	mm		
		y1	40 mm	y2	860	mm		
2 stirrups in the beam								
Quantity	6	x	$\phi 20$	Area	1884.956	mm ²		
Spacing	70	mm						
Positioning		x1	610 mm	x2	610	mm		
		y1	40 mm	y2	860	mm		
3 stirrups in the beam								
Quantity	6	x	$\phi 20$	Area	1884.956	mm ²		
Spacing	70	mm						
Positioning		x1	680 mm	x2	680	mm		
		y1	40 mm	y2	860	mm		
4 stirrups in the beam								
Quantity	6	x	$\phi 20$	Area	1884.956	mm ²		
Spacing	70	mm						
Positioning		x1	750 mm	x2	750	mm		
		y1	40 mm	y2	860	mm		
5 stirrups in the beam								
Quantity	6	x	$\phi 12$	Area	678.584	mm ²		
Spacing	150	mm						

Positioning	x1	900	mm	x2	900	mm
	y1	40	mm	y2	860	mm
6 stirrups in the beam						
Quantity	6	x	ϕ 12	Area	678.584	mm ²
Spacing	53.3	mm				
Positioning	x1	953.3	mm	x2	953.3	mm
	y1	40	mm	y2	860	mm
7 stirrups in the beam						
Quantity	6	x	ϕ 12	Area	678.584	mm ²
Spacing	53.3	mm				
Positioning	x1	1006.6	mm	x2	1006.6	mm
	y1	40	mm	y2	860	mm
8 stirrups in the beam						
Quantity	6	x	ϕ 12	Area	678.584	mm ²
Spacing	53.3	mm				
Positioning	x1	1059.9	mm	x2	1059.9	mm
	y1	40	mm	y2	860	mm
1 diagonal reinforcement						
Quantity	3.28	x	ϕ 20	Area	1030.442	mm ²
inclination with hor.		45 °				
Positioning						
	x1	40	mm	x3	860	mm
	y1	860	mm	y3	40	mm
	x2	40	mm	x4	1660	mm
	y2	860	mm	y4	40	mm
1 horizontal reinforcement						
Quantity	6.56	x	ϕ 20	Area	2060.885	mm ²
Positioning	x1	40	mm	x2	1460	mm
	y1	360	mm	y2	360	mm
	x3	40	mm	y3	860	mm
2 horizontal reinforcement						
Quantity	2	x	ϕ 16	Area	402.1239	mm ²
Spacing	90	mm				
Positioning	x1	40	mm	x2	1460	mm
	y1	450	mm	y2	450	mm
3 horizontal reinforcement						
Quantity	2	x	ϕ 16	Area	402.1239	mm ²
Spacing	90	mm				
Positioning	x1	40	mm	x2	1460	mm
	y1	540	mm	y2	540	mm
1 longitudinal prestressing						
strands	12	x	ϕ 12.9	Area,i	100	mm ²
inclination with hor.		4.24 °		Area	1200	mm ²
Positioning	x1	0	mm	x2	2000	mm
	y1	670	mm	y2	521.7253	mm

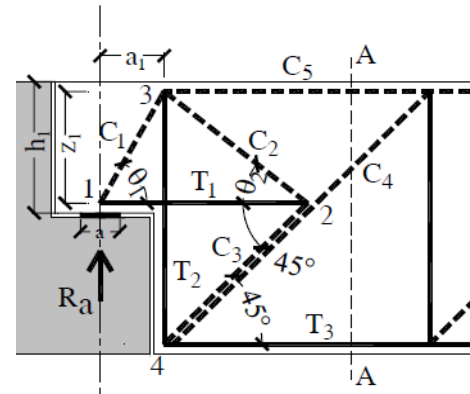
Lower bound: MODEL A

Geometry

$\tan\theta_1$	1.39	-	$\cotan\theta_1$	0.72
$\tan\theta_2$	1.56	-	$\cotan\theta_2$	0.64
θ_1	0.9468	rad	54.27	°
θ_2	1.0015	rad	57.41	°

Model *a* resistance

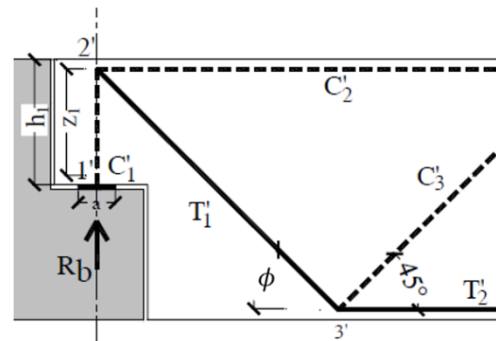
Steel		Rd	
T1		1984500	N
T2		3279823	N
Ra=Rs		2279199	N
Concrete		Ed	Rd
C1		2808506	1107281 N
C2		1188006	1107281 N
C3		1415096	422822.4 N
C4		3223274	1816214 N
Ra=Rc		898596.6	N



Lower bound: MODEL B

Model *b* resistance

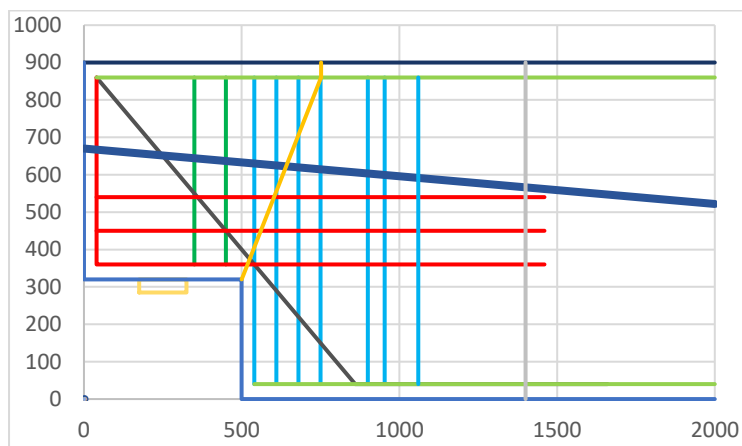
Steel		Rd	
T1		448242.4	N
T2		983946.8	N
Diagonal reinfo. slope		45°	
Rb=Rs		316955.3	N
Concrete		Ed	Rd
C1		316955.3	1100000 N
C3		448242.4	1963500 N
Rb=Rs		316955.3	N



Lower bound: Resistance of the half-joint

V_{Ed}	980	kN
V_p	135.4	kN
V_{LB}	1215.55	kN
unity check	0.695	

Upper bound: KINEMATIC METHOD

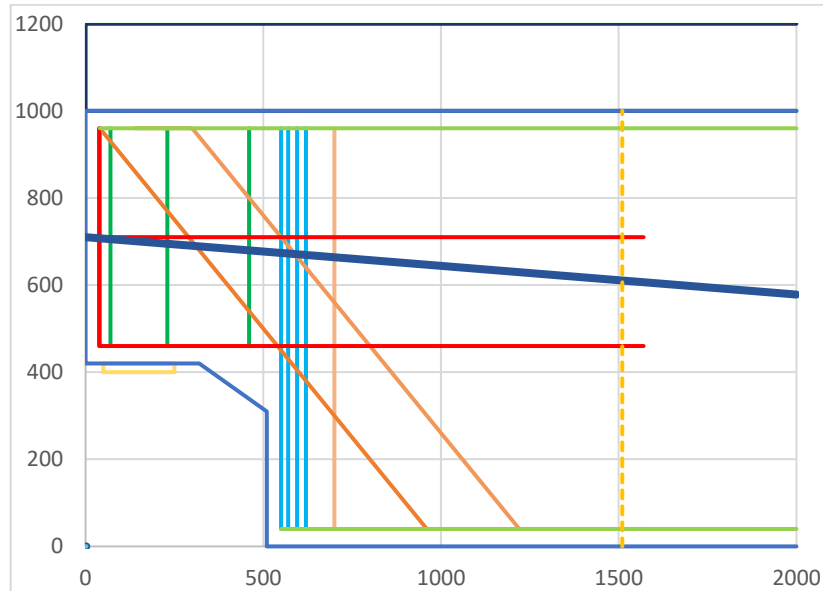


Crack slope: 65°

	As	f_{yd}	T	arm	M_{rd}	
	mm ²	N/mm ²	N	mm	kNm	
Hr1	2061	435	8.96E+05	500.0	448.2	
Hr2	402	435	1.75E+05	410.0	71.7	
Hr3	402	435	1.75E+05	320.0	56.0	
Vr1	1885.0	435	8.20E+05	211.8	173.7	
Vr2	1885.0	435	8.20E+05	141.8	116.3	
Vr3	1885.0	435	8.20E+05	71.8	58.9	
Dr1	1030.4	435	4.48E+05			
			448242	500.0	224.1	h
			448242	211.8	94.9	V
Ap_long1	1200.0	837	907804.2			55% efficiency
			905320	162.2	146.8	h
			67118	111.8	7.5	v
tot	→	→	→	→	1398.17	kNm
a	→	→	→	→	501.81	mm

F_{UB} → → → → 2786.3 kN

A.2 Beam 5



Geometry

height slab	200	mm
height precast	1000	mm
height nib	580	mm
length nib	320	mm
eccentricity of support reaction	170	mm
bearing	2 x	rectangular
bearing width	200	mm
width in the other direction or diameter	300	mm
bearing thickness	20	mm
working width	480	mm

Material

concrete	C55/67	reinforcing steel	QR40	prestressing steel	QP105			
f_{ck}	55	MPa	f_s (A)	335	MPa	f_{pk}	1030	MPa
f_{cd}	36.67	MPa	c	40	mm	f_{pd}	843	MPa
			f_s (B)	335	MPa	σ_p	421	MPa
						anchor	710	mm

Reinforcement layout

1	vertical reinforcement in the nib						
	Quantity	1.16	x	ϕ 10	Area	91.10619	mm ²
	Positioning		x1	40 mm	x2	40	mm
			y1	460 mm	y2	960	mm
2	vertical reinforcement in the nib						
	Quantity	1.16	x	ϕ 10	Area	91.10619	mm ²
	Spacing	30	mm				
	Positioning		x1	70 mm	x2	70	mm
			y1	460 mm	y2	960	mm
3	vertical reinforcement in the nib						
	Quantity	2	x	ϕ 16	Area	402.1239	mm ²
	Spacing	160	mm				
	Positioning		x1	230 mm	x2	230	mm
			y1	460 mm	y2	960	mm
4	vertical reinforcement in the nib						
	Quantity	2	x	ϕ 16	Area	402.1239	mm ²
	Spacing	230	mm				
	Positioning		x1	460 mm	x2	460	mm
			y1	460 mm	y2	960	mm
1	stirrups in the beam						
	Quantity	1.16	x	ϕ 10	Area	91.10619	mm ²
	Positioning		x1	550 mm	x2	550	mm
			y1	40 mm	y2	960	mm
2	stirrups in the beam						
	Quantity	1.16	x	ϕ 10	Area	91.10619	mm ²
	Spacing	20	mm				
	Positioning		x1	570 mm	x2	570	mm
			y1	40 mm	y2	960	mm
3	stirrups in the beam						
	Quantity	2	x	ϕ 16	Area	402.1239	mm ²

Spacing	25	mm					
Positioning	x1	595	mm	x2	595	mm	
	y1	40	mm	y2	960	mm	
4	stirrups in the beam						
Quantity	2	x	$\phi 16$	Area		402.1239	mm ²
Spacing	25	mm					
Positioning	x1	620	mm	x2	620	mm	
	y1	40	mm	y2	960	mm	
1	diagonal reinforcement						
Quantity	2	x	$\phi 16$	Area		402.1239	mm ²
inclination with hor.	45	°					
Positioning	x1	40	mm	x3	960	mm	
	y1	960	mm	y3	40	mm	
	x2	40	mm	x4	1600	mm	
	y2	960	mm	y4	40	mm	
2	diagonal reinforcement						
Quantity	2	x	$\phi 16$	Area		402.1239	mm ²
spacing	100	mm		inclination with hor.	45	°	
Positioning	x1	140	mm	x3	1220	mm	
	y1	960	mm	y3	40	mm	
	x2	300	mm	x4	1860	mm	
	y2	960	mm	y4	40	mm	
1	horizontal reinforcement						
Quantity	2	x	$\phi 16$	Area		402.1239	mm ²
Positioning	x1	38	mm	x2	1570	mm	
	y1	460	mm	y2	460	mm	
	x3	38	mm	y3	960	mm	
2	horizontal reinforcement						
Quantity	2	x	$\phi 16$	Area		402.1239	mm ²
Spacing	250	mm					
Positioning	x1	38	mm	x2	1570	mm	
	y1	710	mm	y2	710	mm	
1	vertical prestressig						
cables	1	x	$\phi 32$	Area		804.2477	mm ²

Positioning		x1	700	mm	x2	700	mm
		y1	40	mm	y2	960	mm
1	longitudinal prestressing				Area,i	94	mm ²
	strands	10	x	ϕ 12.7	Area	940	mm ²
	inclination with hor.	3.77		°			
Positioning		x1	0	mm	x2	2000	mm
		y1	710	mm	y2	578.2119	mm

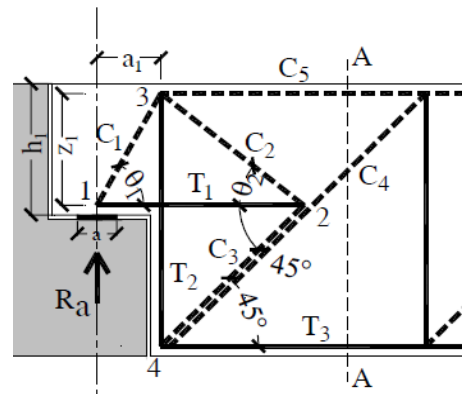
Lower bound: MODEL A

Geometry

$\tan\theta_1$	1.19	-	$\cotan\theta_1$	0.84
$\tan\theta_2$	1.19	-	$\cotan\theta_2$	0.84
θ_1	0.8702	rad	49.88	°
θ_2	0.8721	rad	50.00	°

Model a resistance

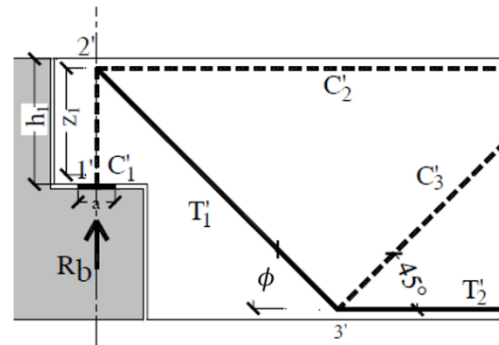
Steel		Rd	
T1		661483.5656	N
T2		664412.5743	N
Ra=Rs		455597	N
Concrete		Ed	Rd
C1	595981.5786	1.97E+06	N
C2	2.73E+05	1.97E+06	N
C3	2.95E+05	1.10E+06	N
C4	6.44E+05	3484166	N
Ra=Rc		455597	N



Lower bound: MODEL B

Model *b* resistance

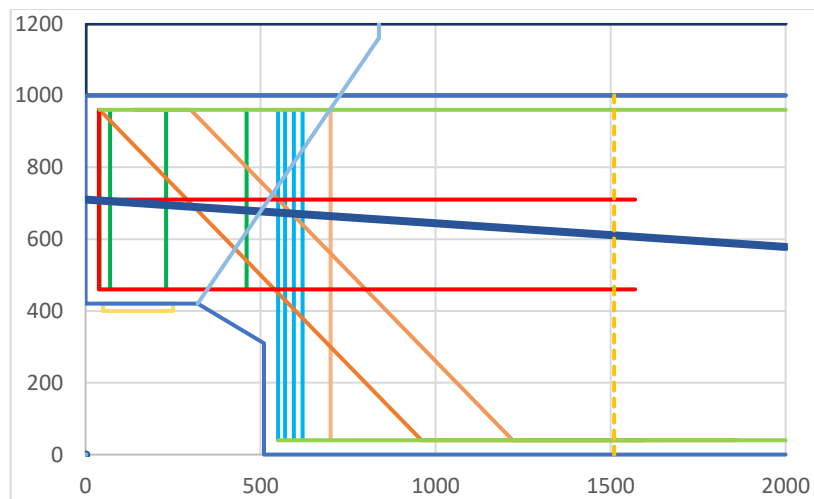
Steel		Rd	
T1		2.65E+05	N
T2		1.24E+06	N
Diagonal reinfo. slope		45°	
Rb=Rs		1.88+05	N
Concrete		Ed	Rd
C1		1.88E+05	2.20E+06
C3		2.65E+05	3.75E+06
Rb=Rs		1.88+05	N



Lower bound: Resistance of the half-joint

V_{Ed}	693.3	kN
V_p	52.2	kN
V_{LB}	643.3	kN
unity check	0.997	

Upper bound: kinematic method

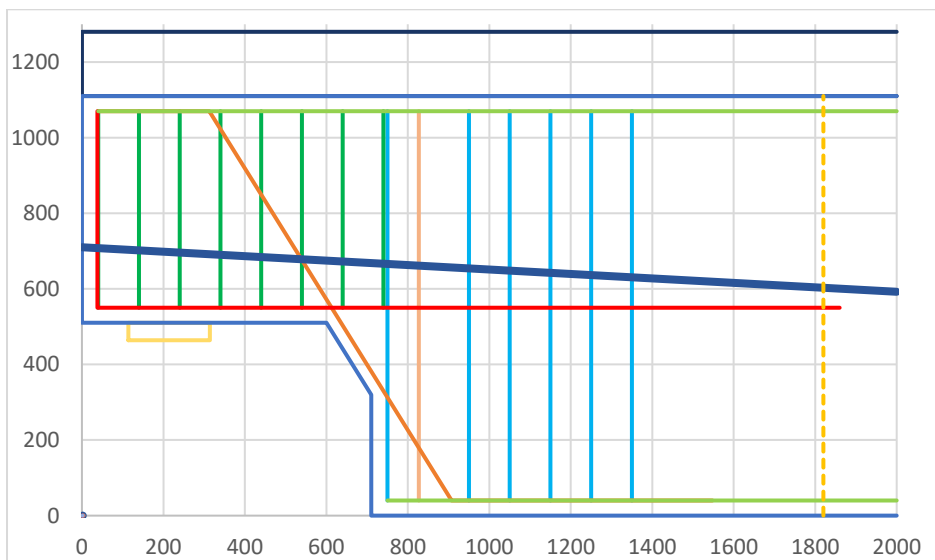


Crack slope: 55°

As	fyd	T	arm	Mrd
----	-----	---	-----	-----

	mm ²	N/mm ²	N	mm	kNm	
Hr1	402	330	1.33E+05	500.0	66.4	
Hr2	402	330	1.33E+05	250.0	33.2	
Vr1	91.1	330	3.01E+04	288.2	8.7	
Vr2	91.1	330	3.01E+04	268.2	8.1	
Vr3	402.1	330	1.33E+05	243.2	32.3	
Vr4	402.1	330	1.33E+05	218.2	28.9	
VrNIB4	402.1239	330	1.33E+05	378.2	50.2	
Dr1	402.1	330	1.33E+05			
			93834	338.2	31.7	h
			93834	570.0	53.5	v
Dr2	402.1	330	1.33E+05			
			93834	148.2	13.9	h
			9.38E+04	375.0	35.2	v
Ap_long1	940.0	464	356124			55% eff.
			355353	502.7	178.6	h
			23416	108.2	2.5	v
tot	→	→	→	→	543.12	kNm
a	→	→	→	→	688.15	mm
F_{UB}	→	→	→	→	789.2409	kN

A.3 Beam 14



Geometry

height slab	170	mm
height precast	1110	mm
height nib	600	mm
length nib	600	mm
eccentricity of support reaction	386	mm
bearing	2 x	rectangular
bearing width	200	mm
width in the other direction or diameter	250	mm
bearing thickness	46	mm
working width	400	mm

Material

concrete	C55/67	reinforcing steel	QR40	prestressing steel	QP190			
f_{ck}	55	MPa	f_s (A)	335	MPa	f_{pk}	1864	MPa
f_{cd}	36.67	MPa	c	40	mm	f_{pd}	1525	MPa
			f_s (B)	335	MPa	σ_p	763	MPa
						anchor	710	mm

Reinforcement layout

1	vertical reinforcement in the nib
Quantity	4 x $\phi 8$ Area 201.0619 mm ²
Positioning	x1 40 mm x2 40 mm y1 550 mm y2 1070 mm
2	vertical reinforcement in the nib
Quantity	4 x $\phi 8$ Area 201.0619 mm ²
Spacing	100 mm
Positioning	x1 140 mm x2 140 mm y1 550 mm y2 1070 mm
3	vertical reinforcement in the nib
Quantity	4 x $\phi 8$ Area 201.0619 mm ²
Spacing	100 mm
Positioning	x1 240 mm x2 240 mm

		y1	550	mm	y2	1070	mm
4	vertical reinforcement in the nib						
	Quantity	4	x	ϕ 8	Area	201.0619	mm ²
	Spacing	100	mm				
	Positioning		x1	340	mm	x2	340 mm
		y1	550	mm	y2	1070	mm
5	vertical reinforcement in the nib						
	Quantity	4	x	ϕ 8	Area	201.0619	mm ²
	Spacing	100	mm				
	Positioning		x1	440	mm	x2	440 mm
		y1	550	mm	y2	1070	mm
6	vertical reinforcement in the nib						
	Quantity	4	x	ϕ 8	Area	201.0619	mm ²
	Spacing	100	mm				
	Positioning		x1	540	mm	x2	540 mm
		y1	550	mm	y2	1070	mm
7	vertical reinforcement in the nib						
	Quantity	4	x	ϕ 8	Area	201.0619	mm ³
	Spacing	100	mm				
	Positioning		x1	640	mm	x2	640 mm
		y1	550	mm	y2	1070	mm
8	vertical reinforcement in the nib						
	Quantity	4	x	ϕ 8	Area	201.0619	mm ³
	Spacing	100	mm				
	Positioning		x1	740	mm	x2	740 mm
		y1	550	mm	y2	1070	mm
1	stirrups in the beam						
	Quantity	4	x	ϕ 8	Area	201.0619	mm ²
	Positioning		x1	750	mm	x2	750 mm
		y1	40	mm	y2	1070	mm
2	stirrups in the beam						
	Quantity	4	x	ϕ 8	Area	201.0619	mm ²

	Spacing	200	mm				
	Positioning	x1	950	mm	x2	950	mm
		y1	40	mm	y2	1070	mm
3	stirrups in the beam						
	Quantity	4	x	$\phi 8$	Area	201.0619	mm ²
	Spacing	100	mm				
	Positioning	x1	1050	mm	x2	1050	mm
		y1	40	mm	y2	1070	mm
4	stirrups in the beam						
	Quantity	4	x	$\phi 8$	Area	201.0619	mm ²
	Spacing	100	mm				
	Positioning	x1	1150	mm	x2	1150	mm
		y1	40	mm	y2	1070	mm
5	stirrups in the beam						
	Quantity	4	x	$\phi 8$	Area	201.0619	mm ²
	Spacing	100	mm				
	Positioning	x1	1250	mm	x2	1250	mm
		y1	40	mm	y2	1070	mm
6	stirrups in the beam						
	Quantity	4	x	$\phi 8$	Area	201.0619	mm ²
	Spacing	100	mm				
	Positioning	x1	1350	mm	x2	1350	mm
		y1	40	mm	y2	1070	mm
1	diagonal reinforcement						
	Quantity	2	x	$\phi 16$	Area	402.1239	mm ²
	inclination with hor.	60	°				
	Positioning	x1	40	mm	x3	907.6708	mm
		y1	1070	mm	y3	40	mm
		x2	313	mm	x4	1547.671	mm
		y2	1070	mm	y4	40	mm
1	horizontal reinforcement						
	Quantity	2	x	$\phi 16$	Area	402.1239	mm ²

Positioning		x1	38	mm	x2	1860	mm
		y1	550	mm	y2	550	mm
		x3	38	mm	y3	1070	mm
1	vertical prestressing						
cables	3	x	ϕ 18.6		Area	815.149	mm ²
Positioning		x1	827	mm	x2	827	mm
		y1	40	mm	y2	1070	mm
1	longitudinal prestressing				Area,i	94	mm ²
strands	10	x	ϕ 12.7		Area	940	mm ²
inclination with hor.		3.37	°				
Positioning		x1	0	mm	x2	2000	mm
		y1	710	mm	y2	592.229	mm

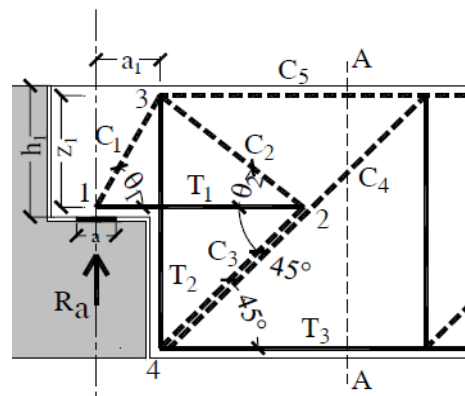
Lower bound: MODEL A

Geometry

$\tan\theta_1$	0.68	-	$\cotan\theta_1$	1.470588
$\tan\theta_2$	1.02	-	$\cotan\theta_2$	0.980769
θ_1	0.5972	rad	34.23	°
θ_2	0.7951	rad	45.58	°

Model a resistance

Steel		Rd	
T1		8.49E+05	N
T2		8.87E+05	N
Ra=Rs		5.09+05	N
Concrete		Ed	Rd
C1	905288.102	1.61E+06	N
C2	5.29E+05	1.61E+06	N
C3	5.34E+05	1.18E+06	N
C4	7.20E+05	3243240	N
Ra=Rs		5.09+05	N

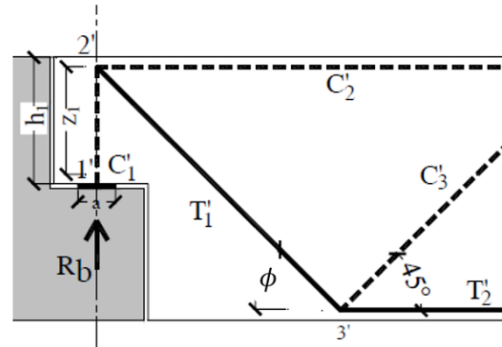


Lower bound: MODEL B

Model *b* resistance

Steel		Rd	
T1		1.33E+05	N
T2		1.24E+06	N
Diagonal reinfo. slope		60°	
Rb=Rs		1.15E+05	N

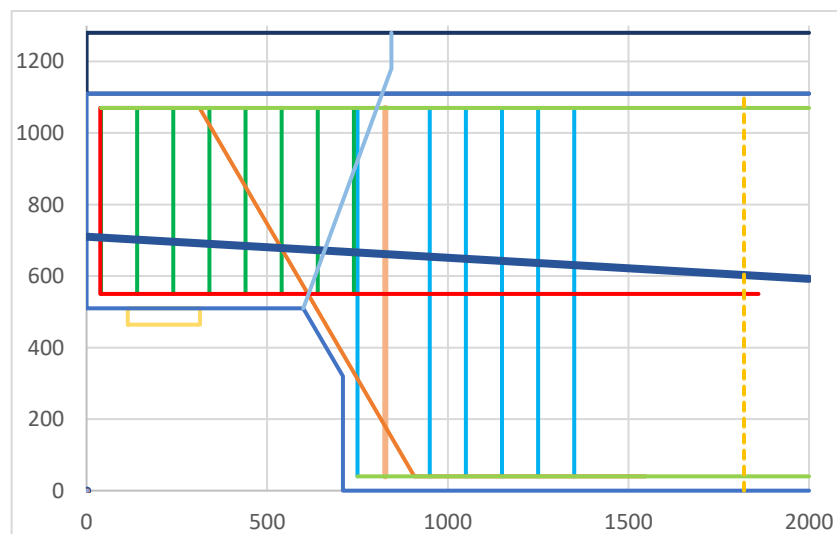
Concrete		Ed	Rd	
C1		1.15E+05	1.83E+06	N
C3		1.63E+05	3.49E+06	N
Rb=Rs			1.15E+05	N



Lower bound: Resistance of the half-joint

V_{Ed}	1001.2	kN
V_p	84.4	kN
V_{LB}	624	kN
unity check	1.47	

Upper bound: kinematic method



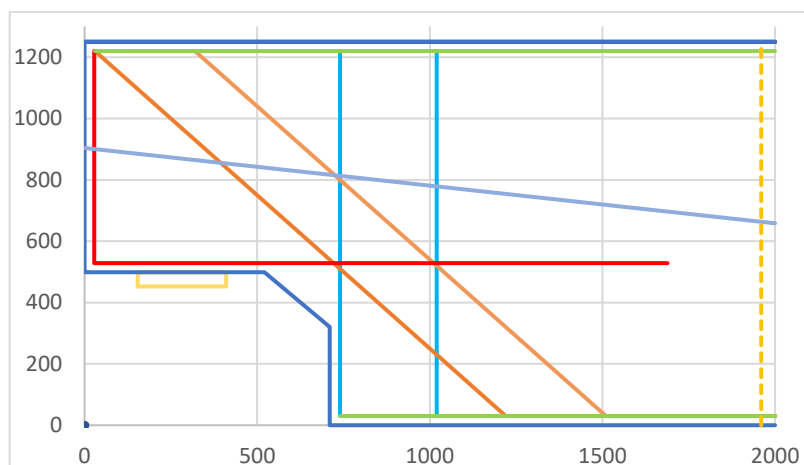
Crack slope: 70°

	As	f_{yd}	T	arm	M_{rd}	
	mm ²	N/mm ²	N	mm	kNm	
Hr1	402	330	1.33E+05	630.0	83.6	
Vr1	201.1	330	6.64E+04	93.9	6.2	
VrNIB7	201.1	330	6.64E+04	203.9	13.5	
VrNIB8	201.1	330	6.64E+04	103.9	6.9	
Dr1	402.1	330	1.33E+05			
			66350	630.0	41.8	h
			114922	243.9	28.0	v
Ap_long1	940.0	839	739640.1			55% eff.
			738361	526.4	388.7	h
			43479	243.9	10.6	v
tot	→	→	→	→	579.36	kNm
a	→	→	→	→	629.86	mm
F_{UB}	→	→	→	→	919.8	kN

A.4 Beam 27

Geometry

height slab	0	mm
height precast	1250	mm
height nib	751.5	mm
length nib	521	mm
eccentricity of support reaction	239	mm
bearing	2 x	rectangular
bearing width	256	mm
width in the other direction or diameter	306	mm
bearing thickness	46	mm
working width	986	mm



Material

concrete	C55/67	reinforcing steel	QR40	prestressing steel	QP170
f_{ck}	55 MPa	f_s (A)	335 MPa	f_{pk}	1670 MPa
f_{cd}	36.67 MPa	c	30 mm	f_{pd}	1366 MPa
		f_s (B)	335 MPa	σ_p	683 MPa
				anchor	904 mm

Reinforcement layout

1	stirrups in the beam						
	Quantity	2.00	x	ϕ 19	Area	567.06	mm ²
	Positioning		x1	740 mm	x2	740	mm
			y1	30 mm	y2	1220	mm
2	stirrups in the beam						
	Quantity	2	x	ϕ 19	Area	567.06	mm ²
	Spacing	280		mm			
	Positioning		x1	1020 mm	x2	1020	mm
			y1	30 mm	y2	1220	mm
1	diagonal reinforcement						
	Quantity	2	x	ϕ 19	Area	567.06	mm ²
	inclination with hor.	45		°			
	Positioning						
			x1	30 mm	x3	1220	mm
			y1	1220 mm	y3	30	mm

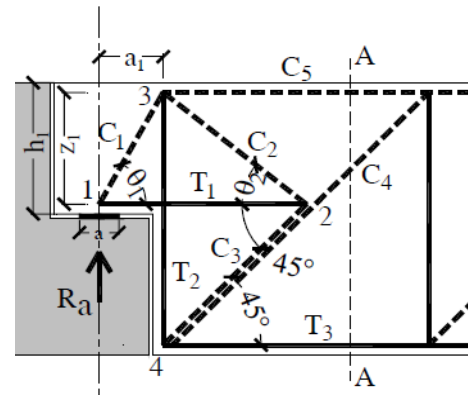
		x2	30	mm	x4	1980	mm
		y2	1220	mm	y4	30	mm
2	diagonal reinforcement						
	Quantity	4	x	ϕ 19	Area	1134.1	mm ²
	spacing	100	mm		inclination with hor.	45	°
	Positioning	x1	130	mm	x3	1510	mm
		y1	1220	mm	y3	30	mm
	Positioning	x2	320	mm	x4	2270	mm
		y2	1220	mm	y4	30	mm
1	horizontal reinforcement						
	Quantity	4	x	ϕ 19	Area	1134.1	mm ²
	Positioning	x1	28	mm	x2	1688.5	mm
		y1	528.5	mm	y2	528.5	mm
		x3	28	mm	y3	1220	mm
1	longitudinal prestressing						
	cables	36	x	ϕ 7	Area	1386	mm ²
	inclination with hor.	7		°			
	Positioning	x1	0	mm	x2	2000	mm
		y1	904	mm	y2	658.43	mm

Lower bound: MODEL A**Geometry**

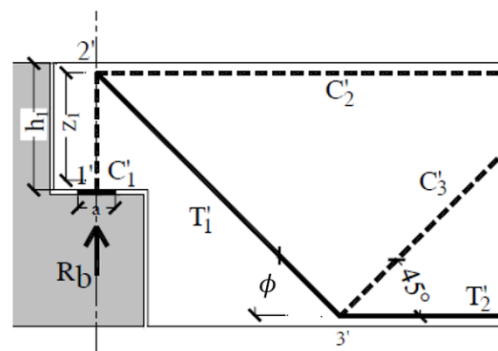
$\tan\theta_1$	1.16	-	$\cotan\theta_1$	0.864786696
$\tan\theta_2$	1.39	-	$\cotan\theta_2$	0.720896602
θ_1	0.8578	rad	49.17	°
θ_2	0.9462	rad	54.24	°

Model *a* resistance

Steel		Rd	
T1		1.32E+06	N
T2		1.87E+05	N
Ra=Rs		1.25+05	N
Concrete		Ed	Rd
C1		164654.3824	5.41E+06 N
C2		7.72E+04	5.41E+06 N
C3		8.85E+04	2.81E+06 N
C4		1.76E+05	9137520 N
Ra=Rs		1.25+05	N

Lower bound: MODEL BModel *b* resistance

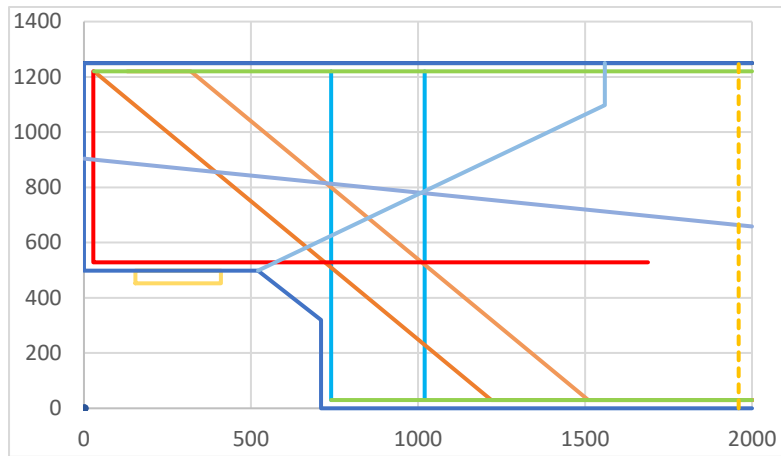
Steel		Rd	
T1		9.17E+05	N
T2		1.22E+06	N
Diagonal reinfo. slope		45°	
Rb=Rs		6.096E+05	N
Concrete		Ed	Rd
C1		6.1E+05	2.87E+06 N
C3		8.62E+05	9.8E+06 N
Rb=Rs		6.096E+05	N



Lower bound: Resistance of the half-joint

V_{Ed}	946.9	kN
V_p	116.3	kN
V_{LB}	734	kN
unity check	1.13	

Upper bound: kinematic method



Crack slope: 30°

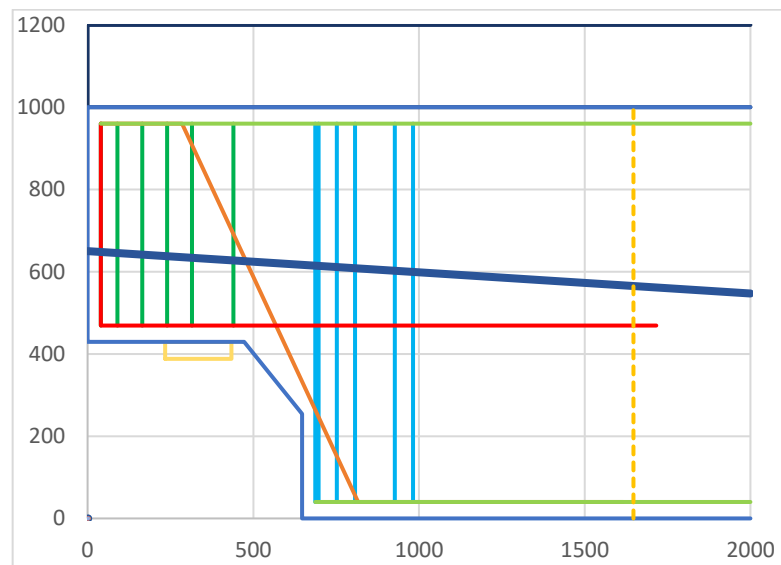
	As	f _{yd}	T	arm	Mrd	
	mm ²	N/mm ²	N	mm	kNm	
Hr1	1134	330	3.74E+05	691.5	258.8	
Vr1	567.1	330	1.87E+05	819.4	153.3	
Vr2	567.1	330	1.87E+05	539.4	100.9	
Dr1	567.1	330	1.87E+05			
			132320	591.5	78.3	h
			132320	989.4	130.9	v
Dr2	1134.1	330	3.74E+05			
			2.65E+05	417.5	110.5	h
			264640	839.4	222.1	v
Ap_long1	1386.0	752	516907.6			55% eff.
			513055	447.5	229.6	h
			62995	869.4	54.8	v
tot	→	→	→	→	1339.18	kNm
a	→	→	→	→	1277.36	mm
F_{UB}	→	→	→	→	1048.39	kN

A.5 Beam 30

Geometry

height slab	200 mm
height precast	1000 mm
height nib	571 mm

length nib	472	mm
eccentricity of support reaction	138	mm
bearing	2 x	rectangular
bearing width	200	mm
width in the other direction or diameter	300	mm
bearing thickness	41	mm
working width	440	mm



Material

concrete	C55/67	reinforcing steel	FeB500	prestressing steel	FeP1860
f_{ck}	55 MPa	f_s (A)	435 MPa	f_{pk}	1860 MPa
f_{cd}	36.67 MPa	c	30 mm	f_{pd}	1522 MPa
		f_s (B)	435 MPa	σ_p	761 MPa
				anchor	650 mm

Reinforcement layout

1	vertical reinforcement in the nib
Quantity	6 x ϕ 12
Area	678.584 mm ²
Positioning	x1 40 mm x2 40 mm
	y1 469 mm y2 960 mm

2	vertical reinforcement in the nib						
Quantity	6	X	ϕ 12	Area	678.584	mm ²	
Spacing	50	Mm					
Positioning		x1	90	mm	x2	90	mm
		y1	469	mm	y2	960	mm
3	vertical reinforcement in the nib						
Quantity	6	x	ϕ 12	Area	678.584	mm ²	
Spacing	75	mm					
Positioning		x1	165	mm	x2	165	mm
		y1	469	mm	y2	960	mm
4	vertical reinforcement in the nib						
Quantity	6	x	ϕ 12	Area	678.584	mm ²	
Spacing	75	mm					
Positioning		x1	240	mm	x2	240	mm
		y1	469	mm	y2	960	mm
5	vertical reinforcement in the nib						
Quantity	6	x	ϕ 12	Area	678.584	mm ²	
Spacing	75	mm					
Positioning		x1	315	mm	x2	315	mm
		y1	469	mm	y2	960	mm
6	vertical reinforcement in the nib						
Quantity	6	x	ϕ 12	Area	678.584	mm ²	
Spacing	125	mm					
Positioning		x1	440	mm	x2	440	mm
		y1	469	mm	y2	960	mm
7	vertical reinforcement in the nib						
Quantity	6	x	ϕ 12	Area	678.584	mm ³	
Spacing	50	mm					

	Positioning		x2	490	mm	x3	490	mm
			y2	469	mm	y3	960	mm
8	vertical reinforcement in the nib							
	Quantity	6	x	ϕ 12		Area	678.584	mm ³
	Spacing	50	mm					
	Positioning		x2	540	mm	x3	540	mm
			y2	469	mm	y3	960	mm
1	stirrups in the beam							
	Quantity	4	x	ϕ 12		Area	452.39	mm ²
	Positioning		x1	687	mm	x2	687	mm
			y1	40	mm	y2	960	mm
2	stirrups in the beam							
	Quantity	2	x	ϕ 25		Area	981.75	mm ²
	Spacing	10	mm					
	Positioning		x1	697	mm	x2	697	mm
			y1	40	mm	y2	960	mm
3	stirrups in the beam							
	Quantity	4	x	ϕ 12		Area	452.39	mm ²
	Spacing	55	mm					
	Positioning		x1	752	mm	x2	752	mm
			y1	40	mm	y2	960	mm
4	stirrups in the beam							
	Quantity	4	x	ϕ 12		Area	452.39	mm ²
	Spacing	55	mm					
	Positioning		x1	807	mm	x2	807	mm
			y1	40	mm	y2	960	mm
5	stirrups in the beam							
	Quantity	4	x	ϕ 12		Area	452.39	mm ²
	Spacing	120	mm					
	Positioning		x1	927	mm	x2	927	mm
			y1	40	mm	y2	960	mm

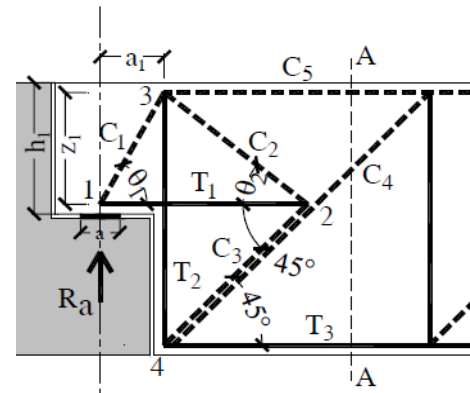
6	stirrups in the beam						
Quantity	4	x	$\phi 12$	Area	452.39	mm ²	
Spacing	55	mm					
Positioning		x1	982	mm	x2	982	mm
		y1	40	mm	y2	960	mm
1	diagonal reinforcement						
Quantity	4	x	$\phi 20$	Area	1256.64	mm ²	
inclination with hor.	60	°					
Positioning		x1	40	mm	x3	816.162	mm
		y1	960	mm	y3	40	mm
		x2	285	mm	x4	1616.16	mm
		y2	960	mm	y4	40	mm
1	horizontal reinforcement						
Quantity	4	x	$\phi 20$	Area	1256.63	mm ²	
Positioning		x1	40	mm	x2	1716	mm
		y1	469	mm	y2	469	mm
		x3	40	mm	y3	960	mm
1	longitudinal prestressing			Area,i	94	mm ²	
strands	21	x	$\phi 12.7$	Area	1974	mm ²	
inclination with hor.	2.95	°					
Positioning		x1	0	mm	x2	2000	mm
		y1	650	mm	y2	546.93	mm

Lower bound: MODEL A**Geometry**

$\tan\theta_1$	1.30	-	$\cotan\theta_1$	0.769857
$\tan\theta_2$	1.14	-	$\cotan\theta_2$	0.873727
θ_1	0.9147	rad	52.44	°
θ_2	0.8527	rad	48.88	°

Model *a* resistance

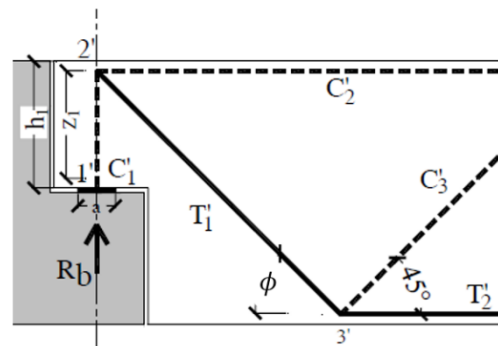
Steel		Rd	
T1		2.05E+06	N
T2		1.21E+05	N
Ra=Rs		8.61+05	N
Concrete		Ed	Rd
C1		1086110.529	1.74E+06 N
C2		4.70E+05	1.74E+06 N
C3		5.00E+05	1.04E+06 N
C4		1.22E+06	3193819 N
Ra=Rs		8.61+05	N



Lower bound: MODEL B

Model *b* resistance

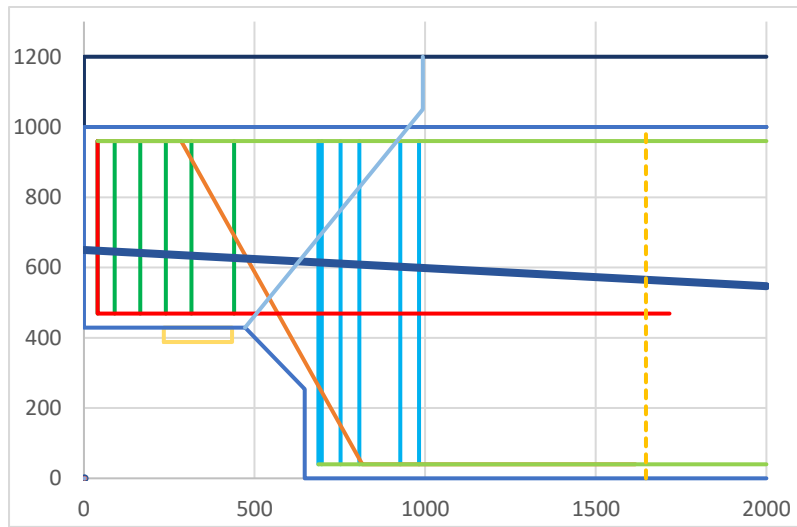
Steel		Rd	
T1		5.47E+05	N
T2		1.64E+06	N
Diagonal reinfo. slope		60°	
Rb=Rs		5.73E+05	N
Concrete		Ed	Rd
C1		4.73E+05	2.20E+06 N
C3		6.69E+05	3.44E+06 N
Rb=Rs		5.73E+05	N



Lower bound: Resistance of the half-joint

V_{Ed}	823	kN
V_p	77.4	kN
V_{LB}	1334	kN
unity check	0.6	

Upper bound: kinematic method



Crack slope: 50°

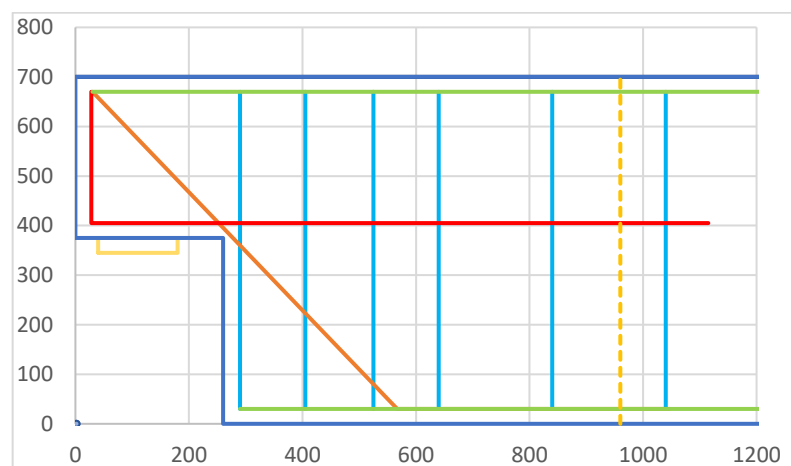
	As	f _{yd}	T	arm	M _{rd}	
	mm ²	N/mm ²	N	mm	kNm	
Hr1	1257	435	5.47E+05	581.0	317.6	
Vr1	452.4	435	1.97E+05	306.1	60.2	
Vr2	981.7	435	4.27E+05	296.1	126.4	
Vr3	452.4	435	1.97E+05	241.1	47.4	
Vr4	452.4	435	1.97E+05	186.1	36.6	
Dr1	1256.6	435	5.47E+05	968.1		
			2.73E+05	511	147.9	
			473402	541.1	256.1	
Ap_long1	1974.0	837	1264010			55% eff.
			1262335	433.3	547.0	
			65052	336.1	21.9	
tot	→	→	→	→	1561.20	kNm
a	→	→	→	→	659.08	mm
F_{UB}	→	→	→	→	2368.754	kN

A.6 Laboratory test

Geometry

height slab	0 mm
height precast	700 mm

height nib	325	mm
length nib	260	mm
eccentricity of support reaction	150	mm
bearing	2 x	rectangular
bearing width	140	mm
width in the other direction or diameter	200	mm
bearing thickness	30	mm
working width	400	mm



Material

concrete	C30/37	reinforcing steel	-	prestressing steel	-			
f_{ck}	30	MPa	f_s (A)	539	MPa	f_{pk}	-	MPa
f_{cd}	20	MPa	c	30	mm	f_{pd}	-	MPa
			f_s (B)	529	MPa	σ_p	-	MPa
						anchor	-	mm

Reinforcement layout

1	stirrups in the beam							
	Quantity	2	x	$\phi 10$	Area	157.0796	mm ²	
	Positioning		x1	290	mm	x2	290	mm
			y1	30	mm	y2	670	mm
2	stirrups in the beam							

	Quantity	2	x	$\phi 10$		Area	157.0796	mm ²
	Spacing	115	mm					
	Positioning		x1	405	mm	x2	405	mm
			y1	30	mm	y2	670	mm
3	stirrups in the beam							
	Quantity	2	x	$\phi 10$		Area	157.0796	mm ²
	Spacing	120	mm					
	Positioning		x1	525	mm	x2	525	mm
			y1	30	mm	y2	670	mm
4	stirrups in the beam							
	Quantity	2	x	$\phi 10$		Area	157.0796	mm ²
	Spacing	115	mm					
	Positioning		x1	640	mm	x2	640	mm
			y1	30	mm	y2	670	mm
5	stirrups in the beam							
	Quantity	2	x	$\phi 10$		Area	157.0796	mm ²
	Spacing	200	mm					
	Positioning		x1	840	mm	x2	840	mm
			y1	30	mm	y2	670	mm
6	stirrups in the beam							
	Quantity	3	X	$\phi 10$		Area	235.6194	mm ²
	Spacing	200	Mm					
	Positioning		x1	1040	mm	x2	1040	mm
			y1	30	mm	y2	670	mm
1	diagonal reinforcement							
	Quantity	4	x	$\phi 12$		Area	452.3893	mm ²
	inclination with hor.		50	°				
	Positioning		x1	30	mm	x3	567.0238	mm
			y1	670	mm	y3	30	mm
			x2	30	mm	x4	1047.024	mm
			y2	670	mm	y4	30	mm
1	longitudinal sup. reinforcement							
	Quantity	5	x	$\phi 20$		Area	1570.796	mm ²

Positioning	x1	30	mm	x2	2000	mm
	y1	670	mm	y2	670	mm
2 longitudinal inf. reinforcement						
Quantity	5	x	ϕ_{24}	Area	2261.947	mm ²
Positioning	x1	290	mm	x2	2000	mm
	y1	30	mm	y2	30	mm
1 horizontal reinforcement						
Quantity	3	x	ϕ_{12}	Area	339.292	mm ²
Positioning	x1	28	mm	x2	1115	mm
	y1	405	mm	y2	405	mm
	x3	28	mm	y3	670	mm

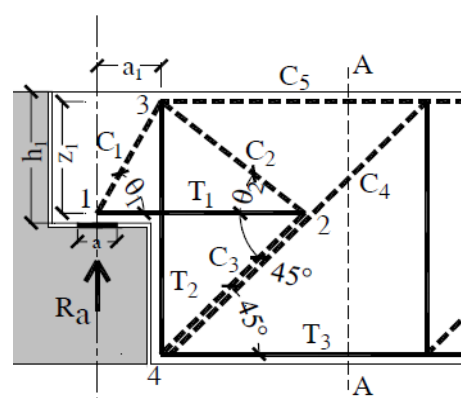
Lower bound: MODEL A

Geometry

$\tan\theta_1$	1.12	-	$\cotan\theta_1$	0.896226
$\tan\theta_2$	0.71	-	$\cotan\theta_2$	1.415094
θ_1	0.8401	rad	48.16	°
θ_2	0.6152	rad	35.27	°

Model a resistance

Steel	Rd		
T1	1.83E+06	N	
T2	1.69E+05	N	
Ra=Rs	1.24E+05	N	
Concrete	Ed	Rd	
C1	165842.5855	5.57E+05	N
C2	7.94E+04	5.57E+05	N
C3	6.48E+04	5.59E+05	N
C4	1.75E+05	1245024	N
Ra=Rs	1.24E+05	N	

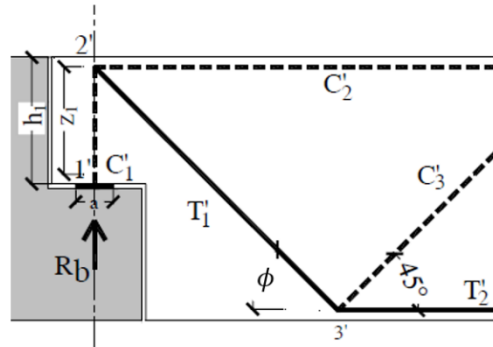


Lower bound: MODEL B

Model *b* resistance

Steel		Rd	
T1		2.39E+05	N
T2		1.20E+06	N
Diagonal reinfo. slope		45°	
Rb=Rs		1.83E+05	N

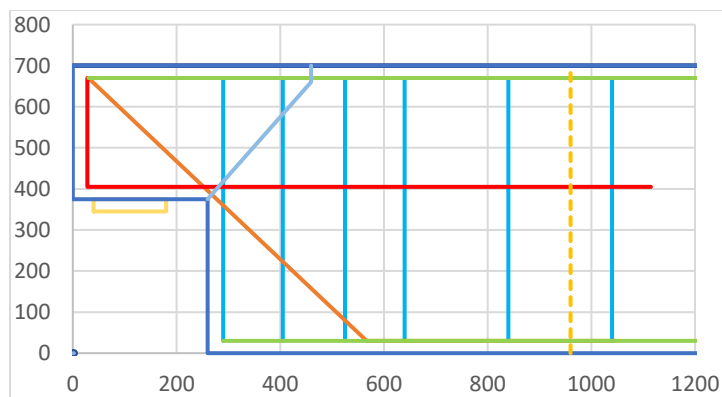
Concrete		Ed	Rd	
C1		1.83E+05	5.60E+05	N
C3		2.59E+05	1.19E+06	N
Rb=Rs			1.83E+05	N



Lower bound: Resistance of the half-joint

V_{Ed}	337	kN
V_p	-	kN
V_{LB}	307	kN
unity check	1.1	

Upper Bound: kinematic method



Crack slope: 55°

	As	fyd	T	arm	Mrd	
	mm ²	N/mm ²	N	mm	kNm	
Hr1	339	539	1.83E+05	255.0	46.6	
Vr1	157.1	539	8.47E+04	169.6	14.4	
Vr2	157.1	539	8.47E+04	54.6	4.6	
Dr1	452.4	539	2.44E+05			
			1.72E+05	255.0	44.0	h
			172419	179.6	31.0	v
tot	→	→	→	→	140.54	kNm
a	→	→	→	→	349.56	mm
Ful	→	→	→	→	402.04	kN